

Time-resolved Quantitative Assays and Imaging of Enzymes and Enzyme Substrates Using a New Europium Fluorescent Probe for Hydrogen Peroxide

Dissertation zur Erlangung des Doktorgrades der Naturwissenschaften
(doktorum rerum naturalis, Dr. rer. nat.)

der Fakultät Chemie und Pharmazie,
der Universität Regensburg
Bundesrepublik Deutschland



vorgelegt von

Meng WU

aus Wuhan, China

im December 2003

**Time-resolved Quantitative Assays and Imaging of
Enzymes and Enzyme Substrates Using a New
Europium Fluorescent Probe for Hydrogen Peroxide**

By

Meng WU

A thesis submitted in conformity with the requirements
for the Degree of Doctor of Philosophy (Dr. rer. nat)

Faculty of Chemistry and Pharmacy
in University of Regensburg
Federal Republic of Germany

Copyright[©] by Meng WU 2003

This study was performed at the Institute of Analytical Chemistry, Chemo- and Biosensors of the University of Regensburg between May 2001 and December 2003 under the supervision of Prof. Otto S. Wolfbeis.

Date of defense: 18. 12. 2003

Committee of defense (Prüfungsausschuß):

Chairperson	(Vorsitzender)	Prof. Dr. Manfred Liefländer
First expert	(Erstgutachter)	Prof. Dr. Otto Wolfbeis
Second expert	(Zweitgutachter)	Prof. Dr. Bernhard Dick
Third expert	(Drittprüfer)	Prof. Dr. Claudia Steinem

子曰：「學而時習之，不亦悅乎？」

論語, 學而第一

Confucius said: "Isn't it a pleasure to study and practice what you have learned?"

Konfucius sagte: "Zu lernen und das Erlernte immer wieder auszuüben - ist das nicht eine Freude?"

From THE ANALECTS (Sayings)

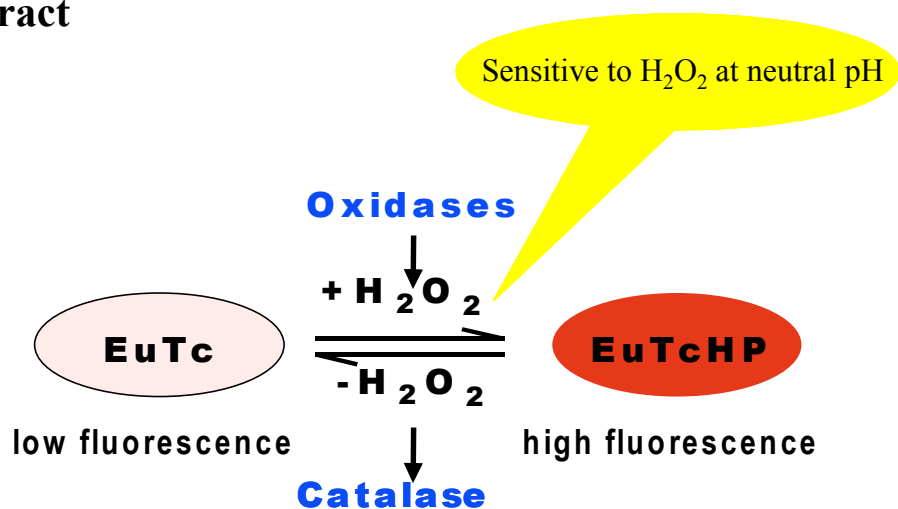
Table of Contents

Graphical Abstract	1
Chapter 1. Introduction	5
1.1. Importance of Hydrogen Peroxide	5
1.2. Overview of Hydrogen Peroxide Based Enzymatic Assays	6
1.3. Overview of Methods for Determination of Hydrogen Peroxide	9
1.3.1. Analytical Methods Based on Physical Properties.....	10
1.3.2. Optical Analytical Methods Based on Chemical Reactions of H ₂ O ₂	10
1.3.2.1. Determination based on simple oxidations.....	11
1.3.2.2. Determination based on enzyme coupling with peroxidases.....	11
1.3.2.3. Determination based on metal H ₂ O ₂ complexes.....	12
1.4. Time-resolved Fluorescence Assays and Imaging	15
1.5. Aim of the Research	16
1.6. Reference	18
Chapter 2. Characterization of the Probe and Time-resolved Assay of H₂O₂	24
2.1. Introduction	24
2.2. Results and Discussion	25
2.2.1. Characterization of the Fluorescent Europium Probe.....	25
2.2.1.1. Absorbance, circular dichroism and fluorescence spectra.....	25
2.2.1.2. Lifetime characterization of EuTc-HP.....	27
2.2.1.3. pH, buffer, temperature and stability.....	29
2.2.1.4. Quenchers and interferents.....	32
2.2.2. Time-resolved Fluorescent Determination of Hydrogen Peroxide.....	33
2.2.2.1. Time-correlated single photon counting (TCSPC) method.....	33
2.2.2.2. Rapid lifetime determination (RLD) method.....	34
2.3. Experimental	38
2.3.1. Time-correlated Single Photon Counting Lifetime Determination.....	38
2.3.2. Rapid Lifetime Determination Assay of H ₂ O ₂ on Microplates.....	38
2.3.3. Time-resolved (gated) and Steady-state Fluorescence Assays.....	38
2.4. References	39

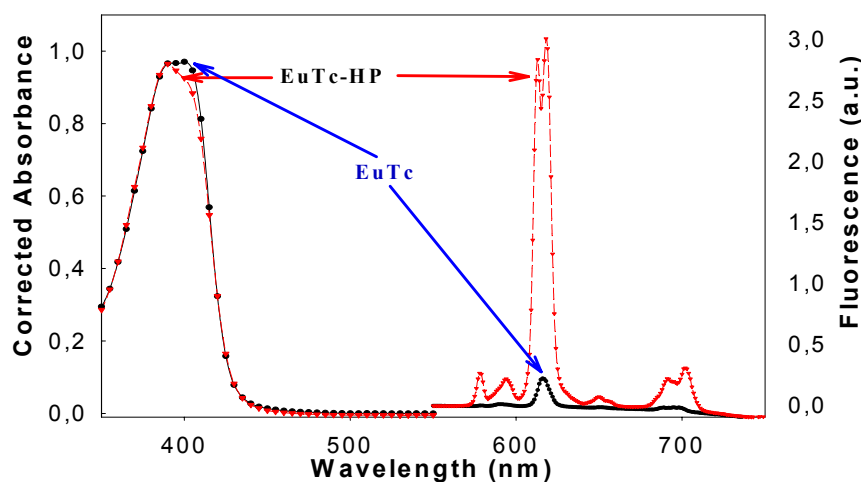
Chapter 3. Direct and Time-Resolved Enzymatic Detection of Glucose	41
3.1. Introduction	41
3.2. Results and Discussion	43
3.2.1. Assay Principle.....	43
3.2.2. Fluorescence Intensity-based Assays.....	45
3.2.3. Time-resolved (gated) Fluorescence Assay.....	48
3.2.4. Comparison.....	50
3.2.5. Analysis of Other Substrates of Oxidases.....	53
3.3. Experimental	54
Glucose Assay Protocol.....	54
3.4. References	55
Chapter 4. Fluorescence Imaging of the Activity of Glucose Oxidase	57
4.1. Introduction	57
4.2. Results and Discussion	58
4.2.1. Principle and Characterization of the Detection System.....	58
4.2.2. Imaging Setup and Analytical Schemes.....	59
4.2.3. Quantitative Aspects of GOx Imaging.....	63
4.2.4. Time-resolved Determination of GOx Using a Microplate Reader.....	64
4.2.5. Comparison.....	64
4.3. Experimental	66
4.4. References	68
Chapter 5. Determination of the Activity of Catalase	70
5.1. Introduction	70
5.2. Results and Discussion	72
5.2.1. Characterization and Optimization of the Assay.....	72
5.2.2. Inhibition and Denaturation of Catalase.....	76
5.2.3. Interferents.....	77
5.2.4. Discussion.....	78
5.3. Experimental	83
Recommended CAT Assay Protocol.....	83
5.4. References	84

Chapter 6. Further Applications and Structure of EuTc-HP	86
6.1. Application of GOx-based ELISA	86
6.2. The Catalase/Glucose Oxidase System	90
6.2.1. The Catalase/Glucose Oxidase System as a Platform for Screening.....	90
6.2.2. Detection of Catalase Independent of H ₂ O ₂	93
6.3. Construction of Microplate Arrays and Sensors	94
6.4. Composition of the Fluorescent Probes	96
6.4.1. Stoichiometry and Structure.....	97
6.4.2. Combinatorial Approach for Discovery of New Lanthanide Probes.....	102
6.5. Experimental	105
6.5.1. Protocol of GOx-labeled Immunoassay.....	105
6.5.2. Coupled GOx-Catalase Enzymatic System.....	106
6.5.3. Construction of Microplate Sensors and Arrays.....	106
6.6. References	107
7. Materials and Instruments	109
7.1. Materials and Reagents	109
7.2. Instruments	110
8. Summary	112
9. Curriculum Vitae	114
10. Patent and List of Recent Publications	115
11. Appendix	117
11.1. Abbreviations and Symbols	117
11.2. Programs	118
11.3. Chinese Summary	125
12. Acknowledgements	127

Graphical Abstract

A. Probe Study

1. The research is based on the finding of the reversible transformation of the weakly fluorescent europium-tetracycline complex (EuTc) to highly fluorescent europium-tetracycline-hydrogen peroxide complex (EuTc-HP) in neutral pH (see figure above).

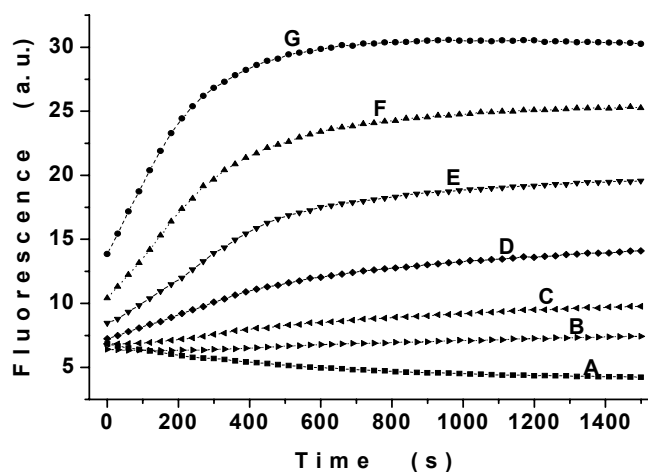


2. EuTc and EuTc-HP have shown not only merits that have made the lanthanide labeling so versatile in bioanalysis, such as large Stokes shift, line-like emission (spectra, above), μs range lifetime, but also compatibility with blue diode laser, as a H_2O_2 fluorescent probe.
3. EuTc and EuTc-HP have been characterized through absorbance, circular dichroism, fluorescence, pH response, temperature response, stability, and etc.
4. A combinatorial approach for discovery of new lanthanide probes has been tested.

B. Assay Study

1. Substrate determinations

The substrates detected in this study are hydrogen peroxide, glucose as an example of the substrates of oxidases (see figure below, a time trace of GOx + glucose with EuTc).

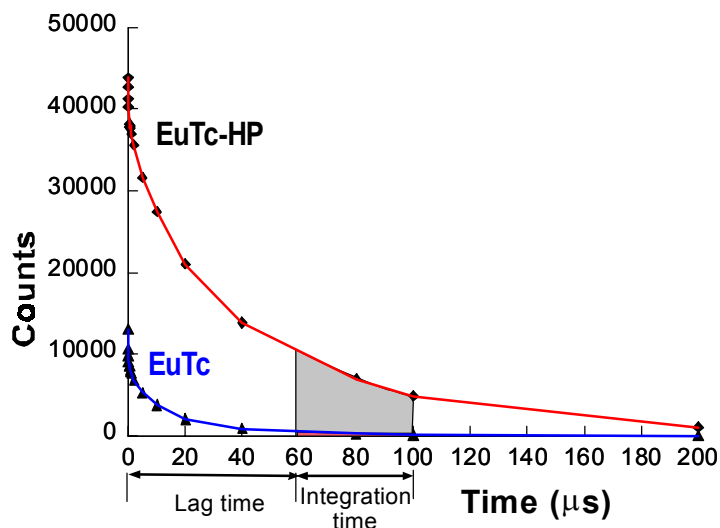


2. Enzyme analysis

Glucose oxidase (GOx) is studied in this thesis as a model enzyme of H_2O_2 producing oxidases, and catalase (CAT) as a model enzyme of H_2O_2 consuming enzymes.

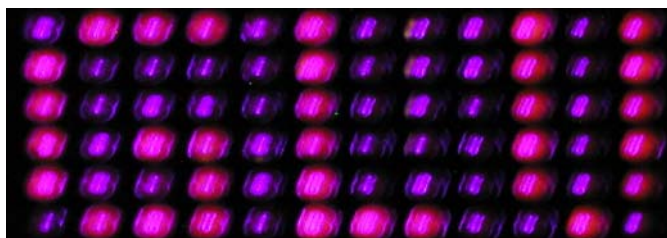
3. Different schemes of detections

Steady-state intensity-based detections, time-resolved “gated” detections (see figure below), and lifetime-based detections of rapid lifetime determination method and time-correlated single photon counting method have been studied in both microplates and cuvettes.

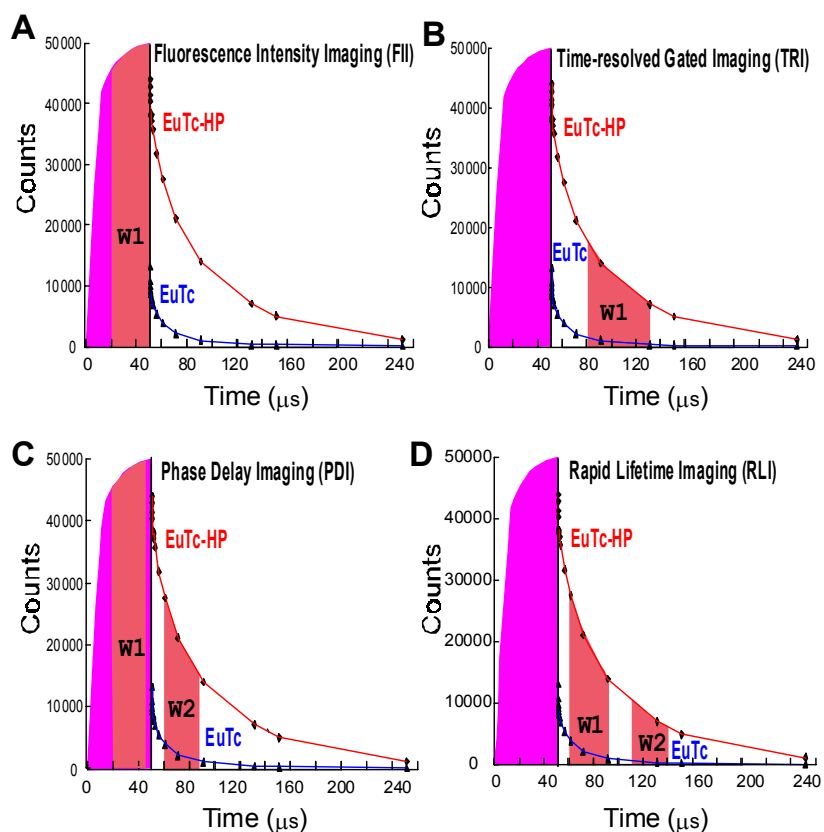


C. Imaging Study

“Seeing is believing”. Visualization through imaging is a better way for bioanalysis (the image below showing “Glu” as glucose). The μs range lifetime of the fluorescent probes has greatly facilitated the imaging here.



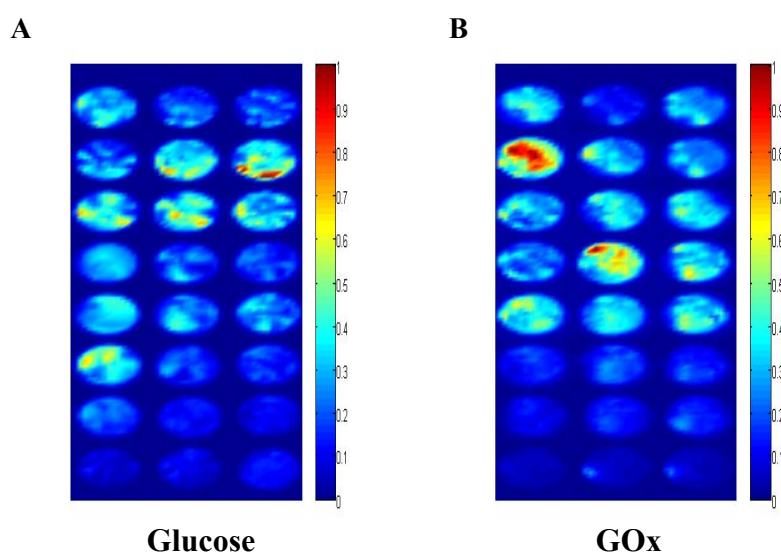
1. Four schemes of imaging (see figure below), that are the conventional fluorescence intensity imaging (FII), the time-resolved ("gated") imaging (TRI), the phase delay ratioing imaging (PDI), and the rapid lifetime determination imaging (RLI), have been used for quantitative analysis.



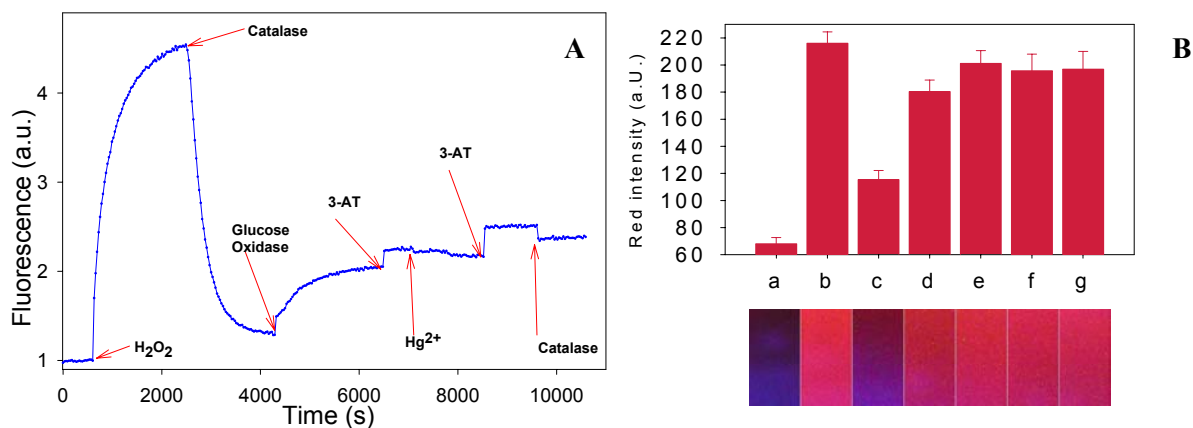
2. Hydrogen peroxide, glucose, and glucose oxidase have been determined by the fluorescence imaging system developed.

D. Further Applications

1. GOx-ELISA, both in sandwich and direct scheme, has been tested without coupling POx.
2. In preliminary studies for arrays and sensors, biotinylated GOx is immobilized on the streptavidin-coated microplates for the quantitative measurement of glucose and for the determination of immobilized GOx (see figure below). It is for multi-enzyme arrays and sensors, which can detect multi-substrates simultaneously on a single shot with microplate arrays.



3. A platform composed of the coupled CAT/GOx system has been constructed for the screening of antioxidative substances and as an alternative for H₂O₂-independent measurement of CAT. The performance of the coupled enzymatic system can be seen in the following figure. The imaging can also be applied for this purpose.



Chapter 1. Introduction

1.1. Importance of Hydrogen Peroxide

Hydrogen peroxide (H_2O_2) is relatively simple molecule as shown in Figure 1.1. However, it is considered as a ubiquitous molecule in almost every aspects of our life, mainly due to the adaptation of nature to the unusual high concentration of oxygen in atmosphere of the earth¹.

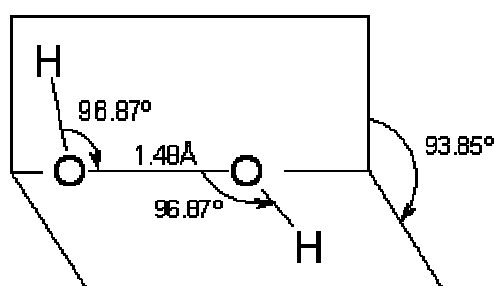


Figure 1.1 Structure of hydrogen peroxide.

Although there are a lot of household and industrial applications^{2,3,4,5} for hydrogen peroxide, the biologically originated hydrogen peroxide is more important and more challenging for bioanalysis. It is of enormous significance in biomedical research for its central role in oxidative stress and peroxidation in general. H_2O_2 as one of the reactive oxygen species (ROS)^{6,7} is viewed as a biomarker for the oxidative stress in cells and as a novel neurotransmitter^{8,9}. The common ROS, their inter-transformation and their energy levels are indicated in Figure 1.2. As a metabolic species produced by almost all oxidases and SOD, and as a substrate for catalase and peroxidases, hydrogen peroxide is acting as a messenger for signal-transduction^{10,11} that regulates cell growth and reduction-oxidation status¹². It is also a potentially harmful metabolic by-product in the presence of metal ions (production of hydroxy radicals through Fenton reaction^{13,14}) that can cause DNA damage^{15,16} and has direct (mostly adverse) effects on cell survival, aging, and cancer development¹⁷.

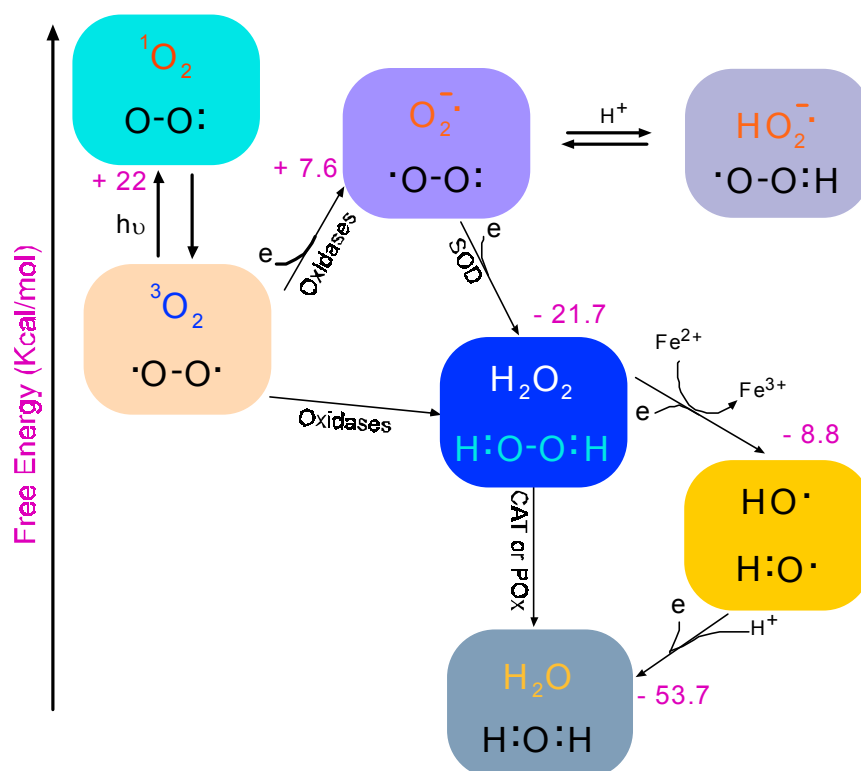


Figure 1.2 Common reactive oxygen species and their energy level.

1.2. Overview of Hydrogen Peroxide Based Enzymatic Assays

Enzymes, as highly specific catalysts in mild reaction conditions, have been used in the diagnosis of disease and bioanalysis for quite a long time. There are lots of reports, reviews and books on their characterization and applications^{18,19,20}. Enzymes have been applied either for the specific detection of enzyme substrates^{21,22}, or for enzymatic amplification immunoassays for biologically important molecules²³, such as antibodies, antigens, nucleic acids, or environmental hazards.

As in Figure 1.3, enzymes, enzyme substrates and enzyme inhibitors can be determined via detectable substrate, products, enzyme cofactors or coenzymes, prosthetic groups and metal ions, and even enzyme itself through the intermediate states if the electrochemical, spectrophotometric, fluorescent, chemiluminescent signals are generated. For

interests of the present research, there have been reports based on fluorescent products, such as resorufin^{24,25} or fused green fluorescent protein (GFP) receptors²⁶; fluorescent cofactors, such as NADH²⁷; fluorescent substrates^{28,29}, such as fluorescein monophosphates³⁰ or other fluorescent peptides³¹; or coupling enzymes³² for the fluorogenic purposes, such as peroxidases (POx).

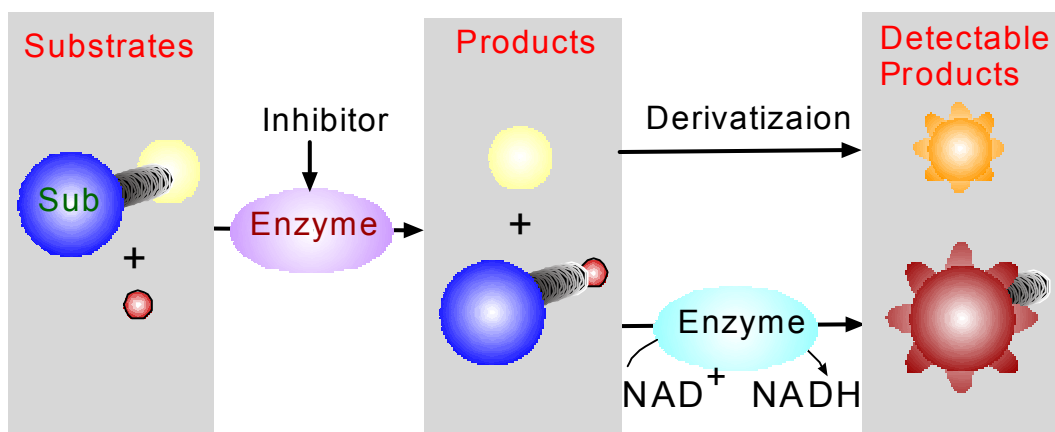


Figure 1.3 Principles for enzyme and enzyme substrate determination.

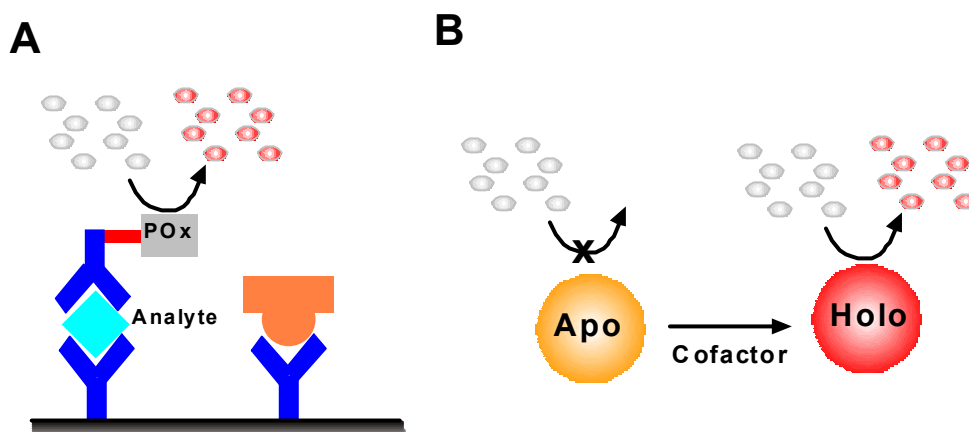


Figure 1.4 Two schemes for enzymatic amplification.

Enzymes for enzymatic amplification are mainly peroxidase, alkaline phosphatase, and β -galactosidase, basically for their high activity and stability. Catalase and glucose oxidase are also sometimes used. There are generally two schemes for enzymatic

amplification as shown in Figure 1.4. One (Figure 1.4 A) is for the amplification reaction of the substrate, while one single enzyme can catalyze multiple substrates into as much as possible detectable products for the measurement of a single analyte. The other is based on the cofactors (Figure 1.4 B) that can be detected by formation of the holo-enzyme, which could generate as much as possible detectable products.

Among different detection schemes (as in Figure 1.3) mentioned above, hydrogen peroxide is of great interests for the following reasons:

- (1) There are numerous H_2O_2 producing oxidases available for the quantitative analysis of biochemically important molecules of clinical interests³³, such as glucose, urate, sarcosine, urea, lactate, etc.
- (2) As a product of enzyme reactions, H_2O_2 does not form a signal background in most biological media.
- (3) There are a variety of cascade enzyme reactions related to H_2O_2 available for the detection of otherwise difficult to detect species, such as creatinine, creatine, etc. Even some NADH related cascade reactions can be further linked with H_2O_2 by NADH oxidase⁴³.
- (4) H_2O_2 consuming enzymes, such as peroxidase, catalase, etc, are usually of high enzyme activity and stability suitable for the enzyme amplification.

In fact, H_2O_2 -related bioassays are of great significance for enzyme substrates, cofactors, enzymes, nucleic acids and cells, as summarized in Table 1.1.

Table 1.1 Application of H₂O₂ assay in biological assays.

	Target	Methods	Note	Ref
Enzyme substrates	Glucose	Chemilum.	+ POx in urinary and blood	34
	L-Lysine	Chemilum.	Lysyl oxidase + peroxidase	35
	Urate (uric acid)	Chemilum.	Uricase + Luminal + Fe ³⁺	36
	Acetylcholine	Fluorescent	Acetylcholinesterase + choline oxidase	37
	Lactate	Fluorescent	Lactate oxidase	38
	Glutamate	Fluorescent	Glutamate oxidase	39
	Sphingomyelin	Fluorescent	Sphingomyelinase + Alk.phosphatase + Cholineoxidase	40
	Sarcosine	Fluorescent	Sarcosine oxidase	41
	Cholesterol	Amperometric		42
Cofactors	NADH(NADPH)	Fluorescent	NADH oxidase	43
Enzymes	Glucose oxidase	Fluorescent	+ POx	34
	Amine oxidase	Fluorescent	Spectrophotometric	44
	Catalase	Fluorescent		45
	Peroxidase	Chemlum.		46
Nucleic acids	Peroxidase	Chemlum.	Peroxidase amplification	47
Cells		Fluorescent		98

1.3. Overview of Methods for Determination of Hydrogen Peroxide

In general, H₂O₂ on its own is thermodynamically reactive, but kinetically relatively poorly reactive (Figure 1.2). It can act both as a mild oxidizing and reducing reagent. Unlike the others of reactive oxygen species, H₂O₂ needs to be activated for the common oxidative reactions in biological systems. Usually only under the activation of transition metals or enzymes containing transition metals, H₂O₂ shows its reactivity. The chemical characteristics of H₂O₂ in this respect consequently made it rather difficult to detect than its brothers of the reactive oxygen species, such as superoxide and hydroxyl radicals.

1.3.1. Analytical Methods Based on Physical Properties

Numerous methods have been developed for H₂O₂ determination. There are a variety of electrochemical, optical, thermal, ultrasonic, chromatographic methods, even mass spectra method⁴⁸, having been reported for H₂O₂ quantitation. Among the electrochemical methods, amperometry is widely used for direct and continuous analysis of H₂O₂ if no other similar electroactive species are present⁴⁹. Furthermore the optical methods by UV detection at 240 nm^{50,51} and mid-IR detection⁵² at 1200 to 1500 cm⁻¹ or 2600 to 3600 cm⁻¹ can also achieve direct and continuous monitoring of H₂O₂, if there are no interferences in the matrix. Since most of H₂O₂ is produced in a biological media, these direct methods based on physical properties of H₂O₂ (as summarized in Table 1.2) are rather restricted by their relatively poor robustness and sensitivities for biomedical applications.

Table 1.2 Analytical methods based on physical properties of H₂O₂

Method	LOD	Dynamic range	pH	Note	Ref.
UV absorbance	~ mM	/	7.0	240 nm, $\epsilon=43.6 \text{ mol}^{-1} \text{ L cm}^{-1}$	50,51
IR spectroscopy	~1%	1-10% (w/w)	/	Peak area or height at 1530-1260 cm ⁻¹ or at 2930-2680 cm ⁻¹	52
Raman scattering	/	/	/	Peak area or height 800-920 cm ⁻¹	53
ESR	/	/	/	/	54
H ₂ O ₂ amperometry	2x10 ⁻⁷ M	2x10 ⁻⁷ -1.1x10 ⁻³	5.5	0.0V vs. SCE	49

1.3.2. Optical Analytical Methods Based on Chemical Reactions of H₂O₂

Alternatively, indirect, usually irreversible reaction-based methods have been exploited for the sensitive determination of H₂O₂. Among them, optical methods, including spectrophotometric, fluorometric, chemiluminescent methods, are mostly used and offer the variety and sensitivity for the biologically originated H₂O₂. These derivation methods can be

categorized into following three approaches: (1) based on simple oxidations; (2) based on enzyme coupling with peroxidases; (3) based on metal H₂O₂ complex.

Table 1.3 Analytical methods based on simple oxidations of H₂O₂

Method	LOD (mol L ⁻¹)	Dynamic range (mol L ⁻¹)	pH	Reaction & Note	Ref
Chemilum.	0.42x10 ⁻⁹	0.42-300x10 ⁻⁹	10.2	Luminol + H ₂ O ₂ + Co ²⁺ , for seawater	64
Chemilum.	25pptv	25pptv-100ppbv	10.8	Luminol + H ₂ O ₂ + Co ²⁺ sensor for gas	55
Chemilum.	1.0x10 ⁻³	3.5-9.0x10 ⁻³	~10	Luminol + H ₂ O ₂ + Fe ³⁺ sensor for immunoassay	56
Chemilum.	/	0.5-100x10 ⁻³	/	Luminol + H ₂ O ₂ + Co foil sensor	57
Chemilum.	1x10 ⁻⁷	/	/	Luminol + H ₂ O ₂ + Co ²⁺ sensor	58
Chemilum.	1x10 ⁻⁷	2.0x10 ⁻⁷ -1x10 ⁻⁴	8-9	Periodate + H ₂ O ₂ + Co ²⁺ sensor for rainwater	59
Fluoresc.	/	0-250 ng/10mL	/	HMPQ + Co	60
Fluoresc.	2.2x10 ⁻⁸	2.3x10 ⁻⁷ -2.3x10 ⁻⁵	/	DTQ	61
Fluoresc.	/	0.1 –10.0x10 ⁻³	/	O ₂ Based sensor	62,63
Spectroph.	/	millimolar	/	Microplates	77

1.3.2.1. Determination based on simple oxidations

The oxidative reaction of H₂O₂ to oxygen (Eq. 1.1) has been applied for the analysis of H₂O₂ to generate detectable products for optical detections (Table 1.3).



As one of the most sensitive optical analytical methods^{64,65}, chemiluminescence assays are based on the luminol-H₂O₂ reaction in basic solution with Co²⁺, Cu²⁺, Fe²⁺ or other metal ion catalysts⁶⁶, with some variations of luminescent substrates, such as periodate⁶⁷, acridinium ester⁶⁸. Subnanomolar H₂O₂⁶⁶ determination has been achieved despite this method is usually restricted by its strongly basic pH.

Alternatively, fluorescent determination has been applied to H_2O_2 based on the oxidation⁶⁹. The generation of oxygen can be measured by the oxygen-sensitive fluorescent probes, such as derivatives of Pd or Pt porphyrins⁷⁰, or directly by oxygen optical sensors⁷¹. Another approach is mainly based on the ROS fluorogenic reactions⁷², especially for fluorescent imaging in biological samples. For example, the general oxidation by H_2O_2 of dichlorofluorescein, dihydrorhodamine and hydroethidine into their oxidized form which are highly fluorescent^{73,74} (Figure 1.5). The most recent advance in this category is the reports based on the fluorescence change of the green fluorescent proteins upon the reaction of H_2O_2 or other ROS⁷⁵. However, these methods usually are not H_2O_2 specific and prone to interferences by other ROS species. In addition, most of the reactions are supposed to happen under peroxidase⁷⁴ available in biological samples.

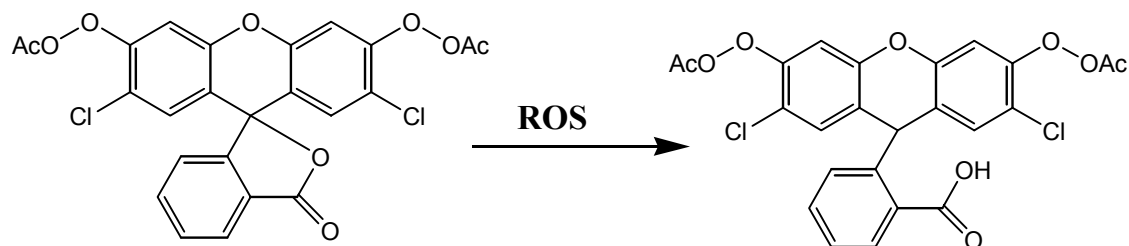


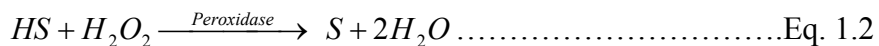
Figure 1.5 ROS based scheme via 2',7'-Dichlorofluorescein.

There are also many reports based on the spectrophotometry and reflectance, such as the decoloration of Prussian blue⁷⁶, or H_2O_2 indicator papers or microplates⁷⁷. Despite their convenience, the sensitivity is not usually good enough for the biologically originated H_2O_2 .

1.3.2.2. Determination based on enzyme coupling with peroxidases

For the relatively poor sensitivity and selectivity of the methods described above, the coupling with POx is introduced for more sensitive and specific H_2O_2 detection. It is based on the specific H_2O_2 reaction with hydrogen donors on the catalysis of POx (Eq. 1.2). The

hydrogen donors (usually phenol derivatives) of POx reaction have been widely explored for the chromogenic⁷⁸, fluorogenic⁷⁹, and chemiluminogenic⁸⁰ purposes.



HS: hydrogen donor, S: oxidized donor

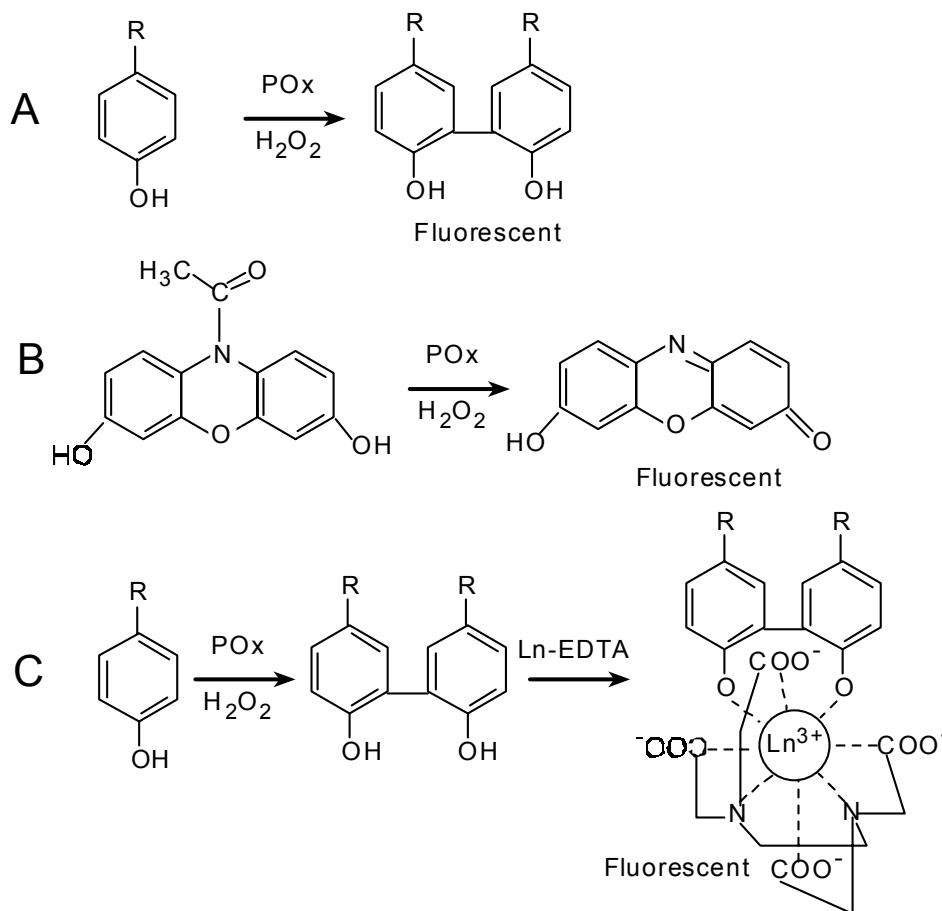


Figure 1.6 Three main variations of the POx –aided detection for H₂O₂.

There are three main variations for POx-aided detection for H₂O₂ as manifested in Figure 1.6. (The products of the POx reaction are usually quantified, either by spectrophotometry, fluorometry, or chemiluminescence, as indicated in Figure 1.6 as fluorescent). One (Figure 1.6 A) is based on the fluorescent or color-changing dimer products of the hydrogen donors reacting with H₂O₂ in the presence of peroxidase, such as

homovanillic acid and derivatives in the earlier reports by Guilbault and co-workers^{81,82}; or Trinder reagent⁸³, such as 2-hydroxy-3,5-dichlorobenzenesulfonate. Another (Figure 1.6 B) is based on the catalytic de-acetylation of the hydrogen donors, such as Amplex Red⁸⁴ and Scopoletin⁸⁵. The last (Figure 1.6 C) is based on recently reported enzyme-amplified lanthanide luminescence (EALL)⁸⁶, through the long-decaying fluorescent lanthanide complexes formed by the dimeric products of the reaction⁸⁷.

Table 1.4 Analytical methods for H₂O₂ based on enzyme coupling with peroxidases

Method	LOD	Dynamic range	Reaction	Ref
Chemilum.	1 nM	5 nM-5mM	Luminol + H ₂ O ₂ + POx sensor	88
Chemilum.	52.2 μM	/	Luminol + H ₂ O ₂ + POx sensor	89
Chemilum.	40 nM	0.1 μM-0.2 mM	Luminol + H ₂ O ₂ + POx sensor	90
Fluoresc.	50 nM	/	POx + Amplex Red, Exc/Em: 530/590 nm	91
Fluoresc.	/	9 nM-1 μM	POx + resorufin, pH 6.4	92
Fluoresc.	2–10 nM	/	POx + Scopoletin Exc/Em: 390/460, pH 8.5-9.5	93
Fluoresc.	2 pmol	0.1-2 nmol	POx + A6550, Exc/Em: 360/460, 590/645, pH7.4	94
Fluoresc.	1.4 nM	0.0-0.2 μM	POx + cyanine	95
Fluoresc.	/	~44 nM-440 nM	POx + Homovanillic acid, Exc/Em: 312/420 nm	96
Spectroph.	4 nM	20-700 nM	DAP, 590 nm absorbance	78
Spectroph.	/	0.1-300 mg/L	4-chloro-1-naphthol	97

Although chemiluminescence or electroluminescence can also be used for determination of H₂O₂ with extreme high sensitivity based on peroxidase reaction (usually performed at pH above 8), and spectrophotometric methods have been developed for the simplicity of the instrumentation⁹⁷, fluorometry is mainly used for biological samples. It is due to its similar sensitivity, reproducibility and optimal neutral pH, in measurements with certain phenols. The characteristics of POx-based optical assays for H₂O₂ are summarized in Table 1.4. The recent development is for the wider application for *in vitro* and *in vivo* detections⁹⁸ and using of POx

mimetics, such as Mn porphyrin, hemoglobin, hemin, Fe calixerene, etc⁹⁹, to overcome the relative instability of the POx protein.

1.3.2.3. Determination based on metal H₂O₂ complexes

From the early development of analysis of transition metals, ternary complexes of transition metal ions (mainly vanadium and titanium) with H₂O₂ have long been recognized for their potential application in the H₂O₂ analysis. The intramolecular energy transfer from the ligands to central metal ions is considered as a smallest metal-antenna system of energy transfer. Although the exact mechanism for the detection is not really clarified from the possible two mechanisms (free-radical mechanism or peroxide complex mechanism¹⁰⁰), there have been several reports of H₂O₂ assays based on this kind of ternary complexes as summarized in Table 1.5.

Table 1.5 Analytical methods based on metal H₂O₂ complexes

Method	LOD	Dynamic range	Reaction	Ref.
Fluoresc.	0.05 μM	0.2-50 μM	Vanadium (V ⁴⁺ or V ⁵⁺) +PTQA+H ₂ O ₂ , 340/490nm, in H ₂ SO ₄	101
Spectroph.	/	10-150 ppm	Vanadium (V ⁴⁺ or V ⁵⁺) 450 nm in 0.6-6 N H ₂ SO ₄	102
Spectroph.	1 μM	4 -60 μM	titanium(IV) peroxo complex 410 nm	103
Spectroph.	0.25 μM	/	Ti (IV)+H ₂ O ₂ + PAR	104,105,106
Spectroph.	/	/	Decoloration of Ti(IV)- complex at 610 nm	107
Fluoresc.	1.8 μM	2-400 μM	Europium-tetracycline complex	108

The earlier studies are mainly photometric methods based on the formation or decoloration of the colored vanadyl complex or the titanium(IV) peroxo complex with H₂O₂. The further development is the introduction of second ligands, such as PAR, to increase the spectrophotometric sensitivity or the search for fluorescent ligands. However, the available

metal-H₂O₂-ligand complex systems are usually in strong acidic range (e.g. 0.15 M H₂SO₄). While the complexes formed usually are at high acidity, the ternary complexes of metal ion, organic ligand, and H₂O₂ can shift the optimal pH to weak acidic pH, such as 5-6.

Only recently, it has been reported by our group of a new europium-tetracycline-H₂O₂ system in the neutral range (optimal pH 6.9)¹⁰⁸. This system has also introduced the characteristic lanthanide fluorescence, such as long Stokes' shift, long lifetime (tens of μ s range), which offers great potential for hydrogen peroxide based enzymatic assays for enzymes, enzyme substrates or enzyme inhibitors, especially in combination with the time-resolved fluorometry and imaging.

1.4. Time-resolved Fluorescence Assays and Imaging

Compared with other optical techniques, fluorometry for enzymatic assays has one advantage, if not more, of multiple parameters available for the measurement. There are mainly two different approaches for fluorometry, based on either spectral or temporal features of the fluorescence emissions¹⁰⁹. Steady-state fluorescence techniques were developed first on the basis of differences of their spectra: peak positions, intensity, excitation, anisotropy, etc. This approach is still widely used in biomedical analysis. But this approach has the following disadvantages: (1) Excitation at UV and visual region of most fluorescent probes results in background fluorescence, despite novel development in near infrared fluorescent probes. (2) The fluctuation of the light source has significant effect on the final intensity readouts. (3) the amount of fluorophores and therefore photobleaching affect the determination. (4) The overlapping of the broad emission spectra of most fluorophores can cause interferences, and restrict their applications in multiplexed assays and imaging.

A different approach is the investigation of the temporal properties of the fluorophores¹¹⁰. The time-resolved gated fluorescence assay¹¹¹ was the first applied as a time delay approach for their simplicity. Gated fluorometry is a method for measurement of fluorescence intensity as a function of analyte concentration. The measurement is proceeded only after the background fluorescence (lifetime < 20 ns) has ceased, while the fluorescence decay of the probe (lifetime > 1 μ s) is still going on. It has the specific feature of enabling the suppression of potentially interfering background fluorescence. However, it still depends on the amount of fluorophores presented, photobleaching and the fluctuation of the light source.

In contrast to gated fluorometry, the lifetime fluorometry¹¹², either phase-domain or time-domain, is a method for measurement of fluorescence lifetime as a function of analyte concentration. The fluorescence lifetime is pre-determined by the nature of the fluorescent probe and only sensitive to the micro-environment around the fluorophores. Therefore, the measurements are usually independent of (1) interfering fluorescence from the background; (2) The fluctuation of the light source; (3) amount of fluorophores and photobleaching. So lifetime detection has been becoming a superb techniques for enzymatic analysis.

Nowadays, the widely used adage that 'seeing is believing' is as true today as it has ever been, with the development of different imaging technologies, such as fluorescence imaging¹¹³, magnetic resonance imaging¹¹⁴, or ultrasonic imaging¹¹⁵. Optical imaging methods have not only attracted attention in life sciences, but also become more and more important for practical processes in bioanalysis and clinical diagnostics¹¹⁶. The combination of fluorescence analysis with imaging represents a useful tool in such diverse applications as mapping of biological samples, or monitoring biological reactions and interactions, especially those in high-throughput screening modes. The fluorescence imaging is certainly preferred

whenever the localization of any fluorophore is required. The two dimensional measurement provide more information than the point spectroscopy. It offers the ability to visualize the distribution of the fluorophores and the newly developed array technologies¹¹⁷ also requires the 2D imaging to offer multi-substrate and multi-enzyme detection¹¹⁸. Same as the point fluorescent detection, the fluorescence imaging is now also achievable by either spectral or temporal approach. Different schemes of fluorescence imaging, such as conventional fluorescent intensity imaging, gated imaging and fluorescence lifetime imaging have offered plenty of possibilities for the bioanalysis, which is the main target of the present research.

1.5. Aim of the Research

The goal of this thesis is, on the basis of a new europium fluorescent probe for hydrogen peroxide, to develop quantitative assays for enzymes and enzyme substrates, in a time-resolved microplate format and imaging format.

Firstly for the probe study, the complete characterization of the fluorescent probe EuTc and EuTc-HP will be done. The structure of EuTc-HP is also of high interest for the discovery of new lanthanide probes.

The second is assay development. Assays for oxidases and their substrates and H₂O₂ consuming enzymes (such as catalase), are intended for the steady-state intensity-based, time-resolved gated and lifetime-based fluorescent detection.

Thirdly, imaging formats have been developed for the two dimensional measurement of the assays.

The last is the further applications of the fluorescent probes, such as for ELISA, for the sensor and microplate-based array construction.

1.6. Reference

1. Georgiou, G; Masip, L. *Science* (2003), 300(5619), 592-594.
2. <http://www.h2o2.com/>
3. Vione, D; Maurino, V; Minero, C; Pelizzetti, E. *Annali di Chimica* (2003), 93(4), 477-488.
4. Grigoropoulou, G.; Clark, J. H.; Elings, J. A. *Green Chemistry* (2003), 5(1), 1-7.
5. Lane, B. S.; Burgess, K. *Chemical Reviews* (2003), 103(7), 2457-2473.
6. Touyz, R. M. *Expert Review of Cardiovascular Therapy* (2003), 1(1), 91-106.
7. Blokhina, O; Virolainen, E; Fagerstedt, K. V. *Annals of Botany* (2003), 91, 179-194.
8. Reth, M. *Nature Immunology* (2002), 3(12), 1129-1134.
9. Wood, Z. A.; Poole, L. B.; Karplus, P. A. *Science* (2003), 300(5619), 650-653.
10. Rhee, Sue Goo; Lee, Seung-Rock; Yang, Kap-Seok; Kwon, Jaeyul; Kang, Sang Won. In: *Signal Transduction by Reactive Oxygen and Nitrogen Species: Pathways and Chemical Principles* (2003), 167-179.
11. Neill, S; Desikan, R; Hancock, J. *Current Opinion in Plant Biology* (2002), 5(5), 388-395.
12. Fandrey, J. *Lung Biology in Health and Disease* (2003), 175(Oxygen Sensing), 67-82.
13. Dunford, H. B. *Coordination Chemistry Reviews* (2002), 233-234 311-318.
14. Pierre, J. L.; Fontecave, M.; Crichton, R. R. *BioMetals* (2002), 15(4), 341-346.
15. Kawanishi, S; Hiraku, Y; Murata, M; Oikawa, S. *Free Radical Biology & Medicine* (2002), 32(9), 822-832.
16. Liang, Fong-Qi; Godley, B. F. *Experimental Eye Research* (2003), 76(4), 397-403.
17. Nathan, Carl F. *Phagocytosis--Past Future* (1982), 391-417.
18. Passonneau, J. V.; Lowry, O. H. *Enzymatic Analysis: A Practical Guide*. (1993) Humana, Totowa, N. J. USA.
19. Yolken, R. H. *Annals of the New York Academy of Sciences* (1984), 428, 223-9.
20. Moss, D. W. *Methods of Enzymic Analysis, Vol. 3: Enzymes 1: Oxidoreductases, Transferases*. (1983) Verlag Chemie, Weinheim, Germany.
21. Urbanke, C. Ed: Bergmeyer, H. U. *Methods Enzym. Anal.* (3rd Ed.) (1983), 1 326-40. Verlag Chem., Weinheim, Germany.
22. Pollack J D. *Methods in Molecular Biology* (1998), 104 79-93.
23. Marko-Varga, G; Dominguez, E. *Trends in Analytical Chemistry* (1991), 10(9), 290-7.
24. Batchelor, R. H.; Zhou, Mingjie. *Analytical Biochemistry* (2002), 305(1), 118-119.
25. Maeda, H; Matsu-Ura, S; Senba, T; Yamasaki, S; Takai, H; Yamauchi, Y; Ohmori, H. *Chemical & Pharmaceutical Bulletin* (2000), 48(7), 897-902.
26. Zarrine-Afsar, A; Krylov, S. N. *Analytical Chemistry* (2003), 75(15), 3720-3724.

27. Saeki Y; Nozaki M; Matsumoto K. *Journal of Biochemistry* (1985), 98(6), 1433-40.
28. Koller, E. *American Biotechnology Laboratory* (1994), 12(12), 14-15.
29. Gao, Wenzhong; Xing, Bengang; Tsien, Roger Y.; Rao, Jianghong. *Journal of the American Chemical Society* (2003), 125(37), 11146-11147.
30. Wang, Q; Scheigetz, J; Gilbert, M; Snider, J; Ramachandran, C. *Biochimica et Biophysica Acta* (1999), 1431(1), 14-23.
31. Noble, J E.; Ganju, P; Cass, A. E. G. *Analytical Chemistry* (2003), 75(9), 2042-2047.
32. Vazquez, M. J; Rodriguez, B; Zapatero, C; Tew, D. G. *Analytical Biochemistry* (2003), 320(2), 292-298.
33. Cattaneo, M. V.; Luong, J. H. T. *Proceedings of SPIE-The International Society for Optical Engineering* (1993), 1886, 186-92.
34. Preuschoff, F.; Spohn, U.; Janasek, D.; Weber, E. *Biosens. & Bioelectron.* (1994), 9(8), 543-9.
35. Oshima, N; Matsuyuki, A; Fuje, S. *Jpn. Kokai Tokkyo Koho* (1988), 5 pp. JP 63291600
36. MacDonald R C. *Journal of Neuroscience Methods* (1989 Jul), 29(1), 73-6.
37. Blankenstein, G; Spohn, U; Preuschoff, F; Thoemmes, J; Kula, M. *Biotechnology and Applied Biochemistry* (1994), 20 291-307.
38. McElroy, K. E.; Bouchard, P. J.; Harpel, M. R.; Horiuchi, K. Y.; Rogers, K. C.; Murphy, D. J.; Chung, T. D. Y.; Copeland, R. A. *Analytical Biochemistry* (2000), 284(2), 382-387.
39. He, X; Chen, F; McGovern, M. M.; Schuchman, E. H. *Anal. Biochem.* (2002), 306(1), 115-123.
40. Wagner, M; Jorns, M. S. *Biochemistry* (2000), 39(30), 8825-8829.
41. Carpenter, A; Purdy, W. C. *Analytical Letters* (1990), 23(3), 425-35.
42. Batchelor, R H.; Zhou, Mingjie. *Analytical Biochemistry* (2002), 305(1), 118-119.
43. Nag, S.; Saha, K.; Choudhuri, M. A. *Plant Science* (2000), 157(2), 157-163.
44. Wu, Meng; Lin, Zhihong; Wolfbeis, Otto S. *Analytical Biochemistry* (2003), 320(1), 129-135.
45. Kamidate, T; Ishida, Y; Tani, H; Ishida, A. *Chemistry Letters* (2003), 32(4), 402-403.
46. Spencer, J. P. E.; Jenner, A; Chimel, K; Aruoma, O. I.; Cross, C. E.; Wu, R; Halliwell, B. *FEBS Letters* (1995), 374(2), 233-6.
47. Cranley, P. E.; Allen, J. R.; Danowski, K. L.; McIntyre, J. A.; Miller, T. E., Jr.; Rosner, B. M.; Strickland, A. D.; Subramanian, V.; Sun, L. *PCT Int. Appl.* (2003), 163 pp. WO 2003039483
48. Harms, D; Luftmann, H; Mueller, F. K.; Krebs, B; Karst, Uwe. *Analyst* (2002), 127(11), 1410-1412.
49. Eftekhari A., *Microchim. Acta* (2003)141, 15–21.
50. Aebi H., (1974) in: Bergmeyer H.U. (Ed.), *Methods of Enzymatic Analysis*, Verlag Chemie (Weinheim) and Academic Press Inc. (New York), pp. 680 – 684.
51. Prieve, John F. *Eur. Pat. Appl.* (1999), 29 pp.

52. Voraberger, H.; Ribitsch, V.; Janotta, M.; Mizaikoff, B. *Applied Spectroscopy* (2003), 57(5), 574-579.
53. Yamaguchi, Y; Uenoyama, H; Yagi, M; Xiaoming, Dou. *Eur. Pat. Appl.* (1996), 16 pp.
54. Matoba, T.; Shimokawa, H.; Morikawa, K.; Kubota, H.; Kunihiro, I.; Urakami-Harasawa, L.; Mukai, Y.; Hirakawa, Y.; Akaike, T.; Takeshita, A. *Arteriosclerosis, Thrombosis, and Vascular Biology* (2003), 23(7), 1224-1230.
55. Li, J.; Dasgupta, P. K. *Analytica Chimica Acta* (2001), 442(1), 63-70.
56. Ahmad, M; Murishita, F; Okazaki, S. *Science International* (1998), 10(3), 213-216.
57. Janasek, D; Spohn, U; Beckmann, D. *Sensors and Actuators, B: Chemical*(1998), B51,107-113.
58. Hanaoka, S; Lin, Jin-Ming; Yamada, M. *Analytical Sciences* (2001), 17, a219-a221.
59. Lin, Jin-Ming; Sato, K; Yamada, M. *Microchemical Journal* (2001), 69(1), 73-80.
60. Mori, I; Fujita, Y; Toyoda, M; Kato, K; Yoshida, N; Akagi, M. *Talanta* (1991), 38(6), 683-6.
61. Dong, Su-Ying; Su, Mei-Hong; Nie, Li-Hua; Ma, Hui-Min. *Chinese Journal of Chemistry* (2003), 21(2), 189-191.
62. Posch, H. E.; Wolfbeis, Otto S. *Mikrochimica Acta* (1989), 1(1-2), 41-50.
63. Hynes, J.; Floyd, S.; Soini, A. E.; O'Connor, R.; Papkovsky, D. B. *Journal of Biomolecular Screening* (2003), 8(3), 264-272.
64. Fahrnich, K. A.; Pravda, M.; Guilbault, G. G. *Talanta* (2001), 54(4), 531-559.
65. McCapra, F. *Methods in Enzymology* (2000), 305(Biolumin. and Chemilum., Pt. C), 3-47.
66. Yuan, Jinchun; Shiller, A. M. *Analytical Chemistry* (1999), 71(10), 1975-1980.
67. Lin, Jin-Ming; Sato, K; Yamada, M. *Microchemical Journal* (2001), 69(1), 73-80.
68. Hosaka, S; Uchida, T. *Luminescence Biotechnology* (2002), 305-320.
69. Mori, I; Fujita, Y; Toyoda, M; Kato, K; Yoshida, N; Akagi, M. *Talanta* (1991), 38(6), 683-6.
70. Papkovsky, D. B; O'Riordan, T; Soini, A. *Biochemical Society Transactions*(2000),28(2),74-77.
71. Wolfbeis, O. S.; Oehme, I; Papkovskaya, N; Klimant, I. *Biosensors & Bioelectronics* (2000), 15(1-2), 69-76.
72. Elsner, J; Kapp, A. *Methods in Molecular Biology* (2000), 138, 153-156.
73. Imrich, A; Ning, Yao Yu; Kobzik, L. *Journal of Leukocyte Biology*(1999), 65(4), 499-507.
74. Wang, H.; Joseph, J. A.. *Free Radical Biology & Medicine* (1999), 27(5/6), 612-616.
75. Lu, Canghai; Albano, C. R.; Bentley, W. E.; Rao, G. *Book of Abstracts, 219th ACS National Meeting, San Francisco, CA, March 26-30, 2000* (2000), BIOT-298.
76. Lenarczuk, T.; Glab, S.; Koncki, R. *Journal of Pharmaceutical and Biomedical Analysis* (2001), 26(1), 163-169.
77. Piletsky, S. A.; Panasyuk, T. L.; Piletskaya, E. V.; Sergeeva, T. A.; El'skaya, A. V.; Pringsheim, E.; Wolfbeis, O. S. *Fresenius' Journal of Analytical Chemistry* (2000), 366(8), 807-810.

78. Pappas, A. Ch.; Stalikas, C. D.; Fiamegos, Y. Ch.; Karayannis, M. I. *Analytica Chimica Acta* (2002), 455(2), 305-313.
79. Zhou, Mingjie; Diwu, Zhenjun; Panchuk-Voloshina, N.; Haugland, R. P. *Analytical Biochemistry* (1997), 253(2), 162-168.
80. Hines, K. K.; Feather-Henigan, K; Li, Li; Horneij, I; Clothier, C; Milosevich, G; Lipton, B; Brotcke, T. *Luminescence Biotechnology* (2002), 161-177.
81. Guilbault G G; Brignac P Jr; Zimmer M. *Analytical Chemistry* (1968), 40(1), 190-6.
82. Guilbault G G; Kuan S S; Brignac P J Jr. *Analytical Chemistry* (1969), 47(3), 503-9.
83. Slaughter M. R, O'Brien P. *J. Clin. Biochem.* (2000)33, 525 – 534.
84. <http://www.probes.com/handbook/sections/1005.html>
85. Corbett, J. T. *Journal of Biochemical and Biophysical Methods* (1989), 18(4), 297-307.
86. Evangelista, R. A.; Pollak, A.; Templeton, E. F. *Anal. Biochem.* (1991), 197(1), 213-24.
87. Meyer, J; Karst, U. *Analyst* (2001), 126(2), 175-178.
88. Kiba, N; Tokizawa, T; Kato, S; Tachibana, M; Tani, K; Koizumi, H; Edo, M; Yonezawa, E. *Analytical Sciences* (2003), 19(6), 823-827.
89. Ramos, M. C.; Torijas, M. C.; Diaz, A. N. *Sensors and Actuators, B* (2001), B73(1), 71-75.
90. Zhou, Guo-Jun; Wang, Gang; Xu, Jing-Juan; Chen, Hong-Yuan. *Sensors and Actuators, B: Chemical* (2002), B81(2-3), 334-339.
91. <http://www.probes.com/media/pis/mp22188.pdf>
92. Brotea, G. P.; Thibert, R. *J. Microchemical Journal* (1988), 37(3), 368-76.
93. Zhang, Ling-Su; Wong, George T. F. *Talanta* (1999), 48(5), 1031-1038.
94. Mohanty, J. G.; Jaffe, J. S.; Schulman, Edward S.; Raible, Donald G. *Journal of Immunological Methods* (1997), 202(2), 133-141.
95. Chen, X.-L.; Li, D.-H.; Yang, H.-H.; Zhu, Q.-Z.; Zheng, H.; Xu, J.-G. *Analytica Chimica Acta* (2001), 434(1), 51-58.
96. Ruch, W.; Cooper, P. H.; Baggiolini, M. *J. Immunological Methods* (1983), 63(3), 347-57.
97. Amelin, V.;Kolodkin, I.; Irinina, Yu. A. *Journal of Analytical Chemistry* (2000),55(4), 374-377
98. Barja, G. *Journal of Bioenergetics and Biomembranes* (2002), 34(3), 227-233.
99. Yuan, Hong; Cai, Ruxiu; Pan, Zuting. *Analytical Letters* (2003), 36(2), 277-286.
100. Salem, I. A.; El-Maazawi, M.; Zaki, A. B. *International Journal of Chemical Kinetics* (2000), 32(11), 643-666.
101. Paleologos, E. K.; Giokas, D. L.; Tzouwara-Karayanni, S. M.; Karayannis, M. I. *Analytical Chemistry* (2002), 74(1), 100-106.
102. Kakabadse, G.; Wilson, H. J. *Nature* (1957), 180 861.
103. Almuaibed, A. M.; Townshend, A. *Analytica Chimica Acta* (1994), 295(1-2), 159-63.

104. Liu, J; Lu, B; Xu, L. *Shengwu Huaxue Yu Shengwu Wuli Jinzhan* (2000), 27(5), 548-551.
105. Matsubara, C; Iwamoto, T; Nishikawa, Y; Takamura, K; Yano, S; Yoshikawa, S. *J. of the Chem. Soc., Dalton Transactions: Inorg. Chem.* (1985), (1), 81-4.
106. Li, Jianzhong; Dasgupta, P. K. *Analytical Sciences* (2003), 19(4), 517-523.
107. Fujita, Y; Mori, I; Toyoda, M. *Analytical Sciences* (1991), 7(2), 327-8.
108. Wolfbeis, Otto S.; Duerkop, Axel; Wu, Meng; Lin, Zhihong. *Angewandte Chemie, International Edition* (2002), 41(23), 4495-4498.
109. Valeur, B.; Editor. *Molecular Fluorescence - An Introduction: Principles and Applications*, 1st Ed. (2000), Publisher: Wiley-VCH, Weinheim, Germany
110. Gryczynski, Z; Gryczynski, I; Lakowicz, J R. *Methods in Enzymology* (2003), 360 (Biophotonics, Part A), 44-75.
111. Dahan, M.; Laurence, T.; Pinaud, F.; Chemla, D. S.; Alivisatos, A. P.; Sauer, M.; Weiss, S. *Optics Letters* (2001), 26(11), 825-827.
112. Lin, Hai-Jui; Szmazinski, H.; Lakowicz, J. R. *Analytical Biochemistry* (1999), 269(1), 162-167.
113. Emptage, N. J. *Current Opinion in Pharmacology* (2001), 1(5), 521-525.
114. Juul, A.; Gyllenborg, J.; Scheike, T.; Davidsen, M.; Jorgensen, T. *Circulation* (2003), 107(20), e191-e192.
115. Schutt, E. G.; Klein, D. H.; Mattrey, R. M.; Riess, J. G. *Angewandte Chemie, International Edition* (2003), 42(28), 3218-3235.
116. Cubeddu, R.; Comelli, D.; D'Andrea, C.; Taroni, P.; Valentini, G. *Journal of Physics D: Applied Physics* (2002), 35(9), R61-R76.
117. Lopez, M. F.; Mikulskis, A.; Golenko, E.; Herick, K.; Spibey, C. A.; Taylor, I.; Bobrow, M.; Jackson, P. *Proteomics* (2003), 3(7), 1109-1116.
118. Kasai, S; Hirano, Y; Motochi, N; Shiku, H; Nishizawa, M; Matsue, T. *Analytica Chimica Acta* (2002), 458(2), 263-270.

Chapter 2. Characterization of the Fluorescent Europium Probe and Time-resolved Fluorescent Assay of Hydrogen Peroxide

2.1. Introduction

As described in Chapter 1, the importance of biologically originated H₂O₂ detections has been generally recognized for their applications in developments of biological assays for enzyme substrates, for enzyme inhibitors, for enzymes, and also for enzymatic amplification immunoassays^{1,2}. Among the numerous methods, fluorescence based assays³ have been mainly used in biological applications for their good sensitivity and selectivity. Furthermore, besides the conventional steady-state intensity-based assays, fluorescence determination can also be achieved through other schemes, such as anisotropy polarization, time-resolved and recently time-resolved anisotropy assays. These techniques provide more approaches for improvement of the sensitivity and the selectivity in complicated biological backgrounds over other optical methods. Since H₂O₂ is a small and simple molecule, its anisotropy determination seems to be very difficult. However, the time-resolved assay for H₂O₂ is still possible due to recent developments in lanthanide fluorescence.

There are a lot of time-resolved assays^{4,5} for enzymatical analysis, such as DELFIA⁶, EALL^{7,8}, etc. However, only few research on the direct time-resolved determination of H₂O₂ are reported. Karst⁹ has reported a scheme for H₂O₂ determination based on the EALL method. The approach utilizes the products of POx-catalyzed H₂O₂ reaction to form a terbium complex which has the characteristics of lanthanide fluorescence and consequently can be applied for the time-resolved assay of H₂O₂. The significance of time-resolved fluorometry of H₂O₂ is that it can usually greatly suppress the background fluorescence from biological

samples and increase sensitivity, in addition to the selectivity improvement over the lifetime characteristics. Despite the unbeatable high sensitivity, this method needs further steps for fluorescence development by enhancing solution and usually in extreme basic (i.e. pH ~13) conditions for the formation of the lanthanide complexes, especially those related to H₂O₂.

In this thesis, a fluorescent probe based on europium tetracycline complex has been further characterized and applied for a time-resolved fluorescent determination of H₂O₂. The probe has shown not only merits that have made the lanthanide labeling so versatile in bioanalysis^{10,11}, such as large Stokes shift, line-like emission, μ s lifetime range, but also compatibility with the 405 nm blue laser diodes, and sensitive to H₂O₂ as a fluorescent probe with a optimal pH of 6.9. The time-resolved “gated”, and lifetime-based time-correlated single photon counting detection (TCSPC)¹² have been exploited. Furthermore, a lifetime-based rapid lifetime determination method^{13,14,15} has been borrowed from the fluorescence lifetime imaging microscopy (FLIM)¹⁶ for the on-the-fly measurements of lifetimes on the microplate for H₂O₂ determination.

2.2. Results and Discussion

2.2.1. Characterization of the Fluorescent Europium Probe

2.2.1.1. Absorbance, circular dichroism and fluorescence spectra

The absorbances of EuTc and EuTc-HP are quite similar as indicated in Figure 2.1 (A) and Table 2.1. The absorption band (with peaks at 392 and 401 nm) is caused by the presence of the tetracycline ligand which, in its uncomplexed form, has a slightly blue shift absorption spectrum. The circular dichroism spectra of EuTc and EuTc-HP are offered in Figure 2.1 (B). There are a positive cotton effect at 400 nm and a negative cotton effect at 320

nm different from the circular dichroism spectra of Tc alone, with some other four positive cotton effects from 200 – 300 nm. Few difference is observed in the circular dichroism of EuTc and EuTc-HP.

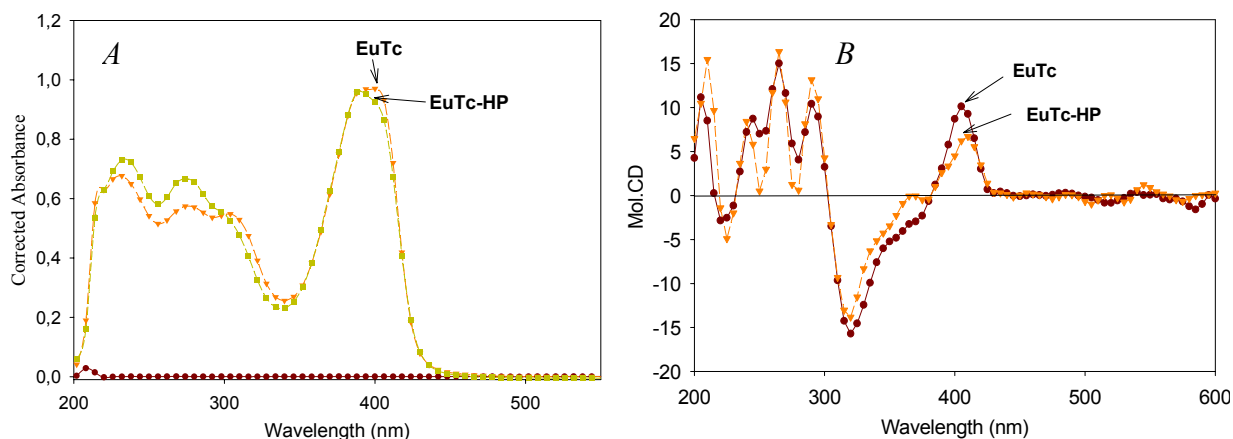


Figure 2.1. Spectra of EuTc and EuTc-HP.

(A) Absorbance spectra of EuTc and EuTc-HP; (B) Circular dichroism spectra of EuTc and EuTc-HP.

Table 2.1 Spectral characterization of EuTc and EuTc-HP

	EuTc		EuTcHP	
Peaks (nm)	392	401	391	401
Molar absorbance ϵ (cm ⁻¹ M ⁻¹)	1.88x10 ⁴	1.88x10 ⁴	1.78x10 ⁴	1.73x10 ⁴
Max. Emission (nm)	617		613 and 619	
Quantum Yield (%)	0.3		4.0	

The fluorescence spectra and absorbance spectra of EuTc and EuTc-HP are shown in Figure 2.2. As in other complexes of this type, the photonic energy absorbed by the ligand is transferred from the triplet state of the ligand to the central Eu³⁺ ion with its typical emission spectra¹⁷ of a main band which peaks at 617 nm (⁵D₀→⁷F₂) and several side bands centered at 579, 597, 654, and 688 nm, respectively. Quantum yield of EuTc-HP is 4.0%, while that of EuTc is 0.3%, with tris(2,2'-bipyridyl)dichlororuthenium(II) hexahydrate (TBDRH) as reference¹⁸. The fluorescence intensity of EuTc-HP is up to 15 times that of EuTc.

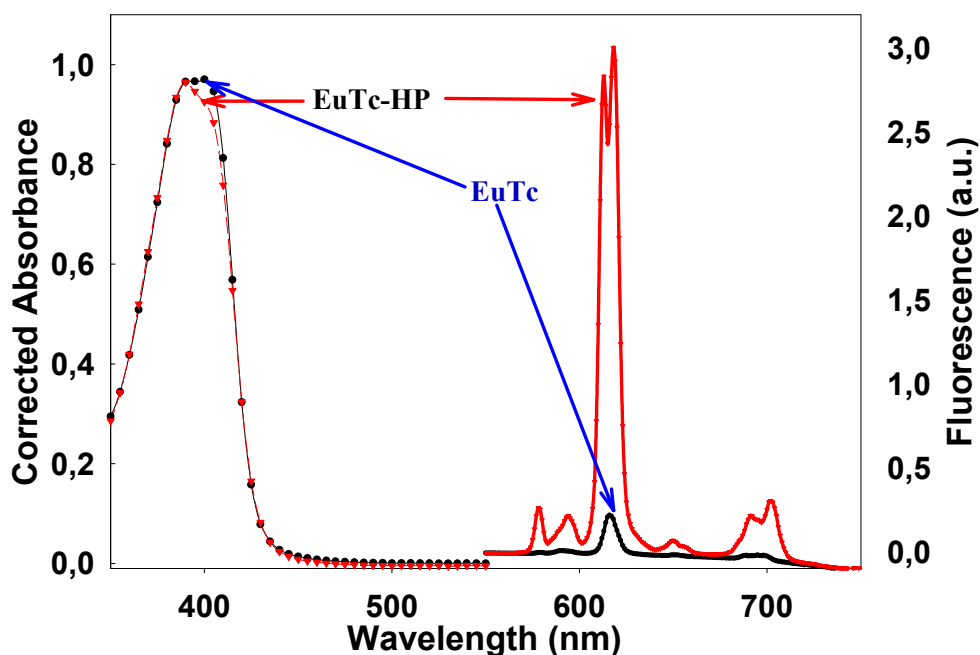


Figure 2.2. Absorption spectra (left) and emission spectra of EuTc and EuTc-HP. Fluorescence spectra were acquired with the AB2 spectrofluorometer and show two peaks. To 2 mL of a solution containing Eu³⁺ (102 $\mu\text{mol L}^{-1}$) and Tc (34 $\mu\text{mol L}^{-1}$) were added 200 μL of a 5 $\mu\text{mol L}^{-1}$ solution of H₂O₂ and 300 μL of MOPS buffer. Fluorescence was recorded after 10 min.

2.2.1.2. Lifetime characterization of EuTc-HP

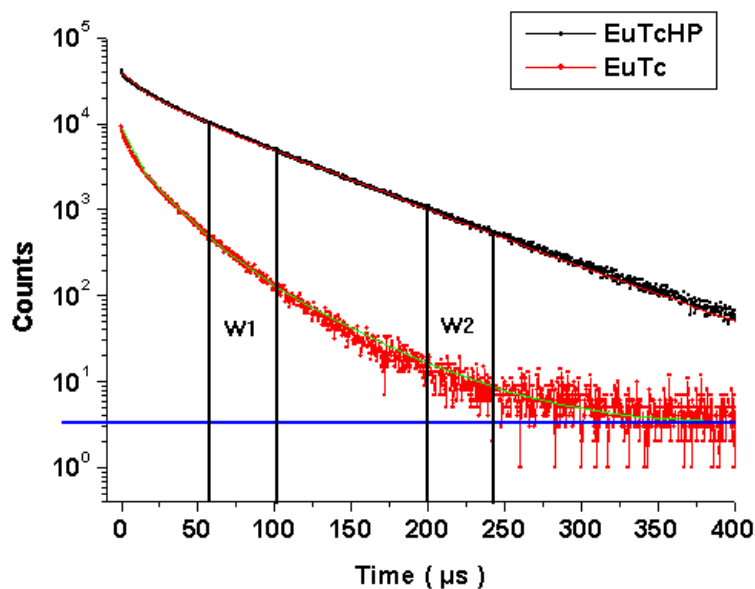


Figure 2.3. Decay profile of the EuTc probe and its complex with H₂O₂ (EuTc-HP). The samples were prepared by addition of different concentrations (0 for EuTc or 1 mmol L⁻¹ for EuTc-HP) of H₂O₂ to a final concentration of EuTc of 53.3 $\mu\text{mol L}^{-1}$ and waiting for 10 min before measurement. W1: window 1, W2: window 2, as applied for Rapid Lifetime Determination (RLD).

The decay profiles of the EuTc and EuTc-HP are shown in Figure 2.3. The decay can be fitted into a three-component exponential decay model according to Eq. 2.1, with all $1 < \chi^2 < 1.1$ and relative residue of the fitting being symmetric and less than 5%.

$$I(t) = \sum_{i=1}^n A_i e^{-t/\tau_i} + B_1 \dots\dots\dots \text{Eq. 2.1}$$

Table 2.2 Lifetime composition of EuTc and EuTc-HP

	EuTc		EuTcHP	
	Decay time (μs)	Rel. Amplitude (%)	Decay time (μs)	Rel. Amplitude (%)
τ ₁	6.8	39.5	10	17.3
τ ₂	24	54.7	34	18.2
τ ₃	53	5.9	61	64.5
Av.	30 μs		60 μs	

The lifetime composition of EuTc and EuTc-HP is summarized in Table 2.2. EuTc has an average lifetime of 30 μs, while EuTc-HP an average lifetime of 60 μs.

The average lifetime for multi-component decays can be described in two ways¹⁹, as in Eq. 2.2 and Eq. 2.3:

$$\tau_1 = \frac{\sum_i A_i * \tau_i^2}{\sum_i A_i * \tau_i} \dots\dots\dots \text{Eq. 2.2}$$

τ₁ : average time the fluorophores remain in their excited state after excitation

$$\tau_2 = \frac{\sum_i A_i * \tau_i}{\sum_i A_i} \dots\dots\dots \text{Eq. 2.3}$$

τ₂ : is proportional to the area under the decay curve

For the case of a single component decay, τ₁ = τ₂. For multi-component decays like EuTc and EuTc-HP, they are different and τ₁ is used throughout, unless otherwise specified,

since the average amount of time the fluorophores remain in their excited state after excitation is more adequate than just the integration of the area under the decay curves.

Because of the complexity of the multi-component decays of EuTc and EuTc-HP, the decay profiles were further studied for the rate constant (k) distributions of Gaussian ln (k) model according to Eq. 2.4. The result is provided in Figure 2.4. The increasing concentration of H₂O₂ resulted in the shift of the distribution from the faster decay to a slower decay.

$$I(t) = \int_k \rho(k)e^{-tk} dk + B_1 \dots\dots\dots\text{Eq. 2.4}$$

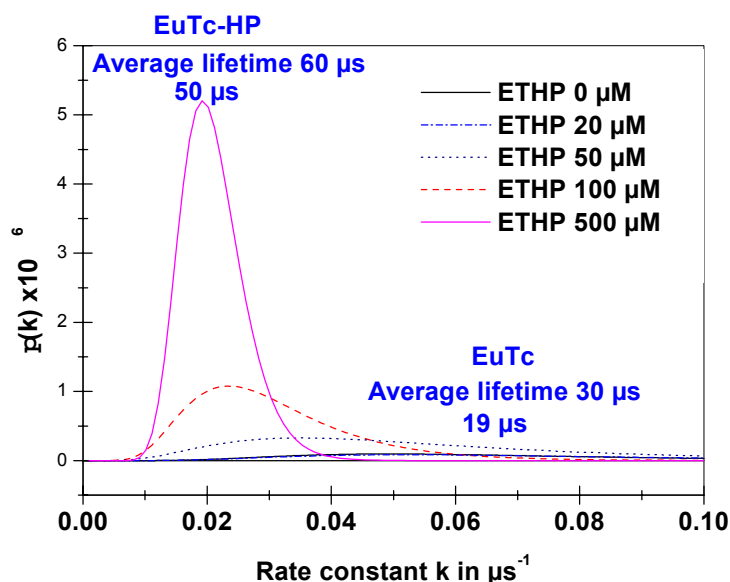


Figure 2.4. Rate constant (k) distributions of Gaussian ln (k) model.

In the same experimental condition as in Figure 2.2. 50 μs as the most frequent lifetime for EuTc-HP, 19 μs as the most frequent lifetime for EuTc.

2.2.1.3. pH, buffer, temperature and stability

The effect of pH on the fluorescence intensity of EuTc-HP was also studied (Figure 2.5). The emission intensity of EuTc-HP is strongest at pH 6.6 – 7.2, and rapidly drops outside this range. In fact, it is only 15% of the maximal intensity at pH 8.0, and 8% at pH 6.0, with the optimum pH at 6.9.

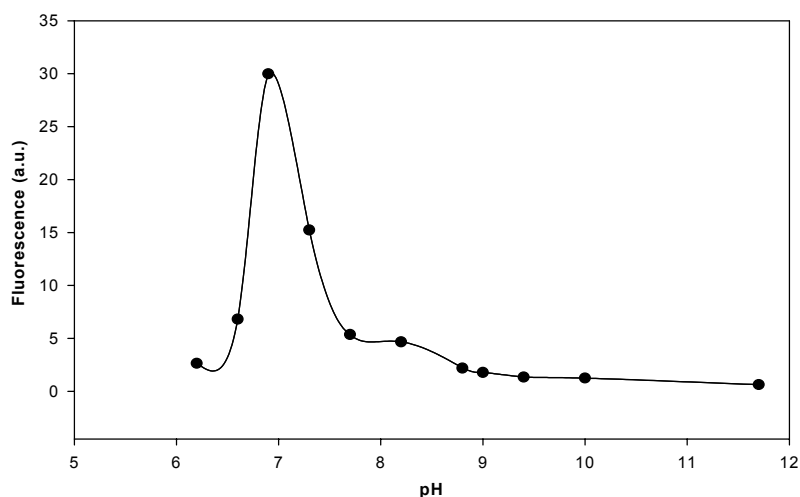


Figure 2.5. The pH optimization for EuTc-HP complex system. 90 μl of 0.2 mmol L^{-1} EuTc, H₂O₂: 240 $\mu\text{mol L}^{-1}$ and 12 mmol L^{-1} MOPS buffer solution (pH 6.9) in 2000 μl cuvette.

The effect of MOPS, Tris, HEPES and phosphate buffers can be seen in Figure 2.6. Phosphate interferes most strongly, while HEPES has a slight quenching effect. Tris buffer does not significantly affect fluorescence, however its best buffer capacity is between pH 7.5 and 9.0 and thus outside the preferred pH range. MOPS buffer is the optimal. Therefore, a 10 mmol L^{-1} MOPS buffer of pH 6.9 was used throughout the experiments.

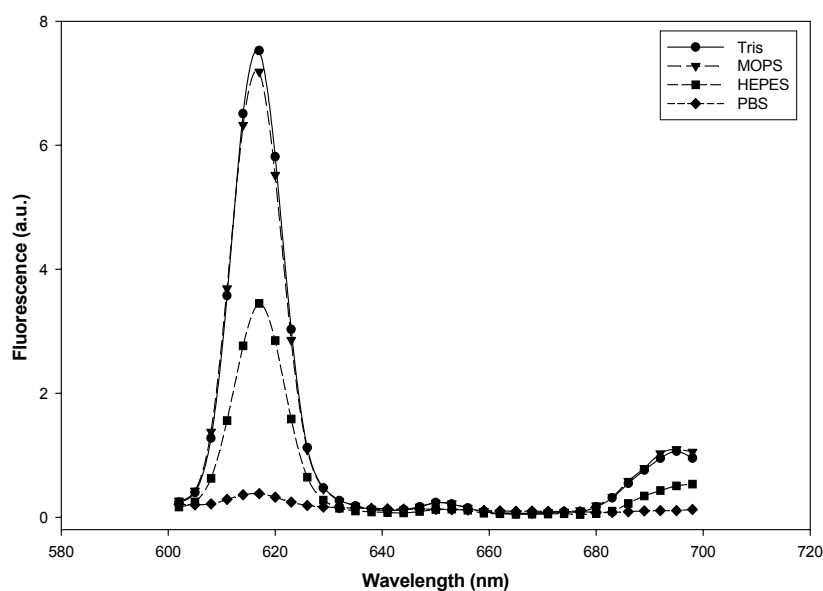


Figure 2.6. Buffer effect on EuTc-HP complex system. 90 μl of 0.2 mmol L^{-1} EuTc, H₂O₂: 240 $\mu\text{mol L}^{-1}$ and 12 mmol L^{-1} MOPS buffer solution: pH 6.9 in 2000 μl cuvette.

The temperature effect on the EuTc-HP is also investigated in Figure 2.7. An increase in temperature results in a decrease of the fluorescence. This is in accordance with the common properties of fluorophores.

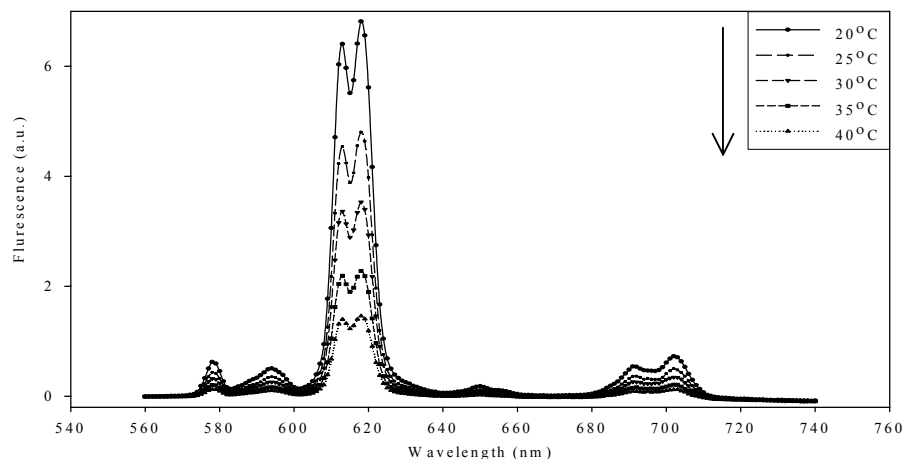


Figure 2.7. Temperature effect on EuTc-HP complex system. EuTc 80 $\mu\text{mol L}^{-1}$, H₂O₂ 400 $\mu\text{mol L}^{-1}$, MOPS to 2 ml. Thermostated at the temperature for 30 min before measurement.

The stability of the EuTc and EuTc-HP were tested. EuTc has shown quite good stability as seen in Figure 2.8. The stability is indicated by the change of the absorbance. Within 45 days, there is only a small deviation less than 1.6%. EuTc-HP is not as stable as EuTc. It is prone to decomposition, but usually stable for more than 4 hours as shown in the time trace of the fluorescence in Figure 2.9, with a constant baseline shift.

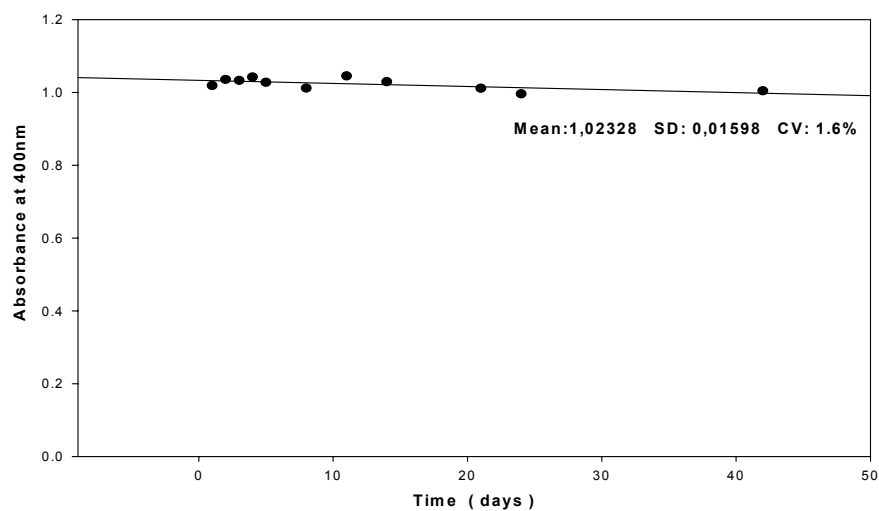


Figure 2.8. The stability of EuTc complex as indicated by the absorbance change. 34 $\mu\text{mol L}^{-1}$ EuTc in MOPS (10mmol L⁻¹, pH=6.9)

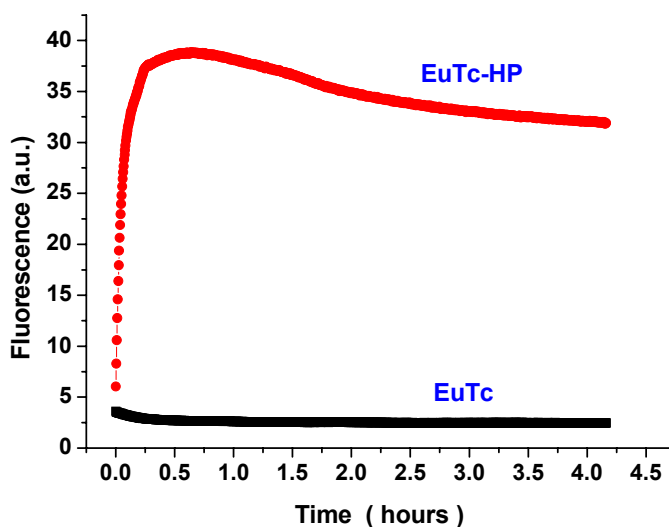


Figure 2.9. The stability of EuTc-HP complex as indicated by the fluorescence change. 60 $\mu\text{mol L}^{-1}$ EuTc in MOPS (10 mmol L^{-1} , pH=6.9) in the wells, H₂O₂ 400 $\mu\text{mol L}^{-1}$ in the wells.

2.2.1.4. Quenchers and interferences

The possible interferences by common anions and cations are also explored (Figure 2.10). The fluorescence of the EuTc-HP complex system is not affected by alkali, alkali earth and ammonium ions, nor by anions including chloride, bromide, iodide, sulfate and nitrate in up to $\sim 100 \text{ mmol L}^{-1}$ concentrations. Fluoride acts as a weak quencher if present in a

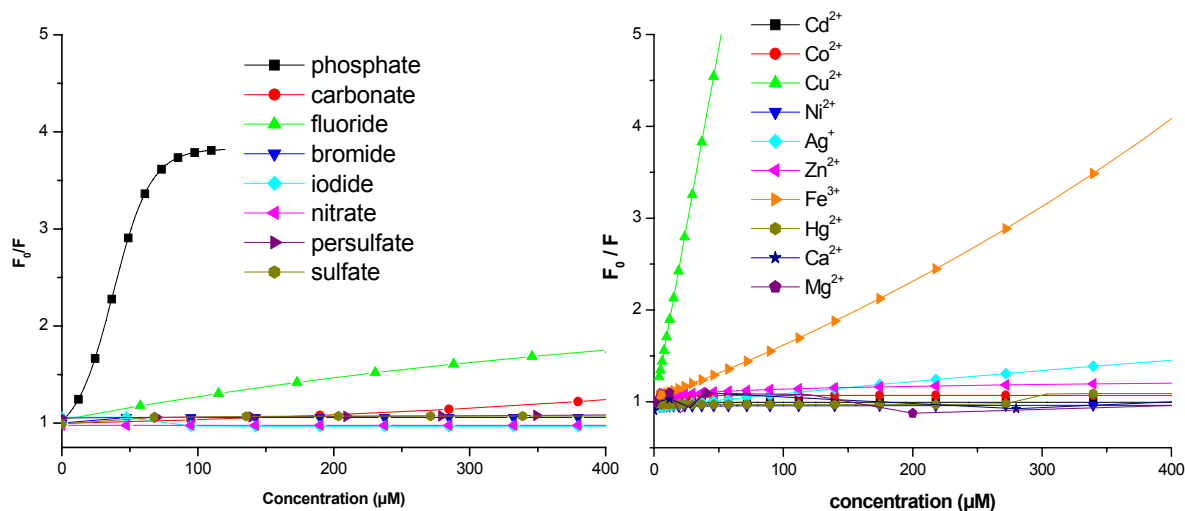


Figure 2.10. The quenchers and interference of EuTc-HP system
The interferences added in EuTc 20 $\mu\text{mol L}^{-1}$, H₂O₂ 400 $\mu\text{mol L}^{-1}$, in the wells

concentration higher than 0.1 mmol L⁻¹. However, phosphate, copper(II) and iron (III) ions are strong quenchers of the system. Furthermore, the fluorescence of the EuTc-HP system is weakly quenched by molecular oxygen. An 11% decrease in fluorescence intensity was observed on going from nitrogen-saturated solutions to air-saturated solutions.

2.2.2. Time-resolved Fluorescent Determination of Hydrogen Peroxide

2.2.2.1. Time-correlated single photon counting (TCSPC) method

Time-correlated single photon counting (TCSPC) method is one of the mostly used methods for photon-counting lifetime detection. This method can be applied for the determination of H₂O₂ with the EuTc fluorescent probe.

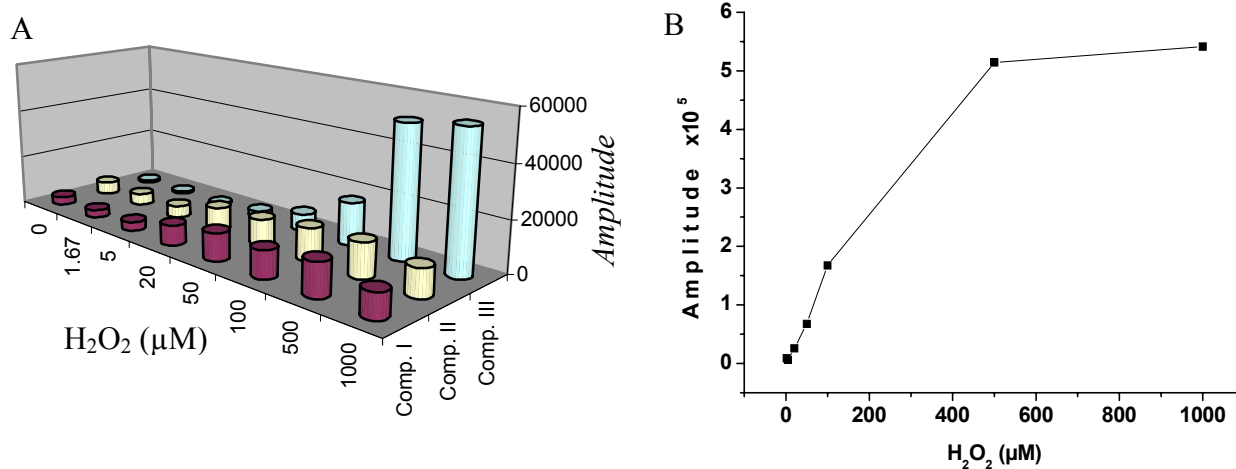


Figure 2.11. A: Three component mode of the decay vs the concen. of H₂O₂ in amplitudes. B: the mainly changed component in amplitudes (Component III, ~60 μs) vs the concen. of H₂O₂. The samples were prepared by addition of different concentrations (0 - 1000 μmol L⁻¹) of H₂O₂ to a final concen. of EuTc of 53.3 μmol L⁻¹ as respect to tetracycline and waiting for 10 min before detection.

As shown in Figure 2.11, the three components of the decay were correlated with the concentrations of H₂O₂. The mainly changed component is component III. The determination

of H₂O₂ can be achieved through the amplitude of component III. The dynamic range is from 0 to 500 μmol L⁻¹ (Figure 2.11 B). For the simplicity, the average lifetimes in different H₂O₂ concentration can also be utilized for the determination of H₂O₂ as in Figure 2.12. The dynamic range is narrower than the mainly changed component method and ranges from 0 to 100 μmol L⁻¹.

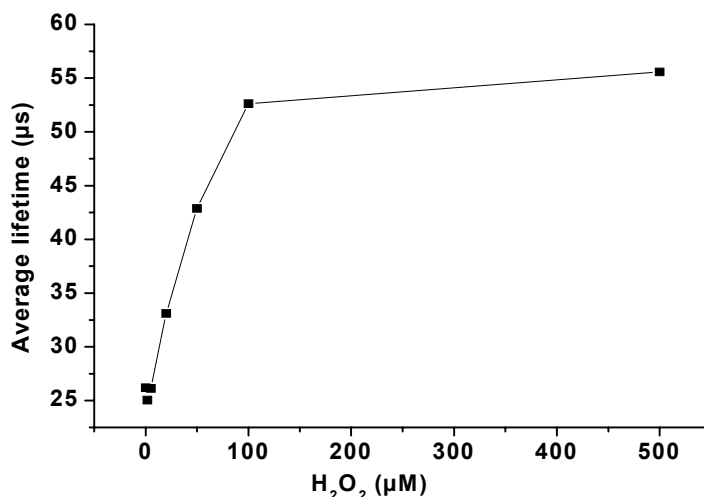


Figure 2.12. Calibration of H₂O₂ in average lifetimes. The samples were prepared by addition of different concentrations (0 - 1000 μmol L⁻¹) of H₂O₂ to a final concentration of EuTc of 53.3 μmol L⁻¹ as respect to tetracycline and waiting for 10 min before measurement.

2.2.2.2. Rapid lifetime determination (RLD) method

Despite the ability of determination of H₂O₂ by the TCSPC method, it is rather complicated both from the instrumental aspects and the data processing aspects. For these reasons, it is mainly used for characterization of the fluorophores rather than quantitative detections. To overcome the relatively tedious procedure of photon counting, there have been several approaches to simplify both the instrumentation and data processing procedure [PDI^{20,21}, and RLD^{22,23}]. Among them, the rapid lifetime determination method (RLD) has been quite thoroughly studied as an alternative for the accurate lifetime determinations, such as the TCSPC method. Unlike TCSPC, RLD detects only two windows in the decay and uses the ratio of the two windows (see Figure 2.2) as an indication of the lifetime as widely used

for imaging, especially helpful for the on-the-fly detection. Here a RLD method is presented for the determination of H₂O₂ on a commercially available microplate reader.

The most favorable experimental conditions were obtained by stepwise optimizations of the delay time, integration time and RLD windows. The best delay time was found to be ~60 μs. The integration time have no signification effect and 40 μs was selected for the detection. The selection of the measurement windows was optimized for the different concentrations of EuTc and different windows, as schematically indicated in Figure 2.3. As from Figure 2.13, among all the windows selected for RLD, the ratio of window 1 (60-100 μs) to window 2 (200-240 μs) has the highest value and still the relative standard deviation is less than 5%. So these two windows were selected for the RLD determination of H₂O₂ on the microplate reader. Data were obtained with 100 times repetition for each data points.

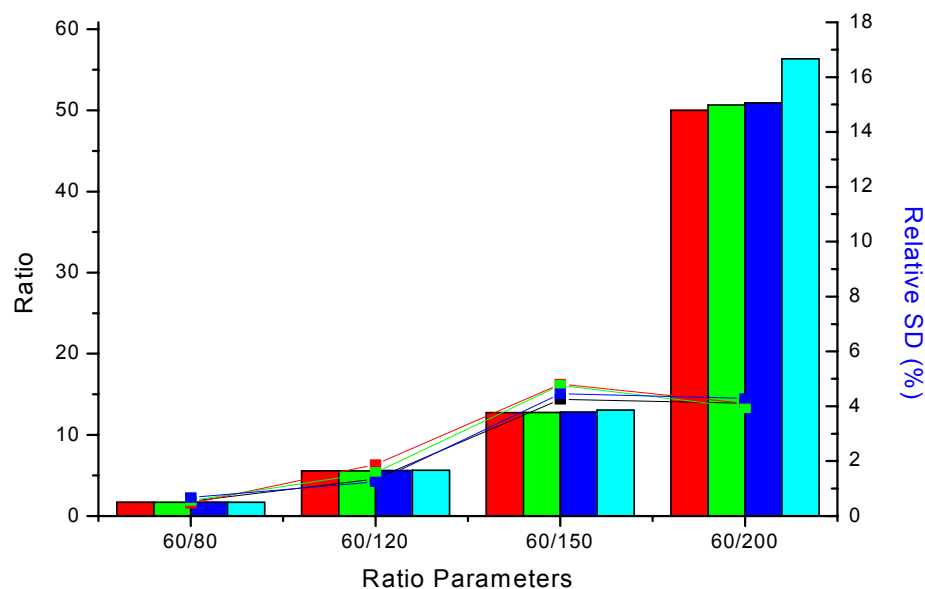


Figure 2.13. Optimization of the measurement windows for the rapid lifetime determination method. The samples were prepared by addition of different concentrations (for each cluster from left to right, 120, 100, 80, 40 μM) of EuTc as respect to tetracycline in the same concentration of H₂O₂ of 20 μM. The measurement was performed in triplicate as detected with different windows.

$$R = \frac{W_1 - Blank}{W_2 - Blank} \quad \dots\dots\dots \text{Eq. 2.5}$$

W1, W2 as in Figure 2.3

The calculation of the RLD method is based on Eq. 2.5. The calibration graph of RLD method is demonstrated in Figure 2.14. The curve can be described as $y = 7.93 + 0.26 * x$ ($r = 0.99$, each point in triplicate), with a dynamic range of 5.2 - 50 $\mu\text{mol L}^{-1}$, and the limit of detection ($3 * \text{SD} / \text{Slope}$) of 5.2 $\mu\text{mol L}^{-1}$. The limit of detection is not improved over the gated methods²⁵ and even intensity-based steady state fluorescent assay²⁶. But it proves the applicability of RLD for multicomponent decays and offers the potential for the high background determination, such as those of plates and fluorescent proteins.

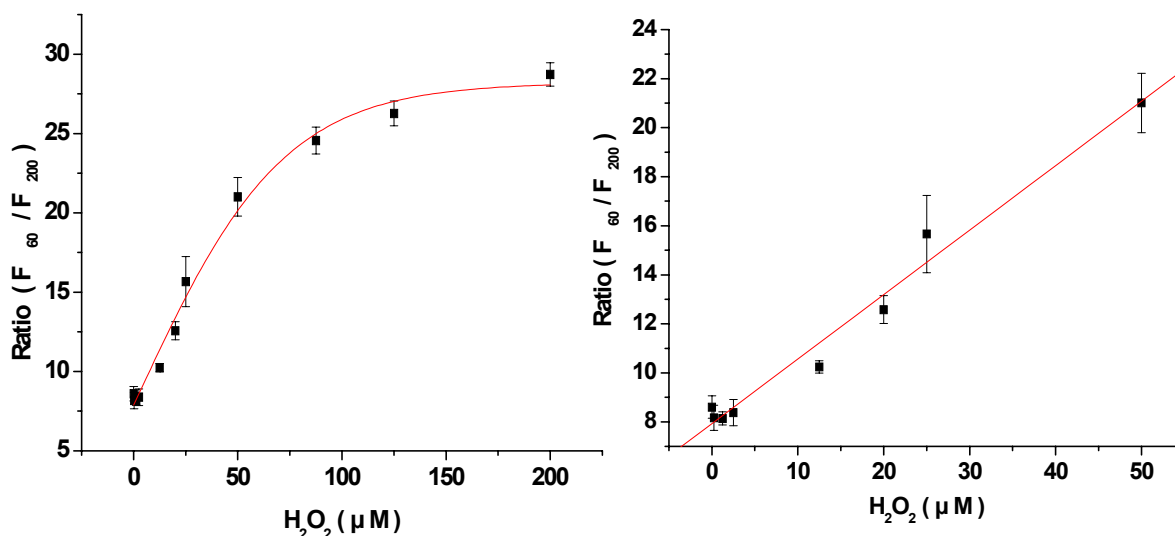


Figure 2.14. Calibration of H₂O₂ in Rapid Lifetime Determination (RLD) method.

See experimental part for the details.

There have been reports on the theoretical optimization of the RLD windows²⁴, from the lifetime data and Monte Carlo calculations. The conclusion from the simulation with around 80% overlap of the measurement windows has been tried in this experiment, but with relatively low ratio as seen in Figure 2.11. The chosen windows have the highest ratio and in

the same time with a less than 5% relative standard deviation. Another aspect that has to be taken into account is that EuTc and EuTc-HP are all composed of three-components of decay. Although theoretical studies have led to the conclusion of a two-component decay²⁴, the optimization of RLD windows might not be suitable for the case used here now. Furthermore, the applicability of the RLD method for EuTc and EuTc-HP may also be in doubt due to their multi-component decay profiles. However, as suggested by others²², the RLD method may still be valid if the monotonic change due to the presence of analyte can be established.

It should be noted that this is the first example for the RLD method to be applied in the microplate assays. The recent developments of fluorescent readers have made it possible to detect simultaneously two windows, which will greatly improve the present method.

2.3. Experimental (Please see Chapter 7 for the reagents and instruments)

2.3.1. Time-correlated Single Photon Counting (TCSPC) Lifetime Determination

The luminescence lifetimes of EuTc and EuTc-HP were detected with a pulsed 392-nm laser (LDH-C-400, PicoQuant GmbH, Berlin, Germany; www.picoquant.de), and an H5783-P04 PMT detector (Hamamatsu) with a newly developed multiphoton-counting board in a special multipass cuvette. The samples were prepared by addition of different conc. (0-1000 $\mu\text{mol L}^{-1}$) of H₂O₂ to a final conc. of EuTc of 53.3 $\mu\text{mol L}^{-1}$ and waiting for 10 min before measurement. Data were processed by the FluoFit software (from PicoQuant GmbH).

2.3.2. Rapid Lifetime Determination Assay of Hydrogen Peroxide on Microplates

Place, in each well of a thermostatted (30 °C) 96-well microplate 100 μL of the EuTc stock solution (0.2 mM with respect to Tc), and MOPS buffer to make up the total volume to 200 μL . The samples (50 μL) containing H₂O₂ in a concentration between 4 and 200 μM were added simultaneously. After 10 min incubation, the rapid lifetime determination scheme with two windows of fluorescence intensity detection at 60 μs to 100 μs and 200 μs to 240 μs is recorded on the FLUOstar OPTIMA reader. The data are the average of 100 measurements for each window for the precision consideration. Control experiments are conducted by adding buffer in place of H₂O₂ samples, to give blank signal denoted as F₀. The blank was subtracted before the calculation. All microplate experiments were done in triplicate.

2.3.3. Time-resolved (gated) and Steady-state Fluorescence Assays

Conventional steady-state and time-resolved “gated“ fluorescence assays were performed with the same samples and microplates as described above.

2.4 References

1. Wolfbeis, O; Wu, M; Lin, Z. Ger. Offen. (2003), 16 pp. DE 10155160 A1 20030522
2. Duerkop, A. Eur. Pat. Appl. (2002), 29 pp. EP 1239049 A2 20020911
3. Lakowicz, J. R. Principles of Fluorescence Spectroscopy. Second Edition (1992), Plenum Press, New York, N. Y. USA.
4. Dickson Gudgin, Eva F.; Pollak, Alfred; Diamandis, Eleftherios P. Pharmacology & Therapeutics (1995), 66(2), 207-35.
5. Ekins, R. P.; Chu, F. W. Clinical Chemistry (1991), 37(11), 1955-67.
6. Soini, Erkki; Hemmila, Ilkka. Clinical Chemistry (1979), 25(3), 353-61.
7. Evangelista, Ramon A.; Pollak, Alfred; Templeton, Eva F. Gudgin. Analytical Biochemistry (1991), 197(1), 213-24.
8. Gudgin Dickson, Eva F.; Pollak, Alfred; Diamandis, Eleftherios P. Journal of Photochemistry and Photobiology, B: Biology (1995), 27(1), 3-19.
9. Meyer, Jorg; Karst, Uwe. Analyst (2000), 125(9), 1537-1538.
10. Gudgin Dickson, Eva F.; Pollak, Alfred; Diamandis, Eleftherios P. Journal of Photochemistry and Photobiology, B: Biology (1995), 27(1), 3-19.
11. Lee, Y. C. Analytical Biochemistry (2001), 297(2), 123-127.
12. Nowak, Steven A.; Lytle, Fred E. Applied Spectroscopy (1991), 45(5), 728-33.
13. Waters, P. Dean; Burns, David H. Applied Spectroscopy (1993), 47(1), 111-15.
14. Ballew, R. M.; Demas, J. N. Analytica Chimica Acta (1991), 245(1), 121-7.
15. Ballew, Richard M.; Demas, J. N. Analytical Chemistry (1989), 61(1), 30-3.
16. Holub, O.; Seufferheld, M. J.; Gohlke, C.; Govindjee; Clegg, R. M. Photosynthetica (2000), 38(4), 581-599.
17. Stump, N; Chen, G.; Peterson, J; Haire, R. Inorganica Chimica Acta (1992), 196(2), 209-11.
18. Van Houten, J; Watts, R. J. Journal of the American Chemical Society (1975), 97(13), 3843-4.
19. M. Wahl. R. Erdmann, Time-Correlated Single Photon Counting in Fluorescence Lifetime Analysis Photonik 1-2 (2000) 1

20. Liebsch, Gregor; Klimant, Ingo; Krause, Christian; Wolfbeis, Otto S. *Analytical Chemistry* (2001), 73(17), 4354-4363.
21. Hartmann, Paul; Ziegler, Werner. *Analytical Chemistry* (1996), 68(24), 4512-4514.
22. Sharman, Kristin K.; Periasamy, Ammasi; Ashworth, Harry; Demas, J. N.; Snow, N. H. *Analytical Chemistry* (1999), 71(5), 947-952.
23. Woods, R. J.; Scypinski, Stephen; Love, L. J. Cline. Transient digitizer for the determination of microsecond luminescence lifetimes. *Analytical Chemistry* (1984), 56(8), 1395-400.
24. Chan, Sing Po; Fuller, Z. J.; Demas, J. N.; DeGraff, B. A. *Analytical Chemistry* (2001), 73(18), 4486-4490.
25. W. Lei, A. Dürkop, Z. Lin, M. Wu, O. S. Wolfbeis, *Microchim. Acta* (2003)
26. Wolfbeis, Otto S.; Duerkop, Axel; Wu, Meng; Lin, Zhihong. *Angewandte Chemie, International Edition* (2002), 41(23), 4495-4498.

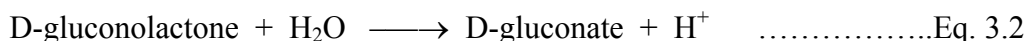
Chapter 3. Direct and Time-Resolved Enzymatic Detection of Glucose

3.1. Introduction

Glucose is of great importance for its roles in diabetes¹, in central carbon metabolism², and in diet-related biomedical research^{3,4}. It is also of interest with respect to monitoring industrial processes such as bio-fermentation, brewing, etc⁵. There have been continuous intensive efforts to develop continuous and discontinuous assays, the former often with respect to non-invasive, real-time glucose sensors^{6,7,8}.

Numerous optical (sensory) methods have been proposed. One approach is based on the glucose binding capability of concanavalin A (ConA) that can be followed by fluorescence resonance energy transfer (measured in either intensity or decay time)^{9,10}. However, the method is limited by the tendency of ConA and its conjugate to form aggregates. Another more recent approach is based on boronic acid receptors which can recognize glucose (and other polyols) and thereby trigger a fluorescent signal^{11,12,13}. A lot of efforts have been made to improve the performance of the method, e.g. by making use of an aniline/anilineboronic acid copolymer that is capable of binding saccharides and thereby undergoes a color change¹⁴. Glucose binding proteins conjugated to fluorescent proteins have also been investigated with respect to their possible application in glucose assays^{15,16}.

Despite recent advances, enzymatic methods based on (a) glucose oxidase (GOx) that converts glucose and oxygen into gluconate and H₂O₂, and (b) reduction of glucose by a dehydrogenase¹⁷ still are the most widely used methods. In GOx-based assays (see Eq. 3.1 and 3.2), the consumption of oxygen¹⁸, changes in pH¹⁹ and the intrinsic fluorescence of glucose oxidase²⁰ have been exploited, mainly for sensory purposes.



Notwithstanding the utility of these approaches, methods based on the direct detection of H₂O₂ produced (by GOx) according to Eq. 3.1 are of particular interest since H₂O₂ does not form a signal background in most biological matter. Unfortunately, no *reversible* optical indicators (probes) do exist for H₂O₂. On the other side, H₂O₂ can be irreversibly converted into colored products using peroxidase (POx), thereby enabling single shot (irreversible) tests, partially in the form of tests strips for diabetics^{21,22,23}. Chromogenic reagents used include, in particular, the so-called Trinder reagents since they can result in many different hues of colors²². Guilbault et al.^{24,25,26} have shown that certain hydroxyphenyl acetic acids and homovanillic acid undergo POx-catalyzed oxidative dimerization with H₂O₂ to form strongly fluorescent products. These findings forms the basis for widely used and very sensitive assays for H₂O₂ and oxidase-associated enzymatic reactions.

Few direct methods not requiring POx have been reported. Photometric discontinuous assays based on complexes of H₂O₂ with vanadium²⁷, titanium^{28,29,30} or ferric³¹ ions can be performed, however sometimes not at pH 7 because of the precipitation of the respective metal hydroxides. Therefore, these assays are mostly of the endpoint type. More recently, new substrates for H₂O₂ have been introduced, for example certain fluorescent resorufin derivatives^{32,33} and the so-called Amplex Red³⁴ which enable kinetic assays since they can be applied at near-neutral pH. In a recent study³⁵, a lanthanide complex of the product formed from pHPA through POx-assisted oxidation was used for H₂O₂ detection using time resolution. Conceivably, it may be applied to glucose assay. In addition to fluorescent assays, numerous chemiluminescent methods (known for particularly low limits

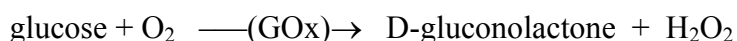
of detection) have been reported³⁶. It should be kept in mind, though, that most glucose assays are applied to sample solutions where analyte concentrations are not extremely low.

A new direct and time-resolved ("gated") glucose detection scheme is presented here based on the detection of H₂O₂ produced by the GOx reaction using a europium-derived fluorescent probe³⁷. It has the specific features that make lanthanide-based probes so popular and versatile^{38,39}, and offers the first H₂O₂-based time-resolved fluorescence assay that does not require the presence of a peroxidase. In addition, it works best at neutral pH.

3.2. Results and Discussion

3.2.1. Assay Principle

The fluorescent probe EuTc has been reported³⁷ to be useful for determination of H₂O₂. The absorption and emission spectra of the probe in absence and presence, respectively, of glucose and glucose oxidase (GOx) are shown in Fig. 3.1. The unique properties of the complex with between H₂O₂ and EuTc (referred to as EuTc-HP) include an absorption maximum around 400 nm, an ~210-nm Stokes' shift, and a line-like fluorescence emission peaking at 616 nm. The principle of the glucose assay is based on the oxidation of glucose by GOx (see Eq. 3.1 and 3.2) and the subsequent conversion of the weakly fluorescent EuTc into the strongly fluorescent EuTc-HP by H₂O₂ according to following equilibrium:



The increase in fluorescence due to the production of H_2O_2 is smaller than would be expected. It is assumed that this is due to the presence of traces of catalase in the GOx as indicated by the provider who gives a catalase activity of ≤ 10 units per mg GOx. Catalase interferes anyway, and the assay reported here requires the absence of any interfering levels of catalase in order to function well. In fact, the EuTc-HP system can be used for the quantitation of catalase⁴⁰.

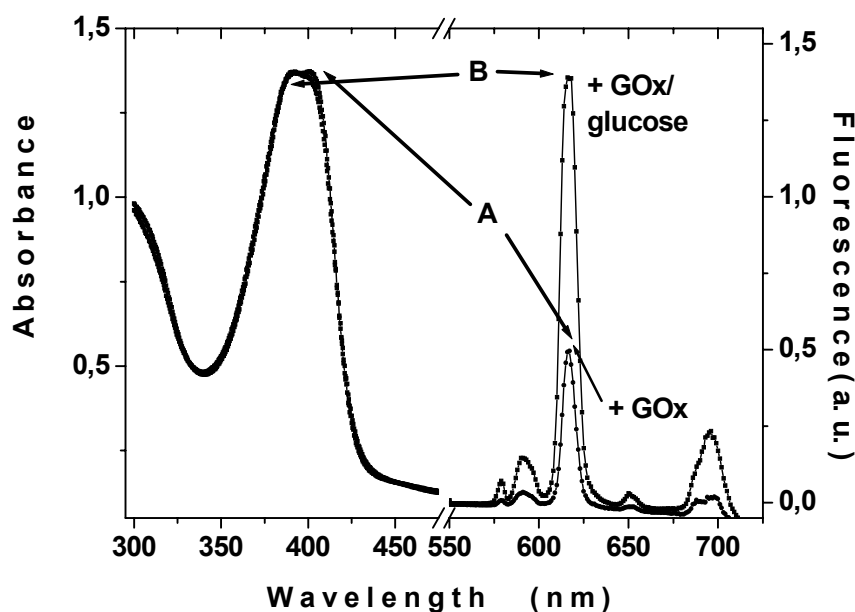


Figure 3.1. Absorbance spectra (left) and emission spectra (right) of the EuTc/GOx system in absence and presence, respectively, of glucose. A: 1 mL of EuTc stock solution plus 200 μL of a 54.1 U/mL glucose oxidase stock solution and 1790 μL of MOPS buffer. B: 10 μL of a 27.7 mmol L^{-1} glucose solution added to A and incubated at room temperature for 30 min with occasional shaking.

Please note that the ratio is only 4 times due to the glucose added.

The kinetic response of the GOx/EuTc system to rising concentrations of glucose (at a constant activity of GOx) is shown in Figure. 3.2. With higher glucose concentrations, and therefore increasing production of hydrogen peroxide, fluorescence intensity increases strongly due to formation of EuTc-HP. Hence, the glucose concentration can be detected directly without further addition of peroxidase or another substrate. Endpoint determination is the preferred format in this case, and the drift can be easily subtracted in a microplate assay.

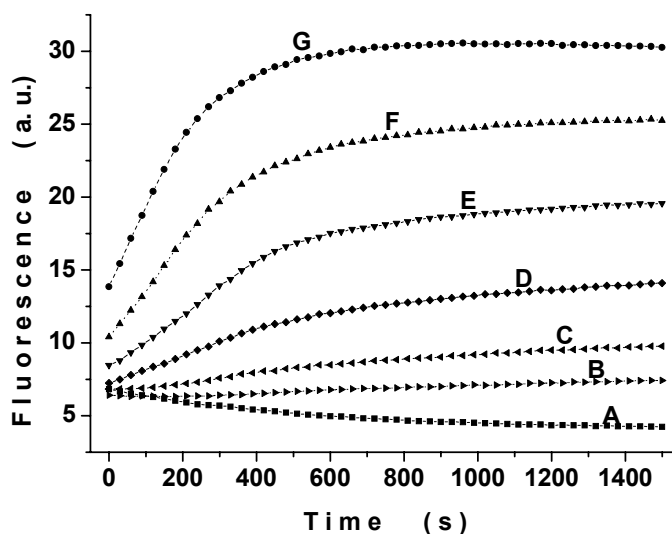


Figure 3.2. Kinetic response over 30 min of the EuTc/GOx system to increasing concentrations of glucose. 100 μL of EuTc 0.2 mmol L^{-1} stock solution, 20 μL of a 54.1 U/mL glucose oxidase stock solution, and MOPS buffer made up to a total volume of 200 μL , with glucose concentrations of 0.0, 13.86, 27.72, 69.3, 138.6, 277, 693 $\mu\text{mol L}^{-1}$ from A to G.

The response of the fluorescent probe is due to the formation of EuTc-HP, rather than to other effects. Glucose alone has no significant effect on the fluorescence of EuTc and of EuTc-HP. In addition, deactivated GOx does not cause any changes over time. While active GOx in the concentrations used here has no effect on EuTc, it did slowly decrease the fluorescence of EuTc-HP (Fig. 3.2, line A). The drift in the baseline of EuTc and GOx in the absence of glucose is likely due to temperature effects or interaction of EuTc with the GOx protein.

3.2.2. Fluorescence Intensity-based Assays

Glucose is present in serum and in many other samples in rather high ($>3 \text{ mmol L}^{-1}$) concentrations. Such levels of glucose are preferably determined in a kinetic way, typically over 5 min. The assay has been adapted to these conditions as described in the Experimental Part so to match glucose concentrations between 0.5 and 10.0 mmol L^{-1} . As can be seen in Figure 3.3, the kinetic response over 5 min is quite linear.

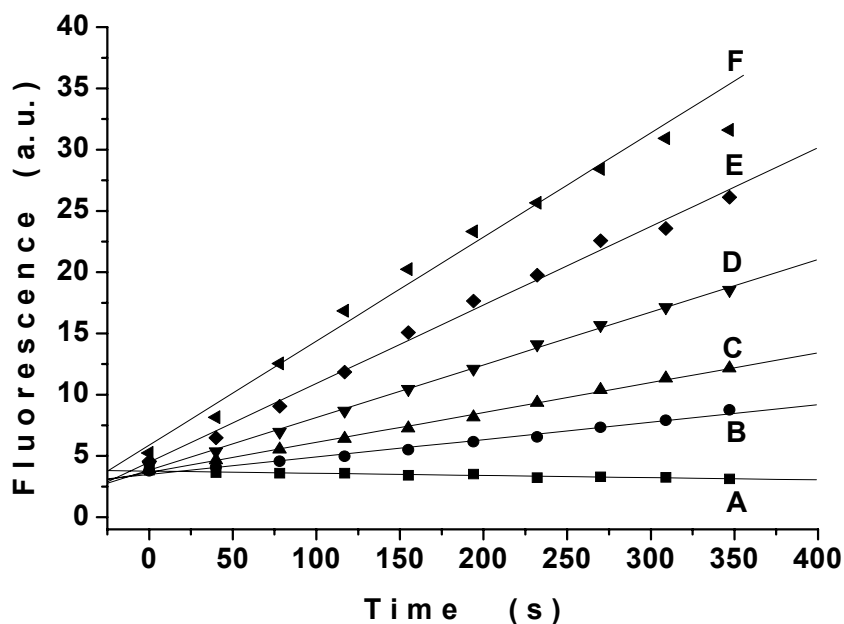


Figure 3.3. Kinetic response over 5 min of the glucose oxidase/EuTc system to increasing concentrations of glucose in the mmol L^{-1} range. Experimental conditions: 100 μL of EuTc 0.2 mmol L^{-1} stock solution, 2 μL of a 55.0 U/mL GOx stock solution, and MOPS buffer made up to a total volume of 200 μL , with glucose conc. (from A to G) of 0, 0.66, 1.32, 2.63, 5.27, 10.5 mmol L^{-1} .

In order to quantify even low concentrations of glucose, an endpoint method is developed, including a 30-min incubation time at 30 °C, and by increasing the activity of the GOx employed and the concentration of EuTc. A stable signal is reached after a >20-min incubation at 30 °C as can be seen from Figure 3.2. The temperature chosen is in the optimal range for GOx⁴¹.

The effect of oxygen as one of reactants was also studied. Although oxygen acts as a weak quencher³⁷ of the fluorescence of EuTc-HP (its intensity decreases by 10% on going from nitrogen-saturated solutions to air-purged solutions), the oxygen supply for the glucose detection is more than adequate as proven by the results obtained with and without shaking, respectively. Under these two conditions, the time trace of the detection is virtually identical. The optimal pH range of detection is 6.6 – 7.2 which is the optimal range for both EuTc-HP

and GOx^{37,41}. Outside this range, the fluorescence intensity drops rapidly, being only 15% of the maximum at pH 8.0, and 8% at pH 6.0.

The interferences of common cations and anions were studied and no significant effects were found for alkali ions and chloride in up to 100 mmol L⁻¹ concentrations, and also for various other cations and anions at up to 100 μmol L⁻¹ levels. Known interferents for the GOx-POx system, such as ascorbic acid, uric acid, and bilirubin, also have no significant effect as shown in Table 3.1, probably because no peroxidase is involved and the transient concentration of free H₂O₂ is never as high as in some other assays. It is likely, though, that in case of higher H₂O₂ concentration there will be interference by ascorbic acid, uric acid, bilirubin, and glutathione. They have a <10% effect if present in concentrations of, respectively, 40, 132.5, 8.6, and 19.8 μmol L⁻¹ in the wells (corresponding to 160, 530, 35, and 79 μmol L⁻¹, respectively, in the 50 μL samples added). Phosphate and citrate ions inhibit or interfere at even micromolar concentrations. Free Cu²⁺ ion interferes with EuTc-HP and inhibits GOx.

Table 3.1. Effect of common interferents for GOx-POx system on EuTc glucose assay.^{a)}

Interferent	Concentrations (μmol L ⁻¹) in the wells (in the stock solution)	Relative fluorescence intensity (%)
ascorbic acid	15.0 (100)	99.5
	37.5 (250)	97.4
uric acid	15.0 (100)	97.4
	30.0 (200)	95.2
bilirubin	3.0 (20)	100.1
	6.0 (40)	94.5

^{a)} Experimental details: test solution: 100 μL of the EuTc stock solution, 20 μL of GOx (54.1 U/mL), 50 μL of glucose solution (2.77 mmol L⁻¹), 30 μL of interference substance (stock concen. as shown above in brackets), and MOPS buffer to make up to a total volume of 200 μL; 30 min incubation at 30 °C ; the relative intensity refers to that of a solution without interferent.

A calibration plot was established for the direct determination of glucose as described in the protocol with the Ascent reader. The linear range is from 2.7 to 100 $\mu\text{mol L}^{-1}$, the linear regression equation being described by $y = -167.1 + 392.5x$ ($r = 0.99$, $n = 3$ for each point). The limit of detection ($S/N = 3$) is 2.7 $\mu\text{mol L}^{-1}$. The kinetic determination of millimolar concentrations of glucose within 5 min results in a linear regression equation described by $y = 0.91 + 0.25 * x$ ($r = 0.98$, $n = 3$ for each point).

3.2.3. Time-resolved (gated) Fluorescence Assay

Lanthanide complexes usually display long decay times, typically between 0.01 and 10 ms. This feature has made them quite popular for time-resolved fluorescent detection, mostly in context with immunoassays, gene assays, and high-throughput screening. The time-resolved ("gated") detection scheme can effectively eliminate background fluorescence, such as the intrinsic short-lived fluorescence of proteins and microplates. EuTc and EuTc-HP can also be applied to this scheme since their average decay times (30 and 60 μs , respectively) are significantly different. In addition, the fluorescence intensity of EuTc-HP is significantly higher than that of EuTc³⁷. In view of this, time-resolved (gated) detection becomes possible by selecting a suitable lag time and integration time as indicated in Fig. 3.4.

Both the lag time and integration time were optimized in the gated assay. The optimal lag time range for the detection is around 50 – 125 μs as shown in Fig. 3.5. We use a 60 μs delay since it gives a good signal-noise ratio, but other lag times may be used as well. The integration time has no significant effect on going from 40 μs to 300 μs . However, the EuTc fluorescence cannot be gated out completely despite the fact that EuTc-HP has a main lifetime twice that of EuTc. This is due to (a) the fact that EuTc with its main component of ~ 30 μs is still present to some extent after 60 μs , and (b) a small but slowly ($> \sim 60$) decaying

component of EuTc which cannot be eliminated by gating. On the other side, gated detection with a lag time of 60 μs is more than adequate to overcome the background fluorescence of the samples and microplates which usually have ns decay times.

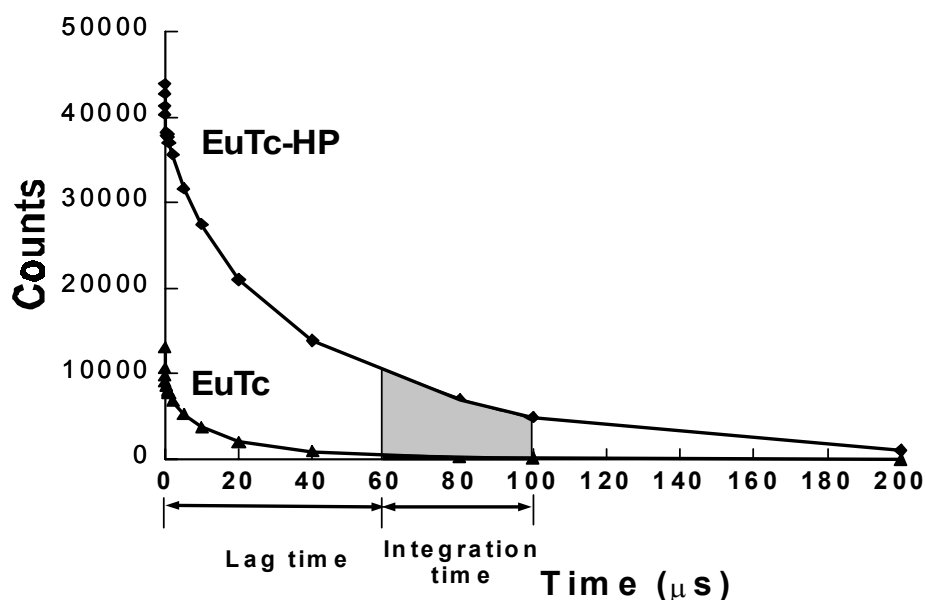


Figure 3.4. Fluorescence decay profiles of EuTc and EuTc-HP, respectively, and a schematic of the time-resolved (gated) assay employed here. By picking a lag time of 60 μs most of the background fluorescence of EuTc is suppressed, while that of EuTc-HP is detected.

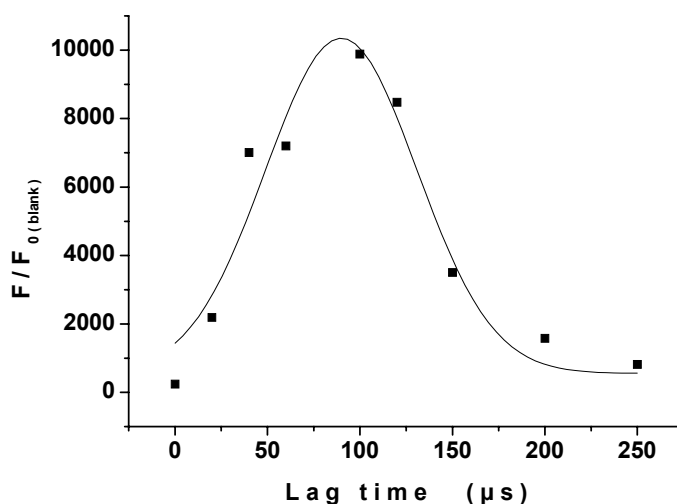


Figure 3.5. Optimization of the lag time of the time-resolved glucose assay. The solution in the well is composed of 100 μL of EuTc stock solution, 20 μL of the 54.1 U/mL GOx, 50 μL of a 2.77 mmol L^{-1} glucose, and 30 μL of MOPS. The blank consists of 200 μL of MOPS. Its fluorescence (F_0 (blank)) is used for background correction. Fluorescence was measured after 30 min at 30 $^{\circ}\text{C}$.

A calibration plot for the gated glucose assay (30 min; described in the recommended protocol) is given in Fig. 3.6. The dynamic range is from 2.2 to 100 $\mu\text{mol L}^{-1}$, the linear regression equation being described by $y = 0.122 + 0.164x$ ($r = 0.99$, $n = 3$ for each point). The calculated limit of detection ($S/N = 3$) is 2.2 $\mu\text{mol L}^{-1}$.

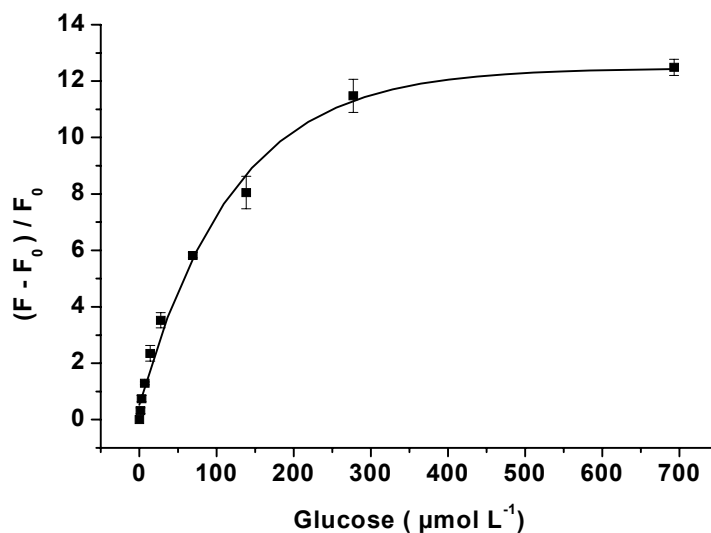


Figure 3.6. Calibration of glucose in the time-resolved (gated) determination. Glucose solutions of different concentrations, 100 μL of EuTc (0.2 mmol L^{-1}) stock solution, 20 μL of 54.1 U/mL glucose oxidase stock solution, and MOPS solution made up to a total volume of 200 μL . Data were acquired after 30 min at 30 $^{\circ}\text{C}$. The lag time of the time-resolved assay was set to 60 μs , and the integration time to 40 μs . The fluorescence intensities (F) obtained with glucose solutions are corrected for F_0 (the fluorescence intensity of a blank containing no glucose).

3.2.4. Comparison

A lot of methods have been described so far for glucose determination. Among those, direct H_2O_2 based optical detection methods based on the use of GOx are still most sensitive and most frequently used as summarized in Table 3.2. The GOx-POx based assay is widely used. However, this coupled enzymatic scheme requires a chromogenic or fluorogenic reaction by POx for the optical signal production, e.g. with Trinder's reagent or Amplex Red. This potentially introduces new interferences, such as by ascorbic acid²³, uric acid, and other

electron-donating substances, and thereby increases the complexity of the detection. Direct H₂O₂ detection without POx can overcome these disadvantages.

Few methods are available for the direct detection of glucose via H₂O₂ without POx. Metal complexes, such as those of vanadium, titanium and ferric ions, have been used since they form colored adducts with H₂O₂. However, these methods mainly exploit changes in absorbance or reflectance. Table 3.2 also lists the optimal pH values. It should be noted, however, that recommended pH values of <6 cannot easily be adjusted to in certain samples.

Recently, a direct glucose assay was presented that is based on the deacetylation of weakly fluorescent acetylresorufin. The fluorescence produced by resorufin is used for the determination of glucose, and common POx interferents remain inert. However, the over-oxidation of fluorescent resorufin or resazurin substrate itself may lead to quenching of the fluorescence and therefore compromise the determination. This is also true for the resorufin analogs such as Amplex red or resazurin.

Compared to other assays (Table 3.2), the method introduced here appears to be the first one that is applicable to gated fluorometry (a) at pH 7, (b) without addition of an enzyme substrate for POx, (c) without the need for addition of POx, and (d) without the need for UV excitation which is known to cause a strong fluorescent background from either the sample or cuvettes and microplates. Moreover, over-oxidation (as in case of resorufin or resazurin) has not been observed (Fig. 3.6). In fact, the fluorescence of the system at glucose concentrations as high as 700 μM (after a 30 min incubation at 30 °C) is constant over time after having reached the endpoint. Finally, the assay reported here is applicable to both kinetic and endpoint determination. Glucose in the concentration range occurring in blood plasma (3 – 20 mM) is preferably determined by kinetic 1-point detection.

Chapter 3. Time-Resolved Enzymatic Detection of Glucose

Table 3.2. Overview on H₂O₂-based optical assays for glucose along with recommended pH values (or pH ranges) ^{a)}

Reagent(s)	Ref.	LOD ($\mu\text{mol L}^{-1}$)	Linear range ($\mu\text{mol L}^{-1}$)	pH range	Remarks
via vanadium complex	27	300	300 – 2400		absorbance measured at 582 nm; end point detection only; ascorbate and uric acid do not interfere
via titanium complex	28,29,30	0.5	0.5 – 500	6.3 – 8.0	absorbance measured at 450 nm; end point detection only; ascorbate and uric acid probably do not interfere
via ferric iron complex	31	10	30 – 200	5.5	absorbance measured at 575 nm; end point detection only; ascorbate and uric acid probably do not interfere
Trinder/POx	21,22,23,42	11.1	11.1 - 55.5	>7.5	absorbance measured at 750 nm; end point detection; ascorbate, uric acid and bilirubin probably interfere
homovanillic acid /POx	24,25,26	1.7	1.7 – 17	8.5	fluorescence measured at exc/em wavelengths of 315/425 nm; UV fluorescence background from biomatter may interfere; kinetic detection and end point detection possible; ascorbate, uric acid and bilirubin probably interfere
Amplex Red /POx	34	1 or 3	~ 3 – 40	7.4	fluorescence measured at exc/em wavelengths of 530-560/~590 nm; kinetic detection and end point detection possible; overoxidation observed at >500 μM glucose; ascorbate, uric acid and bilirubin probably interfere
acetylresorufin	32, 33	200	200 – 2000	7.4	fluorescence determined at exc/em at 568/582 nm; kinetic detection and end point detection possible; ascorbate, uric acid and bilirubin do not interfere; over-oxidation of resorufin to resazurin possible
EuTc	this method	2.2	2.2 - 100	6.5 – 7.5	fluorescence measured at exc/em 405/620 nm; capable of both kinetic and end point detection; time-resolved assay possible; ascorbate, uric acid and bilirubin do not interfere

In conclusion, the glucose assay reported here has several novel and useful features including the good accessibility of the reagent, high sensitivity, large Stokes' shift, stability towards oxygen; and a working pH of ~7. These make it an attractive alternative for glucose-related biomedical research and in diagnosis, not the least because this kind of assay is based on a widely applicable probe so that other assays may be performed with similar or even identical instrumentation.

3.2.5. Analysis of Other Substrates of Oxidases

The EuTc fluorescent probe has also been studied for analysis of galactose, sarcosine and lactate, but without success. As show in Figure 3.7, only glucose oxidase gives the anticipated increase due to the production of H₂O₂. This might partially due to the nature of the enzymes, because (1) the specific activity of GOx is usually much higher than that of the other enzymes, and consequently much more enzyme proteins are in presence, which may interfere and quench the fluorescence of EuTc-HP; (2) the stability of the other enzymes is not as good as GOx; and (3) the nature of EuTc and EuTc-HP itself might also be the reason as will discussed latter in the thesis.

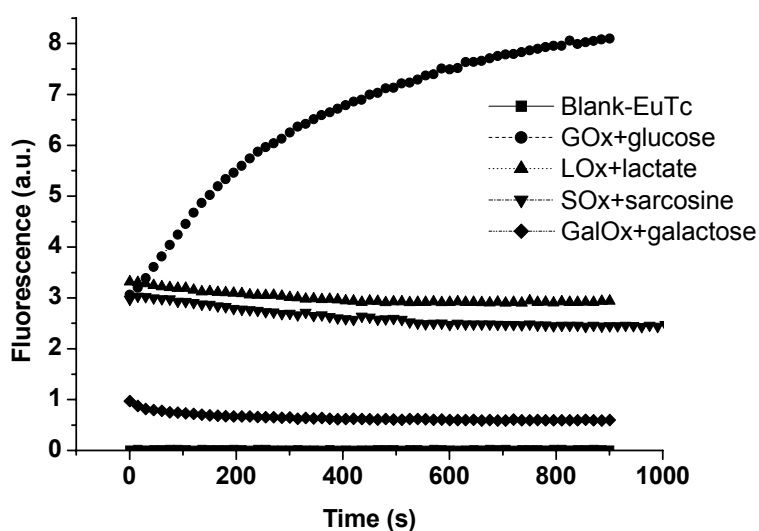


Figure 3.7. Time-trace of the other oxidases.

3.3. Experimental (Please see Chapter 7 for the reagents and instruments)

Glucose Assay Protocol

For determination of glucose in milimolar range (as found in plasma), the assay was optimized for measurement within 5 min. Place, in each well of a thermostatted (30 °C) 96-well microplate, 100 μL of the EuTc solution, 2 μL of GOx (55.0 U/mL), and MOPS buffer to make up the total volume to 200 μL . The samples (95 μL) containing glucose between 0.5 and 10 mmol L^{-1} were added simultaneously, and the plates were read on the GENios+ reader in intervals of shaking over 5 min, with a lag time of 60 μs and an integration time of 40 μs . Control experiments were conducted by replacing glucose samples with buffer, to give blank signal denoted as F_0 . The blank was subtracted from the fluorescence with glucose for the detection. All microplate experiments were done in triplicate.

In order to obtain very low limits of detection, a 30 min incubation at 30 °C and a higher enzyme activity was employed. In each well of a thermostatted (30 °C) 96-well microplate were placed 100 μL of the EuTc solution, 20 μL of GOx solution (54.1 U/mL), and MOPS buffer to make up the total volume to 200 μL . The samples (50 μL) containing glucose in concentrations between 5 and 100 $\mu\text{mol L}^{-1}$ were added thereafter, and the wells were read on the GENios+ reader (under intervals of shaking) as programmed, with a lag time of 60 μs and an integration time of 40 μs . Control experiments were conducted by adding buffer in place of glucose samples to give a signal denoted as F_0 . The blank was subtracted from the fluorescence signal obtained with glucose solutions.

For the steady-state intensity measurement, the same plate composition was used, and measured on the Fluoroskan Ascent reader.

3.4. References

1. Robert J (2002) *Hormone Res.* 57(Suppl. 1):81-84.
2. Fischer E, Sauer, U (2003) *Eur. J. Biochem.* 270:880-91.
3. Folmer V, Soares J, Rocha, J (2002) *Intl. J. Biochem. Cell Biol.* 34:1279-1285.
4. Helander I, Westerblad H, Katz A (2002) *Am. J. Physiol.* 282:C1306-C1312.
5. Dodge T, Gerstner J (2002) *J. Chem. Technol. Biotechnol.* 77:1238-1245.
6. Khalil O (1999) *Clin. Chem.* 45:165-177.
7. Gough D, Armour J, Baker D (1997) *Diabetologia* 40:S102-S107.
8. Wang J (2001) *Electroanalysis* 13:983-988.
9. Meadows D, Schultz J (1988) *Talanta* 35:145-149.
10. Rolinski O, Birch D, McCartney L, Pickup J (2000) *J. Photochem. Photobiol.* B54:26-34.
11. James T, Shinkai S (2002) *Topics Curr. Chem.* 218:159-200.
12. DiCesare N, Adhikari D, Heynekamp J, Heagy M, Lakowicz J. R. (2002) *J. Fluoresc.* 12:147-154.
13. Karnati V, Gao X, Gao S, Yang W, Ni W, Sankar S, Wang B (2002) *Bioorg. Medic. Chem. Lett.* 12:3373-3377.
14. Pringsheim E, Terpetschnig E, Piletsky S, Wolfbeis O (1999) *Adv. Mater.* 11:865-868.
15. Fehr M, Frommer W, Lalonde S (2002) *Proc. Nat. Acad. Sci. USA* 99:9846-9851.
16. Shibasaki S, Ueda M, Tanaka A (2002) *ACS Symp. Ser.* 830:234-247.
17. Ogawa Z, Kanashima M, Nishioka H (2001) *Clin. Chem. Lab. Med.* 39:396-400.
18. Moreno-Bondi M, Wolfbeis O, Leiner M, Schaffar B (1990) *Anal Chem.* 62:2377-2380.
19. Trettnak W, Leiner M, Wolfbeis O (1989) *Biosensors* 4:15-26.
20. Trettnak W, Wolfbeis O (1989) *Anal. Chim. Acta* 221:195-203.
21. Genovesi L, Pedersen K, Sigel G (1989) *Proc. SPIE-Int. Soc. Opt. Eng.* 990:22-28.
22. Charlton S, Kurchacova E (1989) *US Pat.* 4,855,228.
23. Pugia M (1996) *US Pat.* 5,702,955.
24. Guilbault G, Brignac P, Zimmer M (1968) *Anal. Chem.* 40:190-196.
25. Guilbault G, Brignac P, Juneau M (1968) *Anal. Chem.* 40:1256-1263.
26. Guilbault G (1970) *Enzymatic Methods of Analysis*, Pergamon Press.
27. Matsubara C, Ishii K, Takamura K (1981) *Microchem. J.* 26:242-249.
28. Matsubara C, Kudo K, Kawashita T, Takamura K (1985) *Anal. Chem.* 57:1107-1109.
29. Matsubara C, Yokoi Y, Nakamichi N, Takamura K, Yakugaki Z (1994) *J. Pharmaceutical Soc. Jap.* 114:48-53,
30. Yokoi Y, Matsubara C, Takamura K (1995) *Bunseki Kagaku* 44:355-362.
31. Harms D, Meyer J, Westerheide L, Krebs B, Karst U (1999) *Anal. Chim. Acta* 401:83-90.

32. Maeda H, Matsu-Ura S, Nishida M, Senba T, Yamauchi Y, Ohmori H (2001) *Chem. Pharm. Bull.* 49:294-298.
33. Matsu-Ura S, Yamauchi Y, Ohmori H, Maeda H (2002) *Bunseki Kagaku* 51:111-115.
34. Haugland R (2002) *Handbook of Fluorescent Probes and Research Products*, 9th ed.; Eugene, OR, USA; pp.414, 443; <http://www.probes.com/media/pis/mp22189.pdf>
35. Meyer J, Karst U (2000) *Analyst* 125:1537-1538
36. Faehnrich K, Prawda M, Guilbault G (2001) *Talanta* 54:531-559
37. Wolfbeis O, Duerkop A, Wu M, Lin Z (2002) *Angew. Chem., Int. Ed.* 41:4495-4498.
38. Hemmila I, Mikkala V (2001) *Crit. Rev. Clin. Lab. Sci.* 38:441-519.
39. Boisclair M, McClure C, Josiah S, Glass S, Bottomley S, Kamerkar S, Hemmila I (2000) *J. Biomol. Screening* 5:319-328.
40. Wu M, Lin Z, Wolfbeis O (2003) *Anal. Biochem.* 320:129-135.
41. Kalisz H, Hecht H, Schomburg D, Schmid R (1990) *J. Mol. Biol.* 213:207-209.
42. Mizoguchi M, Ishiyama M, Shiga M (1998) *Anal. Comm.* 35:71-74.

Chapter 4. Fluorescence Imaging of the Activity of Glucose Oxidase

4.1. Introduction

Glucose oxidase (GOx, EC 1.1.3.4) is a flavoenzyme that catalyzes specifically the oxidation of glucose into gluconate and hydrogen peroxide (Eq. 4.1).¹ It is one of the most



widely used enzymes for its availability and its stability. As a representative of oxidases, it has been studied in solution as well as in the immobilization on solid surfaces,² or in encapsulation in the microsphere³ for the application in biosensors,⁴ industrial bioreactors,⁵ and bio-fuel cells.⁶ Apo-glucose oxidase has also been utilized in studies for “nanowiring”⁷ of the electron transfer. GOx has been applied not only to the electrochemical and optical determination of glucose,⁸ but also in GOx-labelled enzyme amplification analysis for immunoassays.⁹ GOx based enzyme immunoassays have been used for the quantitation and screening of e.g. steroids, drugs, environmental pollutants, special peptides.¹⁰ Recently, it also has been applied to microchip or microarray technologies for the development of protein chips for proteomics.¹¹

Numerous methods have been developed for the determination of GOx. A set of assays have emerged based on determination of oxygen,¹² pH,¹³ or H₂O₂,^{14,15}. However, methods based on the measurement of H₂O₂ produced by GOx are of particular interest because H₂O₂ does not form a background but is only produced during enzymatic reaction. Since H₂O₂ cannot be easily visualized, it is usually converted into a colored or fluorescent product using peroxidase (POx).

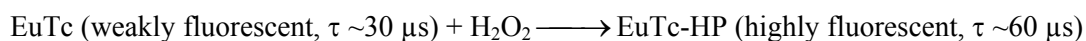
In recent years, fluorescent imaging technologies have attracted substantial attention because of the multitude of information on both the spatial and temporal characterization of the target analyte.^{16,17} Confocal,¹⁸ multi-photon excitation,¹⁹ near-field²⁰ and lifetime-based imaging^{21,22} technologies have been developed for different applications. Unfortunately, known methods for imaging GOx are restricted mainly to scanning electrochemical imaging²³, and scanning chemiluminescence imaging²⁴. This is largely due to the fact that almost all fluorescence imaging methods for GOx are in need for a second enzyme (POx) in order to visualize the H₂O₂ produced by the GOx catalyzed reaction. There have been reports on H₂O₂ based imaging using dihydrorhodamine 123,²⁵ homovanilic acid²⁶, scopoletin²⁷, dichlorodihydrofluorescein diacetate,²⁸ or others²⁹, all in conjugation with POx as the second chromogenic or fluorogenic enzyme.³⁰

Based on the previous reports on the europium tetracycline (EuTc) fluorescent probe,^{31,32} here is presented a direct detection scheme for GOx at neutral pH and without the need for a second enzyme, and a fluorescent imaging to visualize the GOx activity. Due to the long fluorescence decay time of the probe, intensity-based, time-resolved and lifetime-based imaging for quantitative detection of the activity of GOx are also explored.

4.2. Results and Discussion

4.2.1. Principle and Characterization of the Detection System

The direct assay for GOx activity via H₂O₂ is based on the response of EuTc to enzymatically produced H₂O₂ to give the much stronger fluorescent EuTc complex with H₂O₂ (EuTc-HP), as following:



The kinetic response of the glucose/EuTc system with rising activities of GOx is shown in Figure 4.1. With higher activities of GOx, and therefore increasing production of hydrogen peroxide, fluorescence increases due to the formation of the strongly fluorescent europium-tetracycline-hydrogen peroxide (EuTc-HP) system. Glucose and GOx themselves have no significant effect on the fluorescent probe, while ascorbate, uric acid, phosphate and citrate interfere.³² Because of the differences in the average decay times of EuTc ($\sim 30 \mu\text{s}$) and EuTc-HP ($\sim 60 \mu\text{s}$),^{31,32} the time-resolved and decay time based determination and imaging become possible.

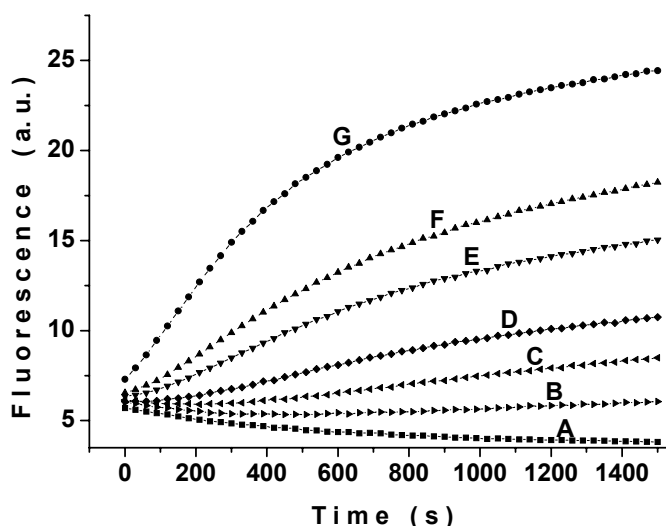


Figure 4. 1. Kinetic response of the glucose/EuTc system to increasing activities of GOx.

100 μL of a 0.2 mmol L^{-1} EuTc stock solution, 15 μL of a 277.2 mmol L^{-1} glucose solution, and MOPS buffer made up to a total volume of 200 μL . Glucose oxidase activities (from A to G): 0.0, 0.27, 0.54, 1.4, 2.7, 5.4 and 13.5 mUnit/mL respectively.

4.2.2. Imaging Setup and Analytical Schemes

The setup of the imaging system is an adapted version of an earlier system^{33,34} that takes into account the larger Stokes shift ($\sim 210 \text{ nm}$), and the μs decay times of the probes. Cut-off optical filters and a common ns pulse generator are adequate for the optimal imaging of GOx.

The four imaging schemes shown in Figure 4.2 have been tested for their suitability for quantitative imaging of GOx activity. Their features are summarized in Table 4.1. In conventional fluorescence intensity imaging (FII)²⁹ one detection window is opened while excitation is on. In contrast to this often applied method, in time-resolved imaging (TRI)^{35,36} the detection window is opened after the excitation pulse. TRI imaging technology is most useful to eliminate (by gating) the autofluorescence of samples and plates with their nanosecond decay times. These two are mainly intensity-based detection schemes.

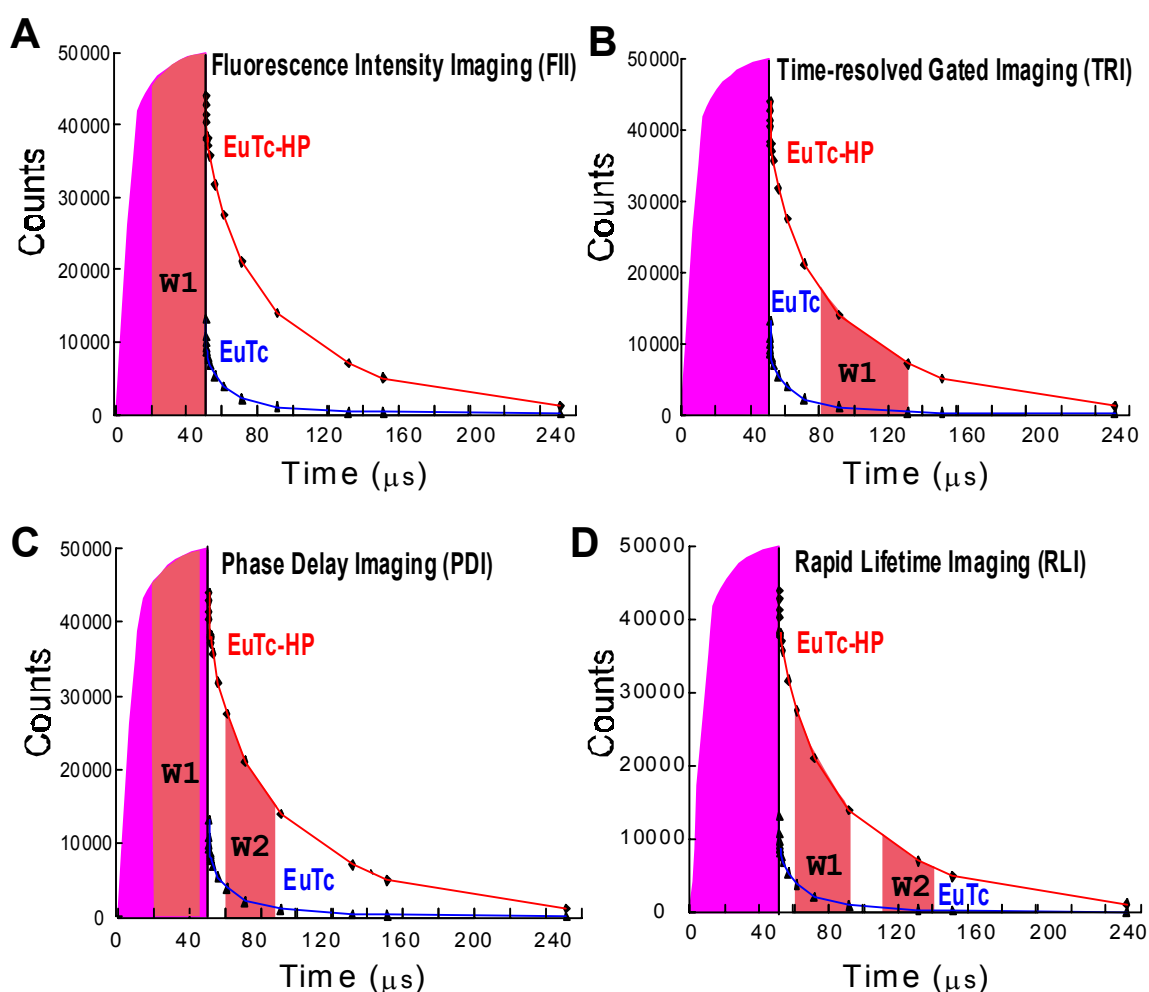


Figure 4.2. Schematic principles of four imaging schemes. Timelines of Window 1 and Window 2 of the four imaging schemes are indicated in Table 1.

Table 4.1. Figures of merit for the four imaging schemes studied in this work.

		FII*	TRI	PDR	RLD
Excitation	t_i	0	0	0	0
	t_t	50	50	50	50
Window 1 (W1)	t_i	0	80	0	80
	t_t	50	130	50	130
Window 2 (W2)	t_i	0	0	100	180
	t_t	0	0	150	300

t_i as the initiating time, t_t as the terminating time, all times in μs .

*: FII: Fluorescent intensity imaging; TRI: Time resolved imaging; PDR: Phase delay rationing imaging; RLD: Rapid lifetime determination imaging.

Luminescence decay time-based detection can also be exploited for imaging purposes and have certain advantages since they are independent of light source and detector fluctuations, the concentration of the fluorophore, and light scatter. The commonly used on-the-fly detection techniques for lifetime are utilized here with a two-window detection and ratiometric quantification as shown in Eq. 4.2:

$$R = \frac{W_1 - W_{\text{dark image}}}{W_2 - W_{\text{dark image}}} \dots\dots\dots \text{Eq. 4.2}$$

Phase delay rationing imaging (PDR)^{34,37} is based on the acquisition of two windows, one in the excitation phase and one in the phase after excitation. The ratio of the two windows can be used for the quantification of the activities of GOx. Rapid lifetime determination imaging (RLD),^{38,39} in contrast, is based on the acquisition of two windows after excitation, the ratio of intensities of the two windows enabling a rapid determination of lifetime.

The resulting intensity-based and lifetime-based GOx images are displayed in Figure 4.3. They indicate that the fluorescent probe EuTc is applicable to all four schemes. The intensity-based (FII, Fig. 4.3 A and TRI, Fig. 4.3 B) images are clearly affected by the intensity fluctuations of the excitation light source and by scattering as indicated by the

inhomogeneity in the wells. In contrast, the lifetime-based images assays (PDR and RLD, see Figures 4.3 C and 4.3 D) in contrast, reveal good homogeneity due to their independence of intensity variation of the excitation light, the quantity of the fluorophore present in the wells, and of scattered light.

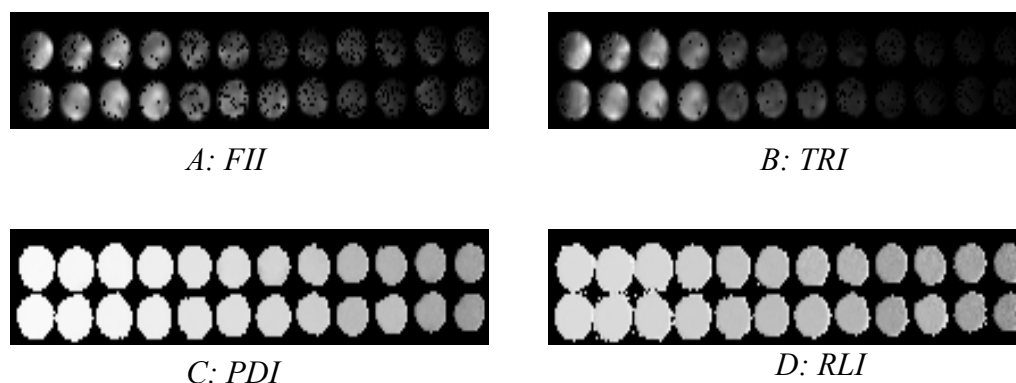


Figure 4.3. Four different images of the activity of glucose oxidase after respective data processing. A: Fluorescent intensity imaging (FII); B: Time-resolved imaging (TRI); C: Phase delay imaging (PDR); D: Rapid lifetime imaging (RLD). Experimental parameters are specified in Table 1, the respective data processing in the experimental part. Composition of the wells in the images (from left to right in duplicate) is as following: Decreasing GOx activities (from 135, 54.1, 27.1, 13.5, 5.4, 2.7, 1.35, 0.54, 0.27, 0.14, 0.05, and 0 (blank) mUnit/mL respectively), 100 μ L of a 0.2 mmol L⁻¹ EuTc, 15 μ L of a 277.2 mmol L⁻¹ glucose, and the total volume made up to 200 μ L with MOPS.

Previous studies have shown that ratiometric methods of PDR and RLD are suitable for on-the-fly detection of the fluorescence lifetime.⁴⁰ For example, the RLD method is most adequate for a mono-exponential decay, however with the possibility of applying it to multi-exponential decays.⁴¹ For multi-exponentially decaying systems like EuTc and EuTc-HP, the precision in the determination of the average lifetimes, however, is known to greatly depend on the selection of the detection windows.⁴² For the same windows, the ratios of the two windows change monotonically with the concentration of H₂O₂ formed by the glucose oxidase reaction as indicated by our experiments above.

4.2.3. Quantitative Aspects of GOx Imaging

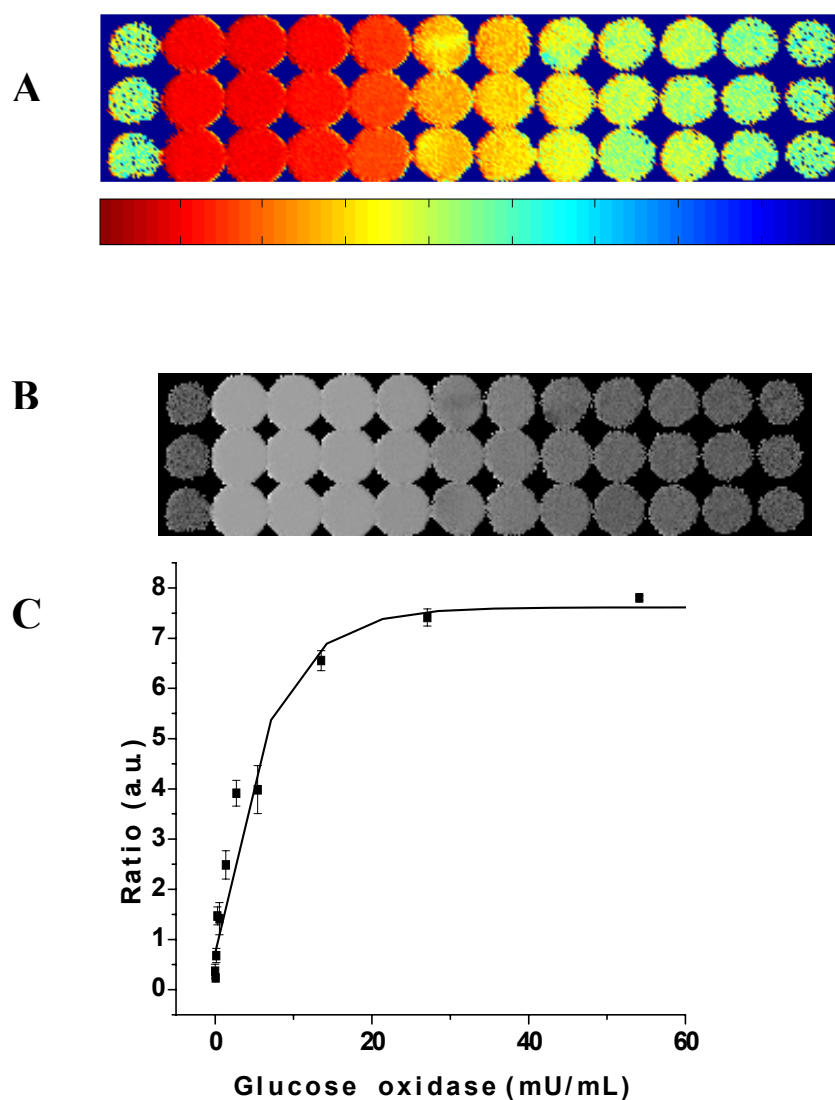


Figure 4.4. Rapid lifetime determination imaging of the activity of glucose oxidase.

A: Normalized ratio of the two images (false color). B: grey scale image of the activity of glucose oxidase; C: The calibration curve of the activity of glucose oxidase. Experiments were performed in triplicate (rows). The composition of the wells in the images is as: from 1 to 12, with glucose oxidase activities from 0 (blank), 135, 54.1, 27.1, 13.5, 5.4, 2.7, 1.35, 0.54, 0.27, 0.14, and 0.05 mUnit/mL respectively, 100 μL of a 0.2 mmol L^{-1} EuTc solution, 15 μL of a 277.2 mmol L^{-1} glucose solution, and the total volume made up to 200 μL with MOPS buffer.

The scheme was optimized with respect to the concentration of glucose and the concentration of EuTc. The optimal response (i.e. the largest change in fluorescence intensity)

was obtained when 20 mmol L⁻¹ glucose and 100 μmol L⁻¹ EuTc in the 200 μL well were used. The steady-state endpoint method is used since the reaction reaches the endpoint after a 30-min incubation, as can be seen from Figure 2. The different activities of GOx result in the different intensities of EuTc-HP. Although kinetic detection also is possible, it is less favored because it is much more complicated than endpoint imaging.

The rapid lifetime determination (RLD) scheme was further exploited for the quantitative imaging of the activity of GOx. The normalized ratio of the two images is shown in Figure 4.4 A. Figure 4.4 B illustrates the ratios in grey scale images after basic calculation, Figure 4.4 C the response of average ratio of the specific wells in the images to the presence of different activities of GOx. Imaging is linear from 0.32 to 2.7 mUnit/mL, with a detection limit of about 0.32 mUnit/mL (1.7 ng mL⁻¹).

4.2.4. Time-resolved Determination of GOx Using a Microplate Reader

Gating may also be applied to the determination of the activity of GOx via a microplate reader. The gated detection with a lag time of 60 μs and a integration time of 40 μs is by far adequate to overcome the background fluorescence of the samples and plates which usually have nanosecond lifetimes. The microplate reader assay resulted in a linear range from 0.32 to 14 mUnit/mL, with a limit of detection (S/N = 3) 0.32 mUnit/mL. The microplate assay, compared to the imaging, usually has a broader dynamic range and smaller standard deviations.

4.2.5. Comparison

The method presented here uses a single fluorescent probe and - to the best of our knowledge - is the first assay of GOx compatible with both time resolution (gating) and

lifetime-based imaging. No lifetime-based oxidase detection or imaging via H₂O₂ has been reported so far. However, an oxygen-based assay of GOx has been reported^{43,44} that is based on the measurement of the phase shift of an oxygen-sensitive fluorescent probe.

On the other hand, lanthanide-based fluorescence has been widely used in time-resolved (gated) assays and in imaging^{35,36} due to decay times of the probes which are in the order of μ s to ms. However, lanthanides are mainly used in the form of covalent labels, sometimes incorporated in microspheres. In the scheme reported here, dissolved EuTc is used as an H₂O₂-sensitive probe. There is no need for reagents other than glucose and EuTc.

Imaging of GOx (and possibly other oxidases such as uricase), offers the possibility of the construction of multi-enzyme or multi-substrate arrays⁴⁵. The capability spatial discrimination also makes imaging applicable to assess enzyme activity in immobilization studies,⁴⁶ such as for testing the quality of glucose biosensors based on GOx.

The methods reported here for imaging GOx activity is possible by both intensity based and lifetime based methods due to the unique features of the fluorescent probe EuTc and its complex formed with H₂O₂ (EuTc-HP). These include easy accessibility, high sensitivity, large Stokes' shift (~210 nm), a line-like fluorescence at 616 nm; an average decay time of ~30 and 60 μ s respectively; compatibility with LED lightsources; stability towards oxygen; and a working pH of ~7. In conclusion, the scheme presented here enables a straightforward method for imaging of GOx activities in microplates that, conceivably, may be extended to enzyme amplification immunoassays, high-throughput screening, immobilization studies and microarray technologies.

4.3. Experimental (Please see Chapter 7 for the reagents and instruments)

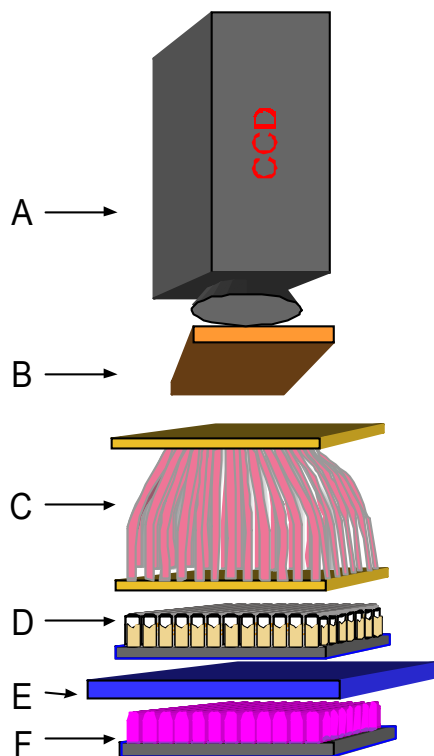


Figure 4.5. Setup of the imaging system. A: fast gateable CCD-camera (SensiMod); B: optical emission filter (KV 550); C: light-guiding adapter, consisting of 96 optical fibers ($\text{\O} = 3 \text{ mm}$); D: 96 well microtiterplate (black one with transparent bottom); E: optical excitation filter (BG 12); F: pulsable LED array with 96 UV light emitting diodes ($\lambda_{\text{max}} = 405 \text{ nm}$).

Imaging Device. The device used in this study has been previously reported^{33,34} and was used with minor modifications. As shown schematically in Figure 4.5, it is composed of a fast gateable CCD-camera (SensiMod; from PCO, Kelheim, Germany; www.pco.de), a pulsable LED array with 96 UV light emitting diodes ($\lambda_{\text{max}} 405 \text{ nm}$, Roithner Laser Technik, Vienna; www.roithner-laser.com/), a pulse generator (Scientific Instruments DG 535, Sunnyvale, California, www.srsys.com, not shown in Figure 1), an optical emission filter (KV 550; Schott, Mainz, Germany; www.schott.com), and an optical excitation filter (BG 12; Schott), with a light-guiding adapter consisting of 96 optical fibers ($\text{\O} = 3 \text{ mm}$) for matching the focus of the CCD camera. A personal computer was used for controlling and visualization

of the experiments as programmed in Interactive Data Language (IDL, Research Systems, Boulder, CO, USA; www.rsinc.com).

The manipulation and calculation of images, such as the rotation and crop of the images, the subtraction of the dark image (blank, without illumination) from the fluorescent image respectively, the ratio of the images and filtration of the background noise, were done by a self-developed program based on Matlab (6.1, Mathwork, Natick, MA, USA; www.mathwork.com). The images of the ratio from lifetime-based detection were inverted to their negatives for a more facile comparison of different methods.

Imaging of the Activity of GOx. To each well of a 96-well microtiter plate with transparent bottom were added 100 μL of the EuTc standard solution, 15 μL of a 277 mmol L^{-1} glucose solution, and enough MOPS buffer to make up the total volume to 200 μL . The samples (50 μL) containing GOx with an activity between 1.2 and 5.6 mUnit/mL were added simultaneously. The images of the plates were taken after a 30-min incubation at 30 $^{\circ}\text{C}$. Blank values (F_0) were obtained by adding buffer in place of GOx. In the time-resolved (gated) non-imaging determination using micro titer plates with a fluorescence reader, a lag time of 60 μs and an integration time of 40 μs were employed³².

4.4. References

1. Raba, J.; Mottola, H. A. *Crit. Rev. in Anal. Chem.* 1995, 25, 1-42.
2. Delvaux, M.; Demoustier-Champagne, S. *Biosens. & Bioelect.* 2003, 18, 943-951.
3. Slomkowski, S.; Basinska, T.; Miksa, B. *Poly. for Adv. Tech.* 2002, 13, 906-918.
4. Chen, L.; Zhang, X.; Xie, W.; Zhou, Y.; Zhang, Z.; Cass, A. E. G. *Biosens. & Bioelect.* 2002, 17, 851-857.
5. Traeger, M.; Qazi, G. N.; Buse, R.; Onken, U. *J. Ferment. and Bioeng.* 1992, 74, 274-81.
6. Tsujimura, S.; Kano, K.; Ikeda, T. *Electrochem.* 2002, 70, 940-942.
7. Xiao, Y.; Patolsky, F.; Katz, E.; Hainfeld, J. F.; Willner, I. *Science* 2003, 299, 1877-1881.
8. Robert, J. *Hormone Res.* 2002, 57(Suppl. 1), 81-84.
9. Kopetzki, E.; Lehnert, K.; Buckel, P. *Clin. Chem.* 1994, 40, 688-704.
10. Tsuji, A.; Maeda, M.; Arakawa, H.; Shimizu, S.; Ikegami, T.; Sudo, Y.; Hosoda, H.; Nambara, T. *J. Steroid Biochem.* 1987, 27, 33-40.
11. Kojima, K.; Hiratsuka, A.; Suzuki, H.; Yano, K.; Ikebukuro, K.; Karube, I. *Anal. Chem.* 2003, 75, 1116-1122.
12. Papkovsky, D. B., O'Riordan, T. C., Guilbault, G. G. *Anal. Chem.* 1999, 71, 1568-1573.
13. Tohda, K.; Gratzl, M. *ChemPhysChem* 2003, 4, 155-160.
14. Guilbault, G. G.; Brignac, P. J., Jr.; Juneau, M. *Anal. Chem.* 1968, 40, 1256-63.
15. Guilbault, G. G.; Brignac, P. J., Jr.; Zimmer, M. *Anal. Chem.* 1968, 40, 190-6.
16. Emptage, N. J. *Curr. Opin. in Pharm.* 2001, 1, 521-525.
17. Gillies, R. J. *J. of Cell. Biochem.* 2002, (Suppl. 39), 231-238.
18. Rastogi, K.S.; Cooper, R.L.; Shi, Z.Q.; Vranic, M. *Endocrine*, 1997, 7, 367-375.
19. Ruan, Q.Q.; Chen, Y.; Gratton, E.; Glaser, M.; Mantulin, W.W. *Biophys. J.* 2002, 83, 3177-3187
20. Kim, J. M.; Ohtani, T.; Sugiyama, S.; Hirose, T.; Muramatsu, H. *Anal. Chem.* 2001, 73, 5984-5991.
21. Szmacinski, H.; Lakowicz, J. R. *Sens. Actuat., B: Chem.* 1995, B29, 16-24.
22. Cubeddu, R.; Comelli, D.; D'Andrea, C.; Taroni, P.; Valentini G. *J. Phys. D Appl. Phys.* 2002, 35, R61-R76.
23. Wilhelm, T.; Wittstock, G.; Szargan, R. *Fresenius' J. Anal. Chem.* 1999, 365, 163-167.
24. Kasai, S.; Zhou, H.; Matsue, T. *Chem. Lett.* 2000, (3), 200-201.
25. Szucs, S.; Vamosi, G.; Poka, R.; Sarvary, A.; Bardos, H.; Balazs, M.; Kappelmayer, J.; Toth, L.; Szollosi, J.; Adany, R. *Cytometry* 1998, 33, 19-31.
26. Pazdzioch-Czochra, M.; Widenska, A. *Anal. Chim. Acta* 2002, 452, 177-184.
27. Gould, K. S.; McKelvie, J.; Markham, K. R. *Plant, Cell and Environ.* 2002, 25, 1261-1269.

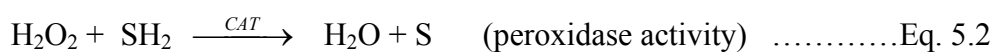
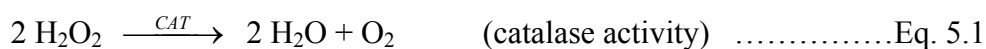
28. Johansson, T.; Petersson, M.; Johansson, J.; Nilsson, S. *Anal. Chem.* 1999, 71, 4190-4197.
29. Borst, J. W.; Uskova, M. A.; Visser, N. V.; Visser, A. J. W. G. *Springer Series on Fluorescence* 2002, 2 (Fluorescence Spectroscopy, Imaging and Probes), pp337-348.
30. Henderson, L. M.; Chappell, J. B. *Eur. J. Bioch.* 1993, 217, 973-80.
31. Wolfbeis, O. S.; Duerkop, A.; Wu, M.; Lin, Z. *Angew. Chem., Int. Ed. Engl.*, 2002, 41, 4495-4498.
32. WU, M.; LIN, Z.; Dürkop, A.; Wolfbeis O.S. *Anal. Bioanal. Chem.* Submitted.
33. Schaeferling, M.; Wu, M.; Enderlein, J.; Bauer, H.; Wolfbeis, O. S. *Appl. Spectr.* in press.
34. Liebsch, G.; Klimant, I.; Krause, C.; Wolfbeis, O. S. *Anal. Chem.* 2001, 73, 4354-4363.
35. Vaisanen, V.; Harma, H.; Lilja, H.; Bjartell, A. *Luminescence* 2000, 15, 389-397.
36. Beeby, A.; Botchway, S. W.; Clarkson, I. M.; Faulkner, S.; Parker, A. W.; Parker, D.; Williams, J. A. G. *J. Photochem. Photobiol. B*, 83-89.
37. Hartmann, P.; Ziegler, W. *Anal. Chem.* 1996, 68, 4512-4514.
38. Sharman, K. K.; Periasamy, A.; Ashworth, H.; Demas, J. N.; Snow, N. H. *Anal. Chem.* 1999, 71, 947-952.
39. Woods, R. J.; Scypinski, Stephen; Love, L. J. Cline. *Anal. Chem.* 1984, 56, 1395-400.
40. Desilets, D. J.; Coburn, J. T.; Lantrip, D. A.; Kissinger, P. T.; Lytle, F. E. *Anal. Chem.* 1986, 58, 1123-8.
41. Chan, S.P.; Fuller, Z. J.; Demas, J. N.; DeGraff, B. A. *Anal. Chem.* 2001, 73, 4486-4490.
42. Sharman, K. K.; Periasamy, A.; Ashworth, H.; Demas, J. N.; Snow, N. H. *Anal. Chem.* 1999, 71, 947-952.
43. Papkovsky, D. B.; O'Riordan, T. C.; Guilbault, G. G. *Anal. Chem.*, 1999, 71, 1568-1573.
44. Papkovsky, D. B.; Ponomarev, G. V.; Trettnak, W.; O'Leary, P. *Anal. Chem.* 67, 4112 – 4117.
45. Kasai, S.; Hirano, Y.; Motochi, N.; Shiku, H.; Nishizawa, M.; Matsue, T. *Anal. Chim. Acta*, 2002, 458 263–270
46. Delvaux, M.; Demoustier-Champagne, S. *Biosens. Bioelectron.* 2003, 18, 943-951.

Chapter 5. Determination of the Activity of Catalase

5.1. Introduction

Catalase (hydrogen peroxide:hydrogen peroxide oxidoreductase, EC 1.11.1.6; here referred to as CAT), is capable of decomposing hydrogen peroxide (H₂O₂) without producing free radicals¹. It has long been recognized as a defense for the oxidative stress² and plays an important role in the compartmentalization of H₂O₂ in biological systems³. Therefore, it has been widely studied for its role in physiological and pathological processes⁴ such as the detoxification of H₂O₂, the modulation of H₂O₂ as a messenger, the brain catalase response for alcohol, and in relation to acute or chronic hepatitis. It has also found applications in environmental monitoring as an early marker of environmental organic pollution⁵, in the food industry for detection of bacteria⁶, and even for the detection of life on the moon⁷. In addition, catalase is often added to biosensor systems in order to prevent any adverse effects of H₂O₂ which is formed during the enzymatic activity of oxidases including glucose oxidase.

Catalase is relatively unique compared to other members of the peroxidase family since it displays both catalase activity (EC 1.11.1.6; see reaction Eq. 5.1) and peroxidase activity (EC 1.11.1.7; Eq. 5.2). Typical substrates of peroxidase activity (SH₂ in Eq. 5.2) include ethanol, methanol, formate, nitrite, phenol, and others.



Numerous methods have been developed for measuring the activity of CAT. The decomposition of H_2O_2 can be monitored spectrophotometrically at 240 nm^{8,9}, or via chemiluminescence^{10,11}. One may also detect the production of oxygen (reaction 1) by either an oxygen electrode¹² or a low-flow gas meter⁷. In order to circumvent spectrophotometry at 240 nm (which is prone to interferences by other absorbers), the competitive consumption of H_2O_2 by catalase and by peroxidase, respectively, can be monitored using chromogenic or fluorogenic substrates¹³. However, spectrophotometric detection at 240 nm still is the most widely used method since it has the advantage of being kinetic, and because other methods usually involve two or more steps or reagents. Unfortunately, the UV photometric method is not easily applicable to complex samples displaying strong intrinsic absorption at 240 nm.

Recently, the weakly fluorescent Eu^{3+} -tetracycline complex (EuTc) has been introduced as a promising new fluorescent probe for detection of H_2O_2 . The latter acts as a fluorescence-enhancing ligand^{14,15}. As little as $1.8 \mu\text{mol L}^{-1}$ concentrations of H_2O_2 are detectable at near neutral pH. In fact, the effect has been used previously to improve the limits of detection in the determination of the drug tetracycline¹⁶ but appears to have an even larger potential in biosciences, since almost all oxidases produce H_2O_2 during their activity.

Here, a novel europium(III) ion derived fluorescent probe is presented for qualitative and quantitative determination of CAT, along with a new one-step fluorescent assay of CAT. The determination is based on the finding that the H_2O_2 in the fluorescent system EuTc-HP can be decomposed by CAT, thus leading to a large decrease in its fluorescence due to formation of the much less fluorescent EuTc.

5.2. Results and Discussion

In light of our previous studies^{14,15}, we found that the fluorescent system formed between H₂O₂ and EuTc (referred to as EuTc-HP) is reversibly decomposed by the enzyme catalase (CAT). Hence, H₂O₂ cannot have oxidized one of the components of the EuTc complex, but rather must be present in a form that makes it acceptable to this highly specific enzyme. Further studies revealed that the EuTc-HP system represents a novel fluorescent probe for CAT that can be used for the direct assay of CAT.

5.2.1. Characterization and Optimization of the Assay

The kinetic response of the EuTc-HP complex system to various activities of CAT is shown in Figure 5.1. The fluorescence of the EuTc-HP system decreases faster with increasing activity of CAT, the slope thus reflecting the actual activity of CAT.

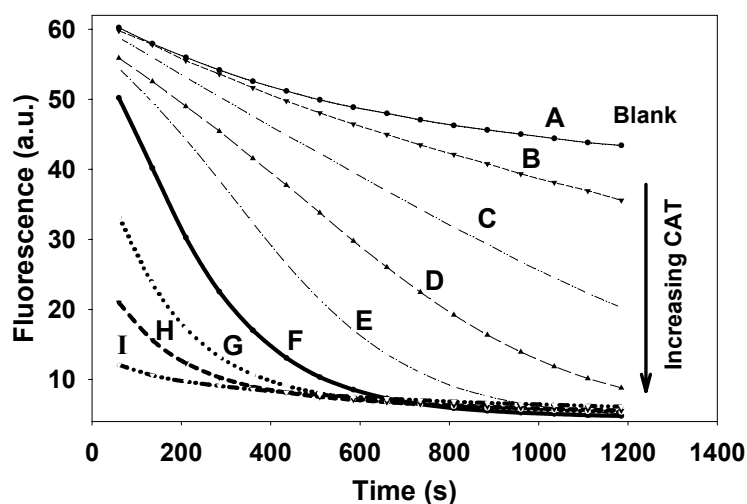


Figure 5.1. Kinetics of the decomposition of the EuTc-HP system by catalase. The activities of catalase are (from top) 0 (= blank), 1.02, 1.53, 3.07, 6.13, 30.7, 51.1, 102.2, and 204.4 unit/mL, respectively. The conc. of EuTc was 52 $\mu\text{mol L}^{-1}$ (with respect to Tc), that of H₂O₂ was 0.4 mmol L^{-1} .

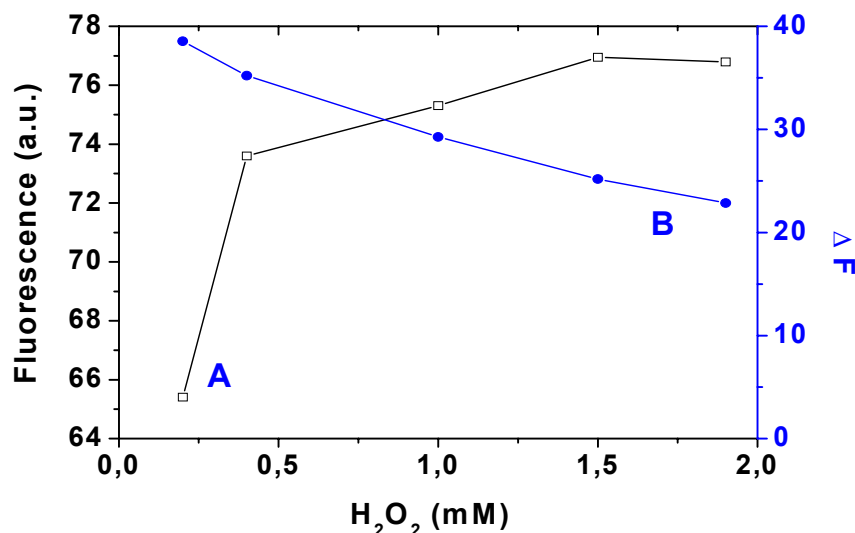


Figure 5.2 Optimization of the concentration of H₂O₂ for the detection of catalase. Curve A: Fluorescence intensity of EuTc-HP without adding catalase. Curve B: difference between blank and fluorescence intensity after 10 min in presence of 10.2 unit/mL of catalase and 0.32 mmol L⁻¹ EuTc (with respect to Tc).

The effect of the concentration of H₂O₂ on the assay can be seen in Figure 5.2. Firstly, an increase in concentration largely enhances the fluorescence of the system (left axis of Figure 5.2). However, higher H₂O₂ concentrations result in a smaller change of the fluorescence on addition of CAT, as seen on the right axis in Figure 5.2. This is due to the fact that the most sensitive range of EuTc to H₂O₂ concentration is at less than 0.6 mmol L⁻¹ (Figure 5.3). Although higher H₂O₂ concentrations resulted in higher fluorescence, the decrease in fluorescence due to the consumption of H₂O₂ was smaller. Consequently, smaller changes are observed at high H₂O₂ levels. In any case, the assay only works in the range where consumption of H₂O₂ makes a difference to the total amount of EuTc-HP. Furthermore, the activity of the CAT is proportional to the concentration of H₂O₂^{13, 19, 20}. The balance of the three aspects led us to use a 0.4 mmol L⁻¹ concentration of H₂O₂ in the well, and this concentration was applied in the recommended procedure. It resulted not only in high fluorescence, but also in relative large signal changes, however without significant deactivation of CAT.

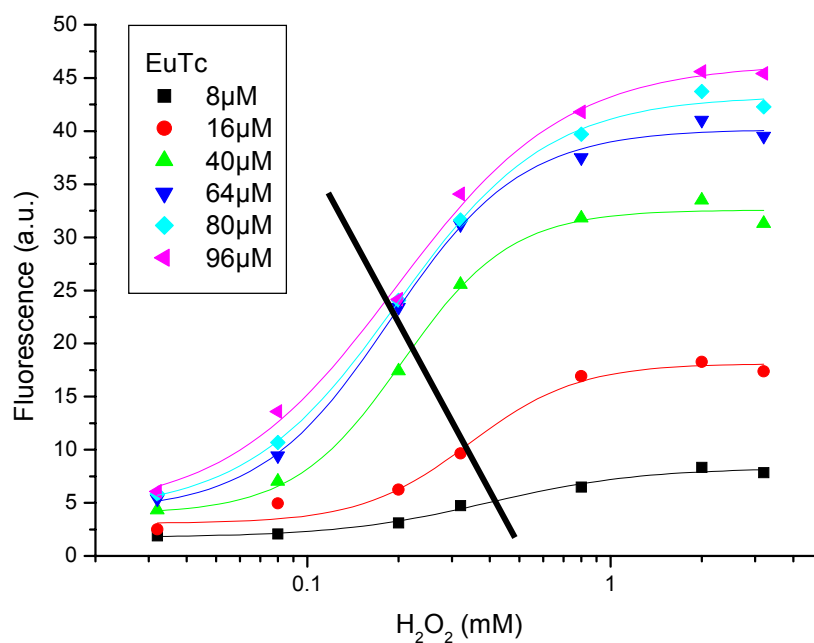


Figure 5.3. Effect of the concentration of hydrogen peroxide on the fluorescence intensity of EuTc-HP; EuTc concentrations (with respect to Tc) ranging from 8 (bottom), to 16, 40, 64, 80 and 96 (top) $\mu\text{mol L}^{-1}$, respectively.

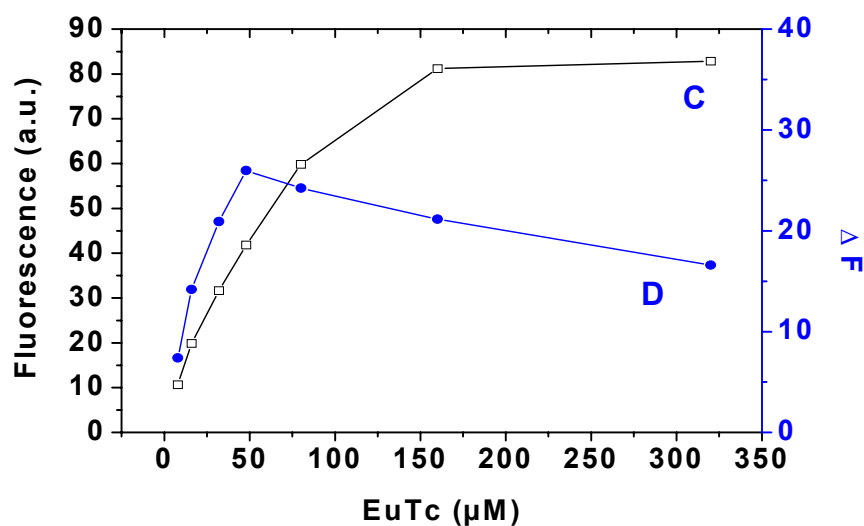


Figure 5.4. Optimization of the concentration of EuTc for the detection of catalase. Curve C: Fluorescence intensity of EuTc-HP (formed from EuTc and H_2O_2) without adding catalase (= blank). Curve D: Difference between blank and fluorescence intensity after 10 min in presence of 1.0 mmol L^{-1} of hydrogen peroxide and 10.22 unit/mL of catalase.

The concentration of the probe EuTc-HP was also optimized. As shown in Figure 5.4, the optimal concentration is at around $50 \mu\text{mol L}^{-1}$. Although an increase in the concentration resulted in an increase in fluorescence intensity, the relative decrease as a result of addition of CAT reached a maximum at a concentration of $50 \mu\text{mol L}^{-1}$, but decreased on further increasing it. As shown in Figure 5.3, the point of inflection shifts with the concentration of EuTc.

A calibration plot for the CAT kinetic assay as described in the recommended protocol is given in Figure 5.5A. The linear range of the catalytic activity of catalase is from 1 to 10 unit/mL, the linear regression equation being described $y = 4.540 + 2.758x$ ($r = 0.99$, $P < 0.0001$). The limit of detection (LOD; $S/N = 3$) is 1.0 unit CAT per mL. The limit of detection was further improved by incubation over 30 min and at 37°C . As shown in Figure 5.5 B, the LOD is 46 milliunit/mL, with a linear range between 46 and 400 milliunit/mL.

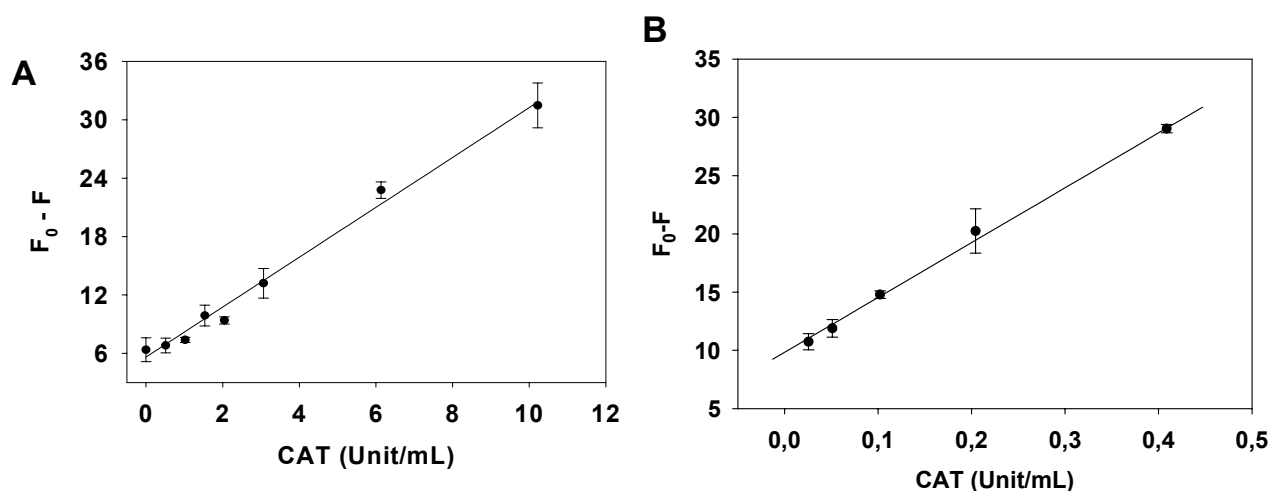


Figure 5.5. Calibration curves for catalase. Graph 6A: calibration curve for catalase with a specific activity between 1 and 10 unit/mL by kinetic detection without incubation. Graph 6B: calibration curve for catalase with a specific activity between 49 and 400 milliunit/mL of catalase by one-point detection after 30 min incubation at 37°C . The solution was $50 \mu\text{mol L}^{-1}$ in EuTc (with respect to Tc), 40mmol L^{-1} in H_2O_2 ; and the total volume ($250 \mu\text{L}$) was made up with MOPS buffer.

Kinetic determination which exploits the time-dependent differences in fluorescence intensity is considered to be advantageous, especially for fast CAT-assisted reactions. When scanning the wells of a microplate, there will be a time delay between the single wells. In case of performing a one-point measurement after typically 30 min, the effect of the time delay of the readings of the single wells will not be significant any more. The improved LOD of the 30-min assay can be further explained by Figure 5.3: a longer incubation time, an increased activity of CAT along with a higher temperature will cause distinctly more H_2O_2 to be consumed in the steepest range of the EuTc-HP fluorescence. Consequently, much less CAT can be quantified.

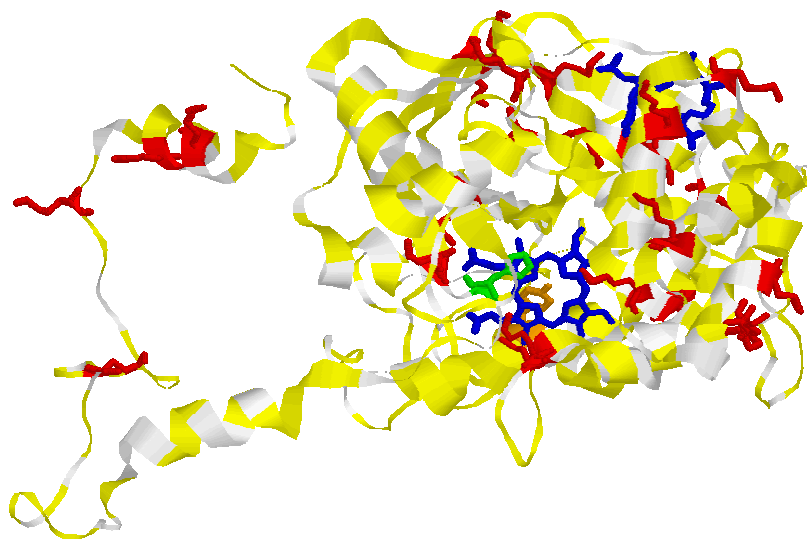


Figure 5.6. Monomer structure of catalase (tetramer). (His 74 in green color)

5.2.2. Inhibition and Denaturation of Catalase

3-Amino-1,2,4-triazole (3-AT) is a specific CAT inhibitor, which in presence of H_2O_2 , inhibits CAT by reacting with the functional groups (His 74) in the active center of CAT (Figure 5.6). The inhibition effect of 3-AT on CAT as monitored via the new probe is

shown in Figure 5.7. 3-AT acts as a specific inhibitor of CAT only in the presence of H_2O_2 . As can be seen from Figure 5.7, 3-AT inhibits the reaction, while 3-AT has little effect on the fluorescence of the EuTc-HP system. If denatured CAT is used, no difference with the blank was observed in fluorescence, while active CAT had a large effect. The inhibition and denaturation experiments show that it the decrease observed in fluorescence is due to the enzymatic consumption of H_2O_2 by CAT, and not by other effects such as interactions between EuTc and CAT.

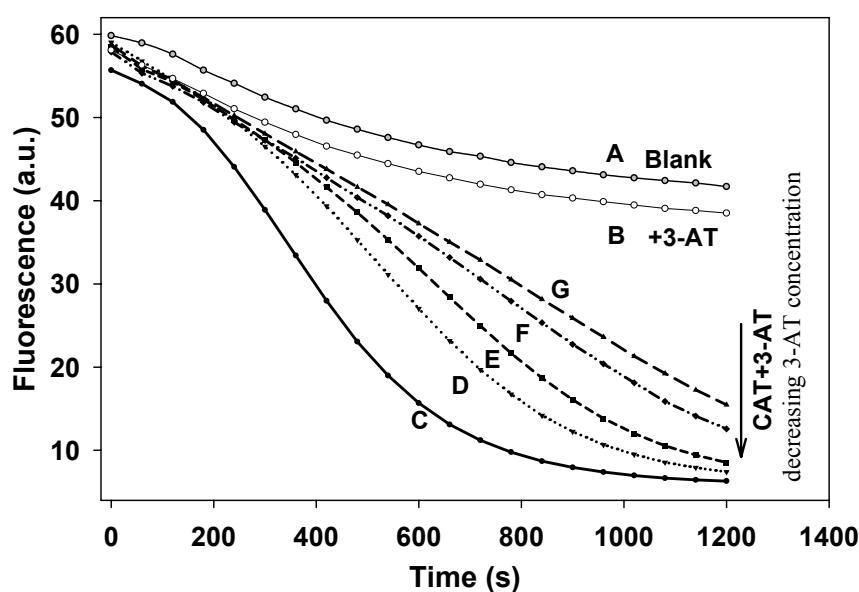


Figure 5.7. Specific inhibition of catalase by 3-amino-1,2,4-triazole (3-AT). A: blank; B: blank plus 3-AT; C: plus catalase but without 3-AT; D to G: plus catalase and 3-AT in concentrations of 2.2, 6.7, 9.0 and 11.2 mmol L^{-1} , respectively. The following concentrations were employed: EuTc: 52 $\mu\text{mol L}^{-1}$ (with respect to Tc); H_2O_2 1 mmol L^{-1} , CAT 10.2 unit/mL).

5.2.3. Interferents

The possible interference of common anions and cations on the detection was also explored. The fluorescence of the EuTc-HP complex system is not affected by alkali, alkali earth and ammonium ions, nor by anions including chloride, bromide, iodide, sulfate and

nitrate in up to ~100 mmol L⁻¹ concentrations. Fluoride acts as a weak quencher if present in a concentration higher than 0.1 mmol L⁻¹. However, phosphate and copper(II) ions are strong quenchers of the system. Furthermore, the fluorescence of the EuTc-HP system is weakly quenched by molecular oxygen. An 11% decrease in fluorescence intensity was observed on going from nitrogen-saturated solutions to air-saturated solutions.

Among the conceivable organic interferents that were tested, ascorbate, uric acid, bilirubin and glutathione interfere weakly in displaying a slight quenching effect on the EuTc-HP system if present in concentrations of >6.4, 40.0, 6.9, and 15.8 μmol L⁻¹ respectively in the wells. Fortunately, these species usually are present in constant concentrations in catalase assays. Alternatively, calibration may be performed in presence of these interferents.

5.2.4. Discussion

Describe here is what appears to be the first direct fluorescent probe for catalase. From the findings presented so far we conclude that the EuTc-HP probe is a ternary complex system, in which H₂O₂, on addition to EuTc, replaces water molecule(s) ligated to Eu³⁺ to form a new ligand, without however undergoing any significant redox reactions. Binding would be weak as anticipated, and in order to create measurable quantities of the EuTc-HP complex, a substantial fraction of "free" H₂O₂ is needed to drive the reaction to the right side.



Hence, Eq. 5.3 is better formulated as Eq. 5.4:



In order to schematically indicate that a fraction of H_2O_2 is present in "free" form. If "free" H_2O_2 is decomposed by catalase, equilibrium (4) is shifted to the left side, i. e. to the less fluorescent EuTc complex. Alternatively, one may assume that the H_2O_2 bound to EuTc in the EuTc-HP complex (Eq. 5.3 and Eq. 5.4) is directly decomposed by CAT (for a schematic description of both situations see Figure 5.8). We do, however, not favor this assumption because (a) H_2O_2 is present in excess, (b) CAT is highly specific for H_2O_2 , and (c) the active site of CAT hardly accessible for the relatively large EuTc-HP complex.

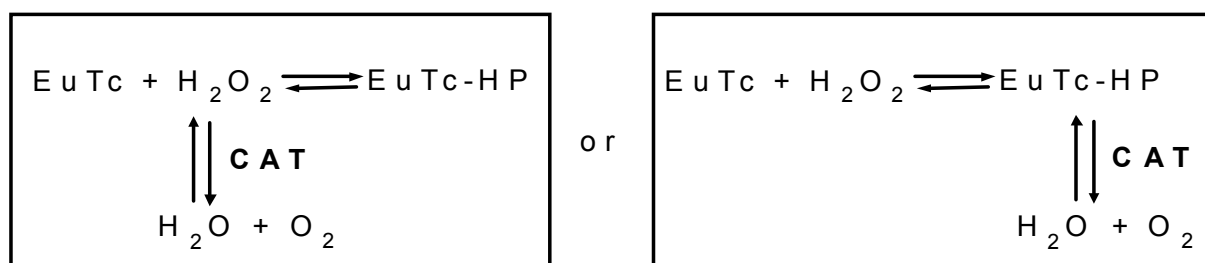


Figure 5.8. Schematic representation of the two conceivable mechanisms of the decomposition of the EuTc-HP system by catalase.

Previous studies have revealed that the effect observed on addition of H_2O_2 is largest if the molar ratio of Eu:Tc is 3:1. We find the same here for the reverse reaction (caused by CAT). The unusual stoichiometry has therefore been the subject of further studies. A Job plot (fluorescence intensity vs. ration of Eu:Tc, see Figure 6.9) gave the same molar ratio (3:1). Attempts failed to obtain crystals for performing an x-ray structural analysis. Circular dichroism spectra and UV spectra (Figure 2.1) are hardly different for EuTc and EuTc-HP, respectively. Thus, the structure of the system is not elucidated yet. The existence of 2:1 complexes such as the Cu_2Tc complex²¹ is noted here, along with the fact that the number of binding sites of Tc is strongly pH dependent²².

Due to the fast reaction rates of CAT¹³, the reaction mechanism does not imply the formation of a detectable enzyme-substrate complex, as is the case in most enzyme-catalyzed reactions. Consequently, the activity of CAT depends on the concentration of H₂O₂ being present initially. Moreover, H₂O₂ in concentrations above 0.1 mol L⁻¹ even deactivates CAT. An optimized H₂O₂ concentration therefore has to be a trade-off between the two features of this unique catalytic system for the optimal sensitive detection. Unlike in other enzyme detection schemes, the concentration of the substrate (H₂O₂) has to be specified when specifying activity. Unfortunately, some researchers have proposed other definitions of activity, but without clearly specifying the working concentrations of H₂O₂, a fact that makes comparison of data from different laboratories rather difficult.

Numerous optical assays for catalase have been developed. Table 5.1 summarizes some features of merits for commonly used assays for catalase. In the recommended photometric assay⁸, the H₂O₂ concentration (as determined by photometry at 240 nm) typically drops from 10.2 to 9.3 mmol L⁻¹. Despite its disadvantages, this method is still widely used, for example when studying catalase overexpression, probably because it is the only direct kinetic method and requires a single substrate only (H₂O₂).

The Trinder reagents²³, like other chromogenic phenols, aromatic amines or aminophenazones, are applied in combination with peroxidase for detection of catalase. In a recent report¹³, 3,5-dichloro-2-hydroxy-benzenesulfonate is used as a chromogenic substrate (see Table 5.1). Unfortunately, any involvement of peroxidase in the detection procedure will change the H₂O₂ concentration in the system and thus will affect the activity of CAT.

The Amplex method²⁴ allows for an ultrasensitive fluorescent determination of CAT. A two-step procedure is recommended to avoid the interference by peroxidase. However, this

two-step endpoint detection limits its applicability to continuous kinetic assays. Chemiluminescence detection of catalase^{10,11} has also been developed, especially for the case of extremely low concentration of H₂O₂. Again, kinetic continuous detection is rather difficult.

Compared to the above methods for CAT detection, the one described here is directly kinetic (or one-point after prolonged incubation), works at a clearly defined H₂O₂ concentration and at neutral pH, and does not require the addition of other substrates or enzymes. The assay can be performed using microplates and is fully compatible with plate readers. Additional features of this probe include a Stokes shift of 210 nm, a line-like emission centered at 616 nm (where background luminescence from biological materials and microplates is weak), a decay time in the μ s range, and excellent compatibility with the 405-nm diode laser. Such features provide distinct advantages over the UV method and two-step or two-reagent methods.

In conclusion, a novel fluorescent probe for the catalase and a one-step kinetic assay for the catalase are introduced. The probe enables an easy, direct, automation-compatible, relative inexpensive alternative to existing methods for detection and quantitation of CAT.

Table 5.1. Overview on commonly used assays for catalase and hydrogen peroxide (H₂O₂), and respective features of merit including limits of detection (LODs).

Method	Ref.	LOD for H ₂ O ₂	LOD for catalase (unit/mL)	H ₂ O ₂ concentration employed	Remarks
UV	8,9	-	~ 10	9.2 – 10.3 mmol L ⁻¹	photometry at 240 nm; kinetic
Amplex Red	24	50 nmol L ⁻¹	0.050	10-20 μmol L ⁻¹	fluorescence; two steps of 30 min each
Trinder	13	-	~ 0.1	unspecified	photometry at 505 nm; color inhibition
Chemiluminescence	10,11	-	~ 0.2	20 - 40 μmol L ⁻¹	in-situ generation of H ₂ O ₂ ; kinetic
EuTc-HP	this method	1.8 μmol L ⁻¹	0.046	400 μmol L ⁻¹	kinetic; gated measurements possible

Data for activity units are based on the Sigma definition:

(One unit decomposes 1 μmole of H₂O₂ per minute at pH 7.0 at 25 °C, while the H₂O₂ concentration falls from 10.3 to 9.2 mmol L⁻¹).

5.3. Experimental (Please see Chapter 7 for the reagents and instruments)

Recommended CAT Assay Protocol

Place, in each well of a thermostatted (30 °C) 96-well microplate, 65 μL of 0.2 mmol L^{-1} EuTc stock solution, 20 μL of a 5 mmol L^{-1} solution of H_2O_2 in water, and MOPS buffer to make up the volume to a total of 250 μL . After 10 min, the samples (50 μL) containing catalase with an activity between 5 and 100 unit/mL were added simultaneously, and the plates were read under intervals of shaking as programmed. Control experiments were conducted without adding catalase under similar conditions.

The kinetic change of the fluorescence was used for the quantification of the activity of catalase. The kinetic changes in fluorescence between 0 and 10 min (F_0 and F respectively) were used for calibration versus the activity determined by UV spectrophotometry at 240 nm. For detection of extremely low activities, a one-point detection (i. e., a single measurement after a fixed period of time) was used with F_0 as the blank without CAT and F as the fluorescence with CAT after a 30-min incubation at 37 °C.

5.4. References

1. Nomenclature Committee of the International Union of Biochemistry and Molecular Biology (NC-IUBMB) (1999) Enzyme Supplement 5. *Eur. J. Biochem.* 264, 610-650
2. Bai, J., Rodriguez, A., Melendez, J., Cederbaum, A. (1999) Overexpression of catalase in cytosolic or mitochondrial compartment protects HepG2 cells against oxidative injury. *J. Biol. Chem.* 274, 26217-26224.
3. Kahlos, K., Soini, Y., Sormunen, R., Kaarteenaho-Wiik, R., Paakko, P., Linnainmaa, K., Kinnula, V. (2001) Expression and prognostic significance of catalase in malignant mesothelioma. *Cancer* 91, 1349-1357,
4. Mittler, R. Berkowitz, G. (2001) Hydrogen peroxide, a messenger with too many roles? *Redox Report* 6, 69-72
5. Nasci, C., Da Ros, L., Campesan, G., Van Vleet, E. S., Salizzato, M., Sporni, L., Pavoni, B. (1999) Clam transplantation and stress-related biomarkers as useful tools for assessing water quality in coastal environments. *Marine Poll. Bull.* 39, 255-260.
6. Kang, D. H., Dougherty, R. H., Clark, S., Costello, M. (2002) Catalase activity for rapid assessment of high-level total mesophilic microbial load in milk. *J. Food Sci.* 67, 1844 - 1846
7. Guwy, A. J., Martin, S. R., Hawkes, F. R., Hawkes, D. L. (1999) Catalase activity measurements in suspended aerobic biomass and soil samples. *Enzyme Microb. Technol.* 25, 669-676.
8. Aebi H., (1974) Catalases, in: Bergmeyer H.U. (Ed.), *Methods of Enzymatic Analysis*, Verlag Chemie (Weinheim) and Academic Press Inc. (New York), pp. 680 – 684.
9. Srivastava S., Dwivedi U. (2001) Plant regeneration from callus of *Cuscuta reflexa* – an angiospermic parasite – and modulation of catalase and peroxidase activity by salicylic acid and naphthalene acetic acid. *Plant Physiol. Biochem.* 39, 529 - 538
10. Mueller S., Riedel H., Stremmel W. (1997) Determination of catalase activity at physiological hydrogen peroxide concentrations. *Anal. Biochem.* 245, 55 – 60
11. Khan S., Jin, E., Sojic N., Pantano P. (2000) A fluorescence-based imaging-fiber electrode chemical sensor for hydrogen peroxide *Anal. Chim. Acta* 404, 213 – 221
12. Kroll R. G., Frears E. R., Bayliss A. (1989) An oxygen electrode-based assay of catalase activity as a rapid method for estimating the bacterial content of foods. *J. Appl. Bacteriol.*, 66, 209 - 217.
13. Slaughter M. R, O'Brien P. J. (2000) Fully-automated spectrophotometric method for measurement of antioxidant activity of catalase. *Clin. Biochem.* 33, 525 – 534.
14. Wolfbeis O., Duerkop A., Wu M., Lin Z. (2002) Europium ion-based luminescent sensing probe for hydrogen peroxide. *Angew. Chem., Int. Ed.* 41, 525–534.

15. Duerkop A. (2002) Determination of hydrogen peroxide in conjunction with oxidases using lanthanoid-ligand complexes as optical indicators. *Eur. Pat. Appl.* EP 1,239,049.
16. Rakicioglu Y., Perrin J. H., Schulman S. G. (1999) Increased luminescence of the tetracycline-europium(III) system following oxidation by hydrogen peroxide. *J. Pharm. Biomed. Anal.* 20, 397-399
17. One unit will decompose 1.0 μmole of H_2O_2 per min at pH 7.0 at 25°C , while the H_2O_2 conc. falls from 10.3 to 9.2 mmol L^{-1} , measured by the rate of decrease of A_{240} . See Sigma website for the details.
18. Schomburg, D., Stephan D. (eds.), *Enzyme Handbook*, Springer, Berlin, 1994, Catalase P3
19. Diaz A., Rangel P., DE OCA Y., Lledias F., Hansberg W. (2001) Molecular and kinetic study of cataclase-1, a durable large catalase of neurospora crassa. *Free Radical Biol. Med.* 31, 1323–1333
20. Kettle, A.J, Winterbourn, C.C. (2001) A kinetic analysis of the catalase activity of Myeloperoxidase, *Biochemistry* 40, 10204-10212
21. Jezowska-Bojczuk, M., Lambs, L., Kozlowski, H., Berthon, G. (1993) Metal ion-tetracycline interactions in biological fluids. 10. Structural investigations on copper(II) complexes of tetracycline, oxytetracycline, chlortetracycline, 4-(dedimethylamino)tetracycline, and 6-desoxy-6-demethyltetracycline and discussion of their binding modes. *Inorg. Chem.*, 32, 428-37.
22. Duarte, H. A., Carvalho, S., Paniago, E. B., Simas, A. M. (1999) Importance of tautomers in the chemical behavior of tetracyclines. *J. Pharm. Sci.* 88, 111-120.
23. Fossati P., Prencipe L., Berti G. (1982) Use of 3,5-dichloro-2-hydroxybenzenesulfonic acid/4-aminophenazone chromogenic system in direct enzymic assay of uric acid in serum and urine, *Clin. Chem.* 26, 227-231.
24. <http://www.probes.com/handbook/sections/1005.html>

Chapter 6. Further Applications and Structure of EuTc-HP

6.1. Application of GOx-based ELISA

Enzyme-linked immunosorbent assays (ELISA)^{1,2,3,4} have been widely utilized as one of the basic immunoassays in clinical research^{5,6,7} for the diagnostic and understanding of diseases, in biochemical research for signal transduction⁸ and other cell regulatory processes⁹, and in pharmaceutical industry for the discovery and screening of potential therapeutic drugs^{10,11,12}. The enzymatic amplification nature has made it one of the most sensitive methods for the analysis of the biologically important molecules. Peroxidase (POx), alkaline phosphatase, and galactosidase have been mostly used as enzyme labels for the fluorescent or chemiluminescent measurements^{13,14,15,16}, while catalase and glucose oxidase (GOx) are only sometimes used due to the lack of direct assays and their available assays always have to be coupled with POx. Time-resolved fluorescent immunoassays, such as dissociation enhanced lanthanide fluoroimmunoassay (DELFLIA)^{17,18,19}, have more advantages than the usual fluorescent assays because of their ability to eliminate the background fluorescence of proteins.

Here, a GOx-based ELISA assay for IgG is presented. Its principle is indicated in Figure 6.1, as an application of the EuTc fluorescent probe for H₂O₂. The GOx ELISA is

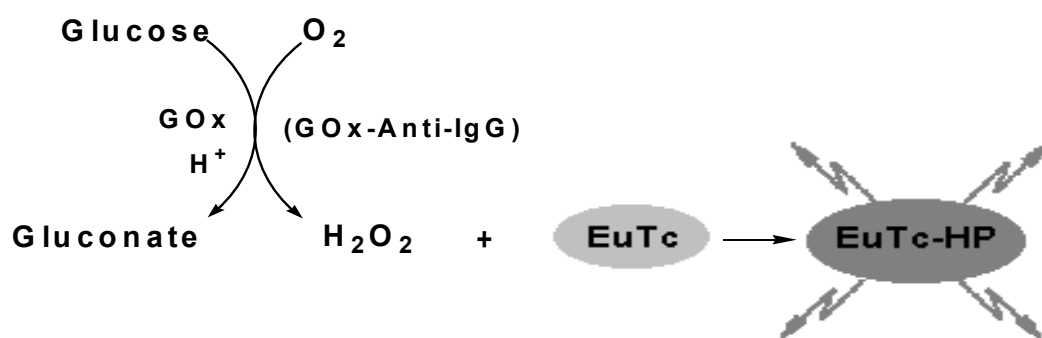


Figure 6.1 Scheme of the principle of GOx-ELISA.

based on the direct determination of H_2O_2 produced by the GOx catalyzed reaction. H_2O_2 binds with EuTc to form EuTc-HP which is highly fluorescent and has a μs lifetime for the potential time-resolved measurements.

Two schemes of ELISA have been tested as shown in Figure 6.2 (see section 6.5.1 for protocol). Sandwich ELISA needs two different antibodies to recognize the target antigens (IgG here) and offers amplification functions, while direct ELISA only need the enzyme-labeled antibody for amplification purposes. Sandwich ELISA usually is more complicated than direct ELISA but with better sensitivity.

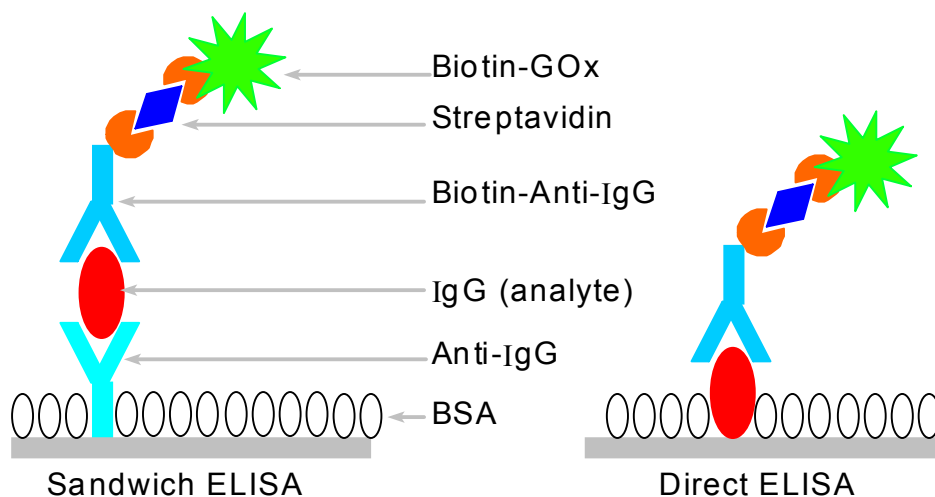


Figure 6.2 Schemes of sandwich (capture) GOx-ELISA and Direct GOx-ELISA.

The kinetic studies on the GOx-ELISA in sandwich format are shown in Figure 6.3. The fluorescence changes as the formation of EuTc-HP through the GOx-labeled anti-IgG, which is immobilized through the immunobinding to the analyte IgG. It catalyzes the oxidation of glucose, thereby forming H_2O_2 . The amount of GOx conjugated anti-IgG can be determined by the fluorescence intensity of EuTc-HP system, and therefore the amount of IgG in sample. Curve (E) is a time trace over 50 min for blank, which is handled exactly the same as other wells, except adding no target molecular IgG. (A) to (C) are curves of kinetic process

with increasing concentration of IgG, and consequently increasing amount of GOx-anti-IgG. With increasing GOx-anti-IgG, from (A) to (C), the slope of curve, as well as the intensity, is increasing, which can be used to analyze IgG. The similar time response is also observed for the direct GOx-ELISA.

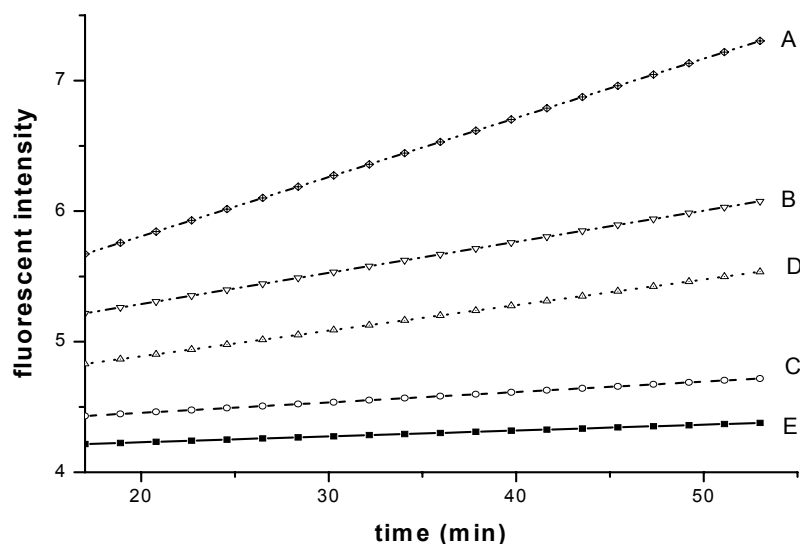


Figure 6.3 Time trace of the formation of EuTc-HP from EuTc and hydrogen peroxide produced by GOx-Anti-IgG conjugate. (A)-(C) trace after incubation of 250, 150, 50, 15 ng/ml of IgG, respectively; (E) blank.

The calibration curves (see 6.5.1 for protocol) of IgG by the end-point of fluorescence are shown in Figure 6.4. It shows that (1) for sandwich GOx-ELISA, its limit of detection ($S/N = 3$) is 3 ng/ml, and the linear range is between 10 – 250 ng/ml, $y = 0.12 + 0.010x$, $r = 0.99$; (2) for direct GOx-ELISA, the limit of detection ($S/N = 3$) is 20 ng/ml, and the linear range is between 50 - 500 ng/ml, $y = 0.051 + 0.005x$, $r = 0.99$; (3) the sandwich GOx-ELISA with the fluorescent EuTc probe is more sensitive than the direct GOx-ELISA; (4) the sandwich GOx-ELISA can fit for the requirements of regular clinical assay and direct GOx-ELISA can be available for the determination of high concentrations of IgG.

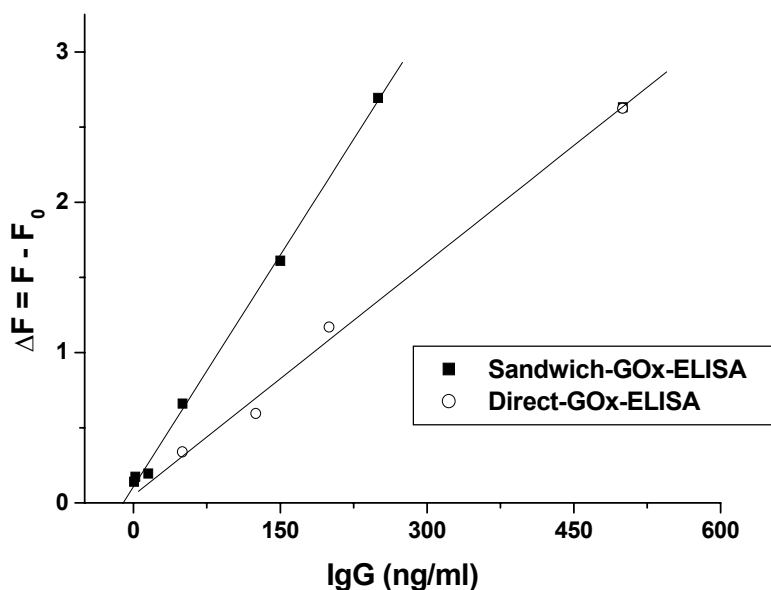


Figure 6.4 Calibration plot for IgG by GOx-Anti-IgG in the well of a microplate versus the increase in fluorescence intensity ($F - F_0$) over 50 min

GOx has been used before for ELISA^{20,21}, but much less than POx or others, partially because most of the GOx assays need POx as well. Compared with earlier GOx-ELISA, the method offered here can be performed without the need of POx and offers the potential of time-resolved application, especially in the light of recent development of protein chip²² array technology. As the most studied enzyme for immobilization, GOx shows much more advantages than POx in chip-based ELISA for the proteomics²³, if a direct measurement without the need of coupling POx is presented as seen here.

6.2. The Catalase/Glucose Oxidase System

Coupled enzyme systems have long been recognized as a superb tool for studying complicated enzymes and as a way of quantifying enzyme substrates. Most of the multi-enzyme systems are cascade systems such as those for creatinine, cholesterol, and choline. Some of them are steady-state system, where the consumption and the production of the substrate reach a steady state. Examples include the catalase-glucose oxidase system, the Krebs cycle, and in biological organelles, such as the peroxisome²⁴. The steady-state enzyme system usually requires the reversible probes rather than irreversible ones to monitor the kinetic changes, if possible in real time. Based on the reversible interaction of EuTc with H₂O₂, a catalase–glucose oxidase system is studied by the EuTc/EuTc-HP fluorescent system as a platform for screening of antioxidative agents, especially those inhibit the oxidases, or those promote catalase.

6.2.1. The Catalase/Glucose Oxidase System as a Platform for Screening

While there are numerous reports on screening platforms for kinases and phosphatases^{25,26}, seldomly any screening platforms for oxidative processes have been studied. The reversible fluorescent EuTc/EuTc-HP system may also be used in studies on peroxisomes, in particular its steady state that is reached by normal chronic response and by emergency acute response, as was shown by Mueller²⁴ et al. for peroxisome proliferation using a flow injection chemiluminescent system for H₂O₂ detection.

As mentioned earlier in this thesis, the fluorescence intensity of EuTc-HP is much higher than that of EuTc, and the highly fluorescent EuTc-HP system (formed from EuTc and

H₂O₂ at neutral pH and at room temperature) is decomposed to the less fluorescent EuTc system. As shown in Figure 6.5, EuTc and EuTc-HP form a reversible system.

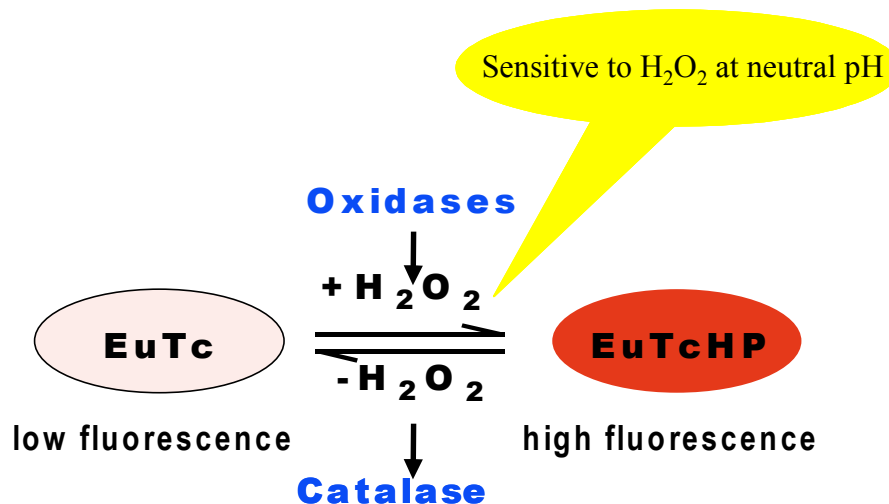


Figure 6.5 Reversible EuTc/EuTc-HP system

The reversibility is confirmed by the following findings: (1) Catalase, which is highly specific for H₂O₂, can decompose H₂O₂ in the EuTc-HP system and turn it back into EuTc if H₂O₂ is fully consumed. (2) The catalase-specific inhibitor 3-AT²⁷, retards the reaction, and increasing quantities of 3-AT result in a distinctly decreased activity; (3) The formation of EuTc-HP and its decomposition are nonoxidative processes in view of the minute differences in the absorbance and circular dichroism (CD) spectra between the two species as in Figure 2.1. In fact, the CD spectra are rather similar, and no significant new peak is observed that would point to reaction products with quite different chemical structure from tetracycline. (4) The reversibility of the fluorescent H₂O₂ system is further demonstrated by a coupled reaction involving glucose, glucose oxidase (GOx) and catalase (catalase) as shown in Fig. 6.6(A) (see section 6.5.2 for experimental details).

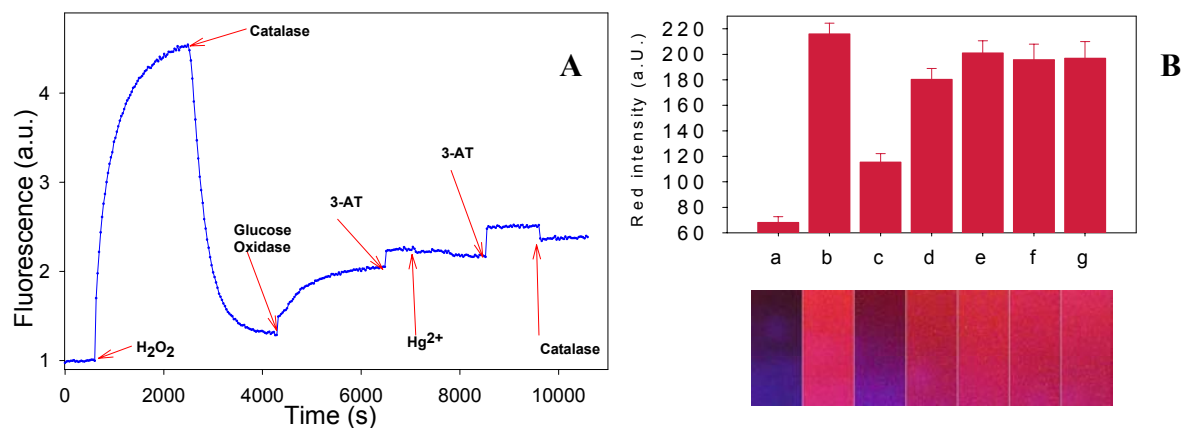


Figure 6.6 The coupled CAT-GOx system as a platform for screening. (A) the kinetic response of the EuTc-HP and the coupled CAT-GOx system. (B) lower part: photographic images of the different steps (a to g) as in experimental section 6.5.2; upper part: the intensity pattern of the red fluorescence of the respective images in the lower part.

The formation of the coupled GOx-CAT enzymatic system is shown in Figure 6.6 A. When H₂O₂ is added to a solution containing EuTc and glucose in MOPS buffer, a large increase in fluorescence is observed due to the formation of EuTc-HP. Subsequently, catalase is added upon which a continuous decrease in fluorescence intensity can be seen (due to catalytic decomposition of H₂O₂ by catalase). On further addition of GOx (which produces more H₂O₂), the system turns into a coupled GOx-CAT enzymatic system, which is known for its production of constant H₂O₂ in steady state for at least hours^{28,29}.

The advantages of the coupled system composed of catalase and glucose oxidase (GOx) are best presented by acting as a model for a screening platform for studying activation and inhibition. As can be seen in Figure 6.6 A, the steady state of the system responds to inhibitors of catalase (3-AT) and GOx (Hg²⁺, a potent GOx inhibitor³⁰). Fluorescence increases as 3-AT is added, and decreases on addition of Hg²⁺, thus forming a new system for antioxidative drug screening. Since screening is often performed in the imaging mode, the digital pictures at different stages of the experiment that reflect the time course of the red fluorescence intensity (Figure 6.6 B) are also taken for the quantitative imaging processing.

The dynamic changes can also be manifested by an animation of the series of the digital photos or video.

6.2.2. Detection of Catalase Independent of H₂O₂

As a alternative to the method of Chapter 5, the activity of catalase may also be determined by the catalase-GOx coupled system, with the additional feature that it will be independent of the actual H₂O₂ concentration in the media. This may help to overcome current limitations when comparing catalase activities which are known to be dependent on substrate concentration. Since in the coupled system described above the final (steady state) concentration of H₂O₂ is proportional to $k_{GOx}/k_{catalase}$ ²⁸, and by keeping the concentrations of glucose and dioxygen at constant levels, the response of the system is a direct parameter of the activity of catalase that is independent of the H₂O₂ concentration. A respective calibration plot is given in Figure 6.7. This approach is much simpler and versatile than the method given in a recent report²⁴.

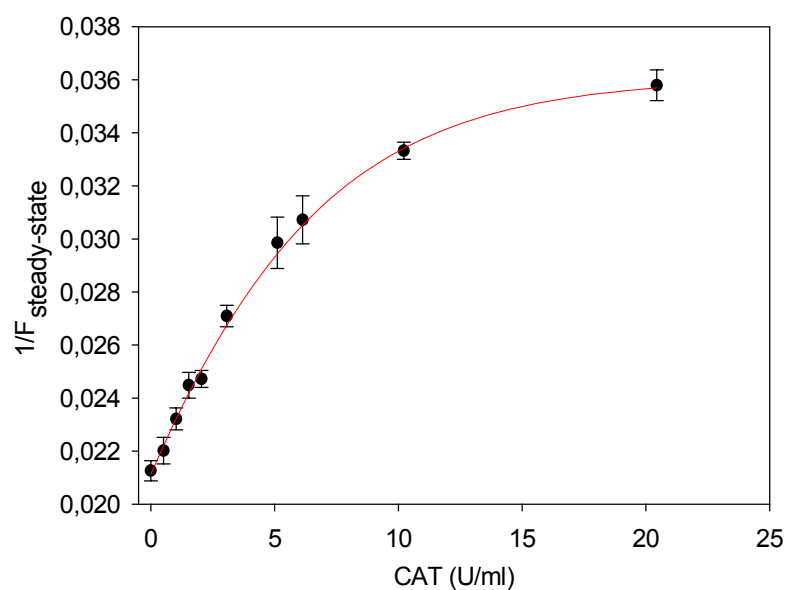


Figure 6.7. Determination of catalase (CAT) activity using EuTc-HP. Calibration graph for a determination based on the catalase-GOx steady-state equilibrium.

6.3. Construction of Microplate Arrays and Sensors

Starting from the earlier single analyte (point) detection, the most recently development of the bioanalysis is the use of two dimensional arrays for high-throughput screening and multi-analyte measurements. Besides different microarrays, such as DNA chips³¹, fluorescence-based fiber optic arrays³², there have been new advances using microplates as the matrix for array construction³³ for the multiple analyte determination.

Initiated by the site-specifically immobilized enzyme arrays³⁴, a study on the construction of arrays and sensors is presented here that is based on the fluorescent EuTc and EuTc-HP probes. The scheme has been integrated into microplate (MTP) technology (in order to form disposable sensor arrays and for the use of fluorescence imaging which allows the reading of all parameters simultaneously).

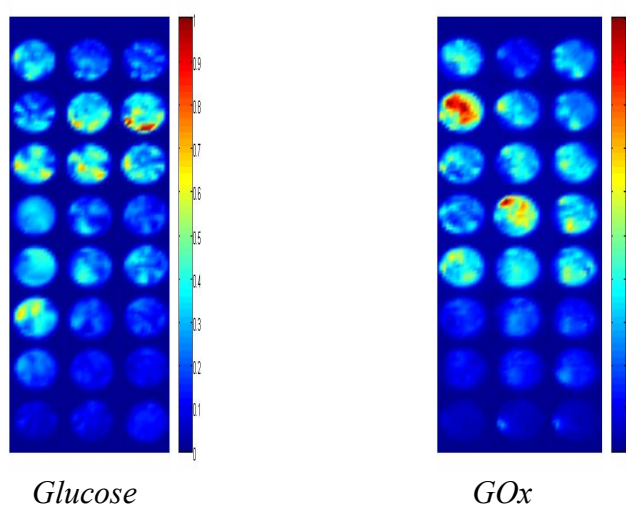


Figure 6.8. Fluorescence images of microplate array and sensor for glucose and GOx.

The microplate sensors and arrays are constructed by the immobilization of biotinylated glucose oxidase on streptavidin-coated microplate through the biotin-avidin interactions. The fluorescence images are shown in Figure 6.8. Figure 6.8 (A) is for the determination of glucose with the same concentration of the biotinylated glucose oxidase,

with increasing concentration of glucose specified in Table 6.1, and in triplicate as shown in column a, b, c. Figure 6.8 (B) is for the measurement of immobilized GOx with the same concentration of glucose, with increasing concentrations of GOx for immobilization specified in Table 6.2, and also in triplicate as column a, b, c. The RLD lifetime-based imaging method was applied as well, with the same composition of the samples in the wells.

Table 6.1 Composition of the samples for glucose sensor (array).

	1	2	3	4	5	6	7	8
GOx-Biotin	0	0	20	20	20	20	20	20
EuTc	0	100	100	100	100	100	100	100
Glucose	0	0	0	1	2	5	8	10
MOPS	200	100	80	79	78	75	72	70
Total	200	200	200	200	200	200	200	200
GOx-Biotin(mU)	0	0	1370	1370	1370	1370	1370	1370
Glucose(mM)	0	0	0	1.39	2.77	6.93	11.01	13.86

Table 6.2 Composition of the samples for glucose oxidase (array).

	1	2	3	4	5	6	7	8
GOx-Biotin	0	20	50	20	50	20	50	85
EuTc	100	100	100	100	100	100	100	100
Glucose	15	15	15	15	15	15	15	15
MOPS	85	85	85	85	85	85	85	85
Total	200	200	200	200	200	200	200	200
Glucose(mM)	20.81	20.81	20.81	20.81	20.81	20.81	20.81	20.81
GOx-Biotin(mU)	0	0.108	0.271	1.082	2.706	10.82	27.06	46.00

As anticipated, the fluorescence intensity imaging is not as homogeneous as the RLD fluorescence imaging. Despite the variation between the triplicates, they still show the same trend as a change of glucose concentrations or the immobilized GOx on microplates. These preliminary results of the images confirm the feasibility of the construction of microplate-based sensors and arrays for the determination of glucose and of GOx immobilized on the microplates. The purpose is for multienzyme arrays for the assay of multi-substrates simultaneously on a single shot of detection with microplates.

6.4. Composition of the Fluorescent Probes

Lanthanide(III) ion complexes have received much attention during the last two decades for their interesting photophysical properties and their usages as candidates for a number of applications. Ln(III) ions, due to their unique luminescence properties, such as long luminescence decay time and narrow emission bands, can form highly luminescent complexes with specific ligands. In such complexes due to strong ligand absorption and efficient energy transfer from the ligand to the metal ion (termed as 'antenna effect'), strong Ln(III) luminescence is observed, overcoming the very small absorption coefficients of the lanthanide(III) ions. There are mainly two classes of such specific ligands³⁵. The first, e.g. cryptands, calixarenes, β -diketones, macrocyclic ligands, carboxylic acid derivatives, and etc, involves the system that are effectively coordinatively saturated by octa- or nonadentate ligands and forming kinetically stable binary complexes (mostly 1:1 complexes). This kind of ligands usually is not affected by the environment and consequently is mainly applied as labels for bioassays. The second class, such as tetracycline, however, usually relates to complexes that are not coordinatively saturated. There are always water molecules involved in the inner field of the coordination field, resulting in smaller quantum yields, shorter lifetimes. This kind of ligands in most cases has lower overall stability and is prone to form ternary complexes, sometimes even multi-nuclear complexes, rather than the 1:1 binary complexes. These complexes are relatively less developed than the first ones. However these complexes can be applied as fluorescent probes rather than fluorescent labels, which are sensitive to certain analytes in the aqueous media, such as the EuTc-HP complex presented here.

In fact, there are quite a few reports about the properties and structure of the europium tetracycline complexes, such as earlier reports by Schulman³⁶, et al. on tetracycline

detection, and Ci, et al.³⁷ on nucleic acid detection. Compared to the earlier research, the EuTc-HP system here is a ternary complex sensitive to H₂O₂, with a peculiar metal-to-ligand ratio of 3:1. In this section, the peculiar composition of the probe will be further studied.

6.4.1. Stoichiometry and Structure

There is an unusual molar ratio (3 to 1) of Eu to Tc as a sensitive probe for H₂O₂. The case only happens for H₂O₂ binding with the EuTc complex. As shown in Figure 6.9 A, Job's plot has been applied for the determination of the molar ratio in the EuTc-HP complex. The fluorescence intensity reaches the highest when the molar ratio of Eu to Tc is 3:1 in the EuTc complex, in different H₂O₂ concentrations. Hence, EuTc is in 3:1 molar ratio as applied in different applications throughout this study. This is quite peculiar, since there have been plenty of reports^{36,38} on the EuTc complex itself. Earlier researches have suggested a 1:2 molar ratio of the complex and later the ratio was corrected to be 1:1 through different methods of characterization. It is also confirmed by our own experiment that, with no H₂O₂ presented, the molar ratio in EuTc complex is 1:1 when fluorescence is the highest.

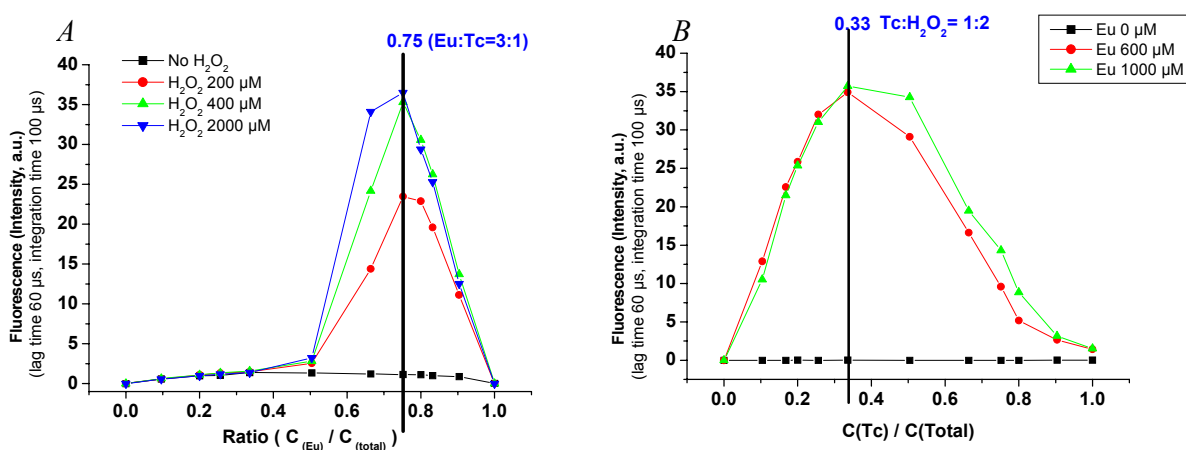


Figure 6.9 Job's plot for EuTc-HP.

A. Eu³⁺ to Tc molar ratio in different conc. of H₂O₂, C_{total}=C_{Eu}+C_{Tc};

B: Tc to H₂O₂ molar ratio in different conc. of Eu³⁺, C_{total}=C_{H2O2}+C_{Tc}.

The exact structure of EuTc, especially EuTc-HP therefore is of great interest. Although a variety of techniques have been used to study the complexation behavior of tetracycline and various derivatives, the results obtained have led to partly contrary assignments of the chelation sites. Depending on the chosen experimental conditions, i.e. nature of the solvent, pH as well as ligand-metal molar ratio, tetracyclines can form complexes exhibiting a 2:1, 1:1, or 1:2 ligand:metal stoichiometry^{39,40}.

For example, Mg^{2+} was reported³⁹ to form a 2:1 metal to ligand complex when in excess, binding to N4-O3 at the A-ring site and O12-O11 at the BCD ring (Figure 6.10). This can be partially supported by the observed shift of the long wavelength band attributed to binding of Mg^{2+} to Tc at N4-O3 and the observed shoulder on the long wavelength absorption band and the observed pronounced increase in the integrated fluorescence intensity attributed to the other Mg^{2+} chelates to O12-O11. Another example is the oxovanadium(IV) ions complexes with Tc⁴⁰, which form a 2:1 metal–ligand binuclear complex with tetracycline at pH 6. The isolated binuclear complex has been characterized with the proposed structure shown in Figure 6.10. Therefore it is reasonable to suggest that tetracycline can also form a 2:1 metal–ligand binuclear complex like Mg^{2+} and oxovanadium(IV) ions.

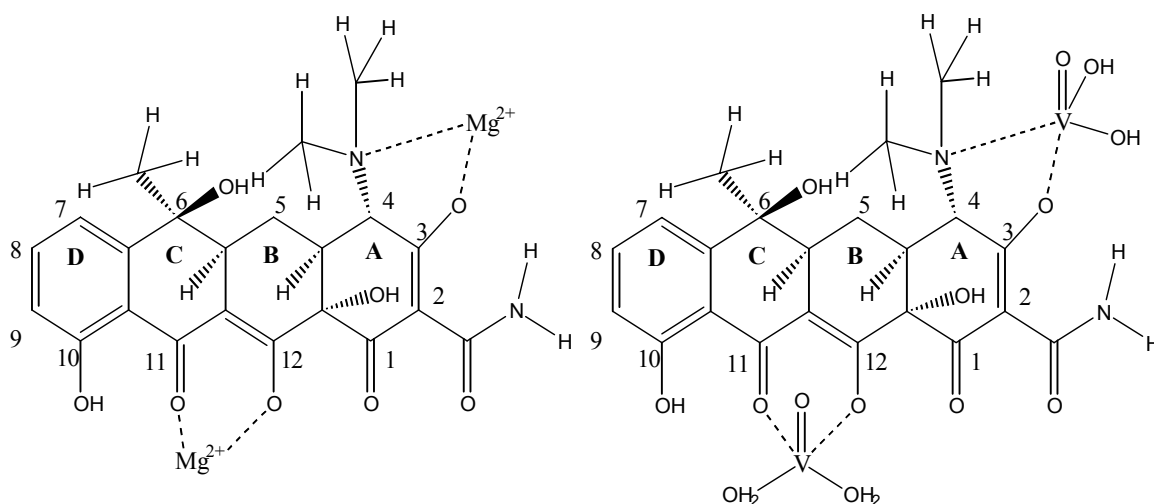


Figure 6.10 Proposed molecular structures of the $2Mg^{2+}$ -Tc and $2VO^{2+}$ -TC complexes.

On the other hand, pH is a significant factor on tetracycline, since that at different pH, Tc can be in different form (even different tautomers) of protonation. The possible binding sites of metal ions depend on the nature of the solvent and the pH value, since chelation occurs predominantly at basic sites, and metal ions (as well as Eu^{3+}) prefer O and N donors. Tetracycline exhibits three macroscopic acidity constants, the assignments of which have been widely accepted, despite some controversy depending on the solvents and presence of metal ions. In aqueous environment the first deprotonation ($\text{p}K_1 \sim 3\text{-}4$) occurs at OH3. The second $\text{p}K$ value is attributed to OH12 ($\text{p}K_2 \sim 7.3\text{-}8.1$), and the third one to the protonated nitrogen of the $(\text{CH}_3)_2\text{-}$ group ($\text{p}K_3 \sim 8.8\text{-}9.8$)^{40,41,42}, as shown in Figure 6.11.

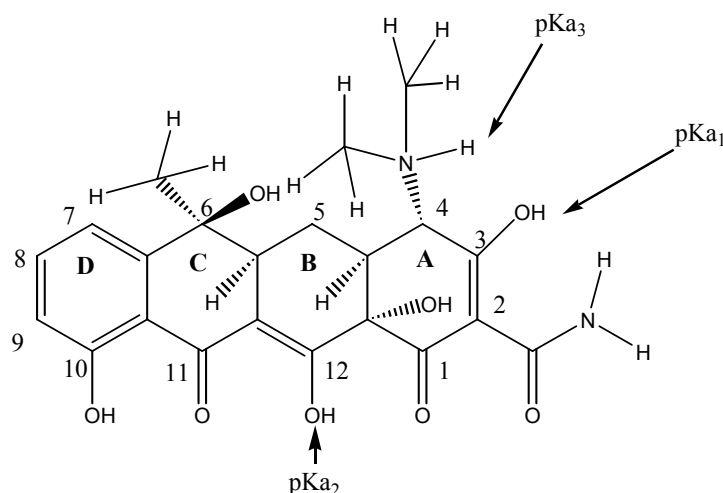


Figure 6.11 Tetracycline structure and assignment of $\text{p}K_{\text{a}}$ s.

As calculated from the $\text{p}K_{\text{a}}$ values of tetracycline (Figure 6.12), the main forms at pH 6.9 which has the highest fluorescence for EuTc-HP, are H_2Tc^- and H_3Tc^0 . In the presence of Eu^{3+} , tetracycline, and H_2O_2 , the pH of the system is determined by the tetracycline protonation, europium hydrolysis and the extremely weak protonation of H_2O_2 , if there is no other reactions involved. Although the optimal pH of 6.9 might be reasonable from the pH additional effects of the presence of the several species, these evidence still can not explain the 3:1 stoichiometry of EuTc-HP, and further clarification is still needed.

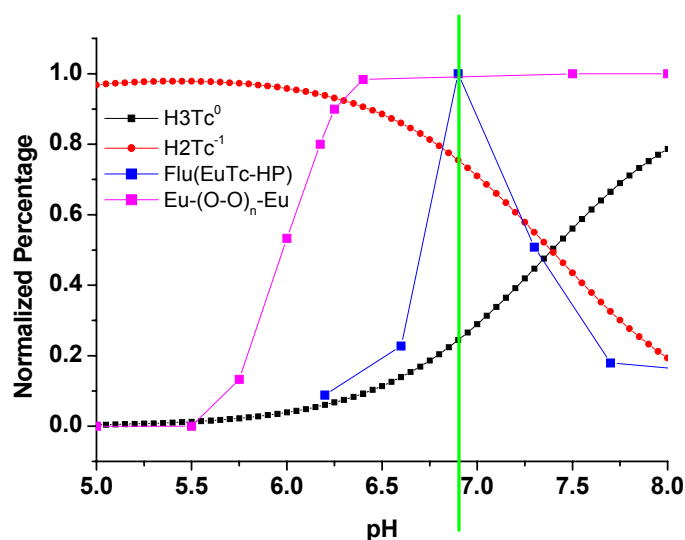
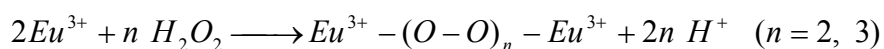


Figure 6.12 pH-dependent form of tetracycline.

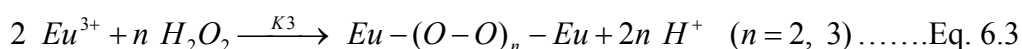
Black and red lines as the pH-dependent percentage of H_3Tc^0 and H_2Tc^{-1} . Blue line as the pH-dependent fluorescence of EuTc-HP. Cyan line as the pH-dependent formation of $Eu-(O-O)_3-Eu^{44}$

First suggested as a mechanism step in the catalytic hydrolysis of RNA⁴³, the following equilibrium was suggested for the reaction between Eu^{3+} and H_2O_2 :



This equilibrium was further tested with pH variation as simulated in Figure 6.12 as the line of $Eu-(O-O)_n-Eu$. At $pH > 6.5$, a fairly stable $Eu^{3+}-(O-O)_n-Eu^{3+}$ ($n=3$) system is formed for the specific accelerated hydrolysis of RNA⁴³.

As a summary of all above arguments, the following mechanism steps are suggested for the explanation of the peculiar molar ratio of Eu to Tc in the EuTc-HP complex:



The possible structure of EuTc-HP is proposed as shown in Figure 6.13. The proposed structure and mechanism up to now offer the only reasonable explanation for the 3:1

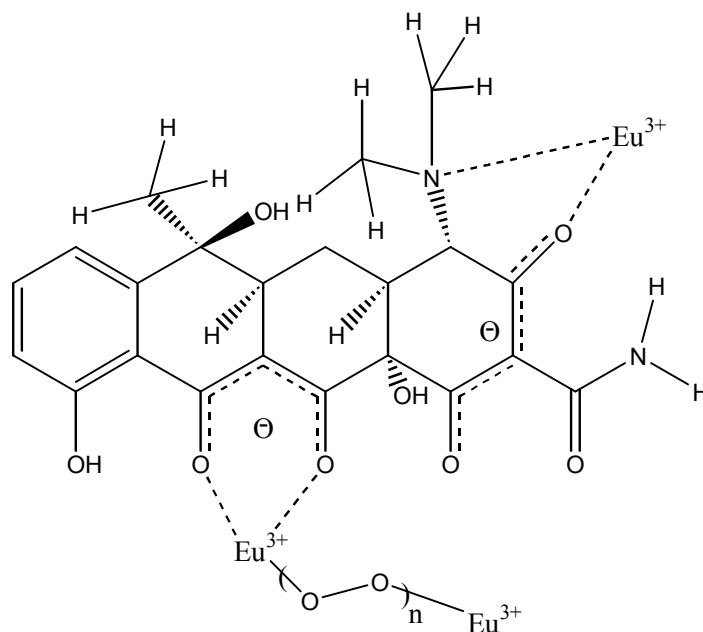


Figure 6.13 Proposed structure of EuTc-HP in the form of EuTc-HP

metal–ligand EuTc-HP complex. The previous considerations on (1) the oxidation of tetracycline; (2) formation of free radicals; (3) formation of peroxo europium ions; and (4) formation of H_2O_2 adduct⁴⁴, were either ruled out (such as tetracycline oxidation, or formation of free radicals), or could not offer a reasonable explanation for the stoichiometry. Furthermore, the proposed structure also results in the enhanced fluorescence and prolonged fluorescence lifetime same as the other possibilities mentioned above. The formation of the Eu complex in the O11-O12 site (or the BCD ring), just as that binding for Mg^{2+} ; the replacement of possible inner field water molecules of the Eu binding to Tc by peroxide linkage, and the possible electron withdrawing effect of the far end Eu^{3+} facilitating the energy transfer from Tc to Eu, all might contribute to the fluorescence characterization of EuTc-HP. In addition, since the K_3 in the mechanism step of Eq. 6.3 is in the range of

$3.3 \times 10^{-31} \text{ M}^2$ ($n=3$) or $1.4 \times 10^{-23} \text{ M}$ ($n=2$)⁴³, the formation of the a fairly stable $\text{Eu}^{3+}-(\text{O}-\text{O})_n-\text{Eu}^{3+}$ is most likely reversible. It also partially gives an explanation of the multi-component luminescence decay of EuTc and EuTc-HP.

It should be noted that this structure is not confirmed yet, partially due to the instability of the peroxide complex, especially in solid form, which has hindered the effort of the further structural characterization. There are also small conflicts, such as the molar ratio of Tc to H_2O_2 as obtained from Job's plot is 1:2 (Figure 6.9 B), rather than 1:3, so that n is more likely to be 2 in $\text{Eu}^{3+}-(\text{O}-\text{O})_n-\text{Eu}^{3+}$ while the $\text{Eu}^{3+}-(\text{O}-\text{O})_2-\text{Eu}^{3+}$ complex has a higher pH to obtain stable complex, such as pH 7.5, although this might be explainable through further calculation of optimal pH in EuTc-HP.

6.4.2. Combinatorial Approach for Discovery of New Lanthanide Probes

The uncertainty of the structure of EuTc-HP results in the combinatorial approach for the further development of new lanthanide–tetracycline fluorescent probes. The basic idea behind the approach is the variation of the tetracycline structure for an even better probe for H_2O_2 . In the experiments, the 3:1 stoichiometry and a pH of 6.9 are also applied.

The preliminary results (structures fluorescence intensities and quantum yields) are summarized in Figure 6.14, Figure 6.15 and Table 6.3.

Analysis of the luminescence spectra and quantum yield leads us to the following conclusions: 1) oxidation in X4 position does not greatly affect the quantum yield of the fluorescent probe, as shown in the case of oxytetracycline as a decomposition product of Tc. This also further rules out the tetracycline oxidation mechanism. 2) The spatial hindrance in X5 position is not important for the generation of the fluorescence, such as with

rolitetraacycline hydrochloride. This offers the possibility for the covalent immobilization of tetracycline for the construction of sensors based on EuTc complexes. 3) The hydroxyl group in X3 is quite important. Without it, the quantum yields are normally low as in the cases of minocycline hydrochloride and minocycline hydrochloride. 4) The spatial hindrance in X2 position has some effects on the fluorescence generation as compared the chlortetracycline hydrochloride and the demeclocycline hydrochloride. 5) In X1 position, the electron donating and withdrawing groups have similar minimal effect, but the spatial hindrance is harmful for the fluorescence.

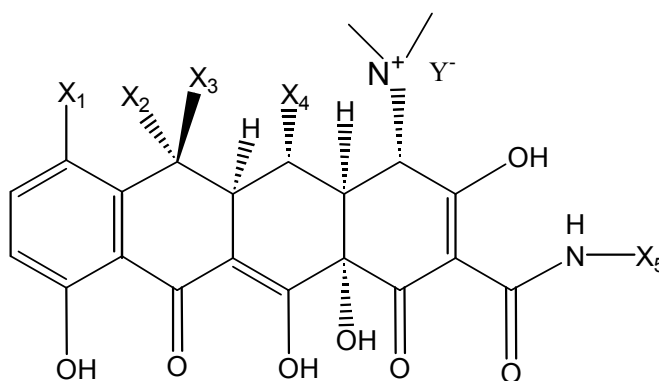
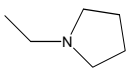


Figure 6.14 The structures of tetracycline and its analogs.

Table 6.3. The structures of tetracycline and its analogs

Name (Tx)	X1	X2	X3	X4	X5	Y	Quantum yield (EuTx-HP, %)	
Tetracycline hydrochloride	A	H	Me	OH	H	H	Cl	4.0
Chlortetracycline hydrochloride	B	Cl	Me	OH	H	H	Cl	1.2
Rolitetraacycline hydrochloride	C	H	Me	OH	H		Cl	4.3
Oxytetracycline hydrochloride	D	H	Me	OH	OH	H	Cl	5.7
Demeclocycline hydrochloride	E	Cl	H	OH	H	H	Cl	2.6
Doxycycline hydrochloride	F	H	Me	H	OH	H	Cl	1.5
Minocycline hydrochloride	G	-N(CH ₃) ₂	H	H	H	H	Cl	0.5
Meclocycline sulfosalicylate salt	H	Cl	=CH ₂	OH	H	Sulfo-salicylate		0.8

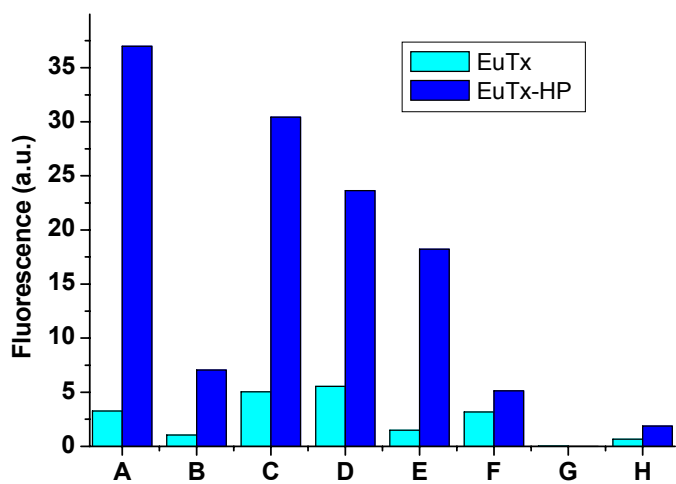


Figure 6.14 Fluorescence of EuTx and EuTx-HP as specified in Table 6.3.

A-H as in Table 6.3

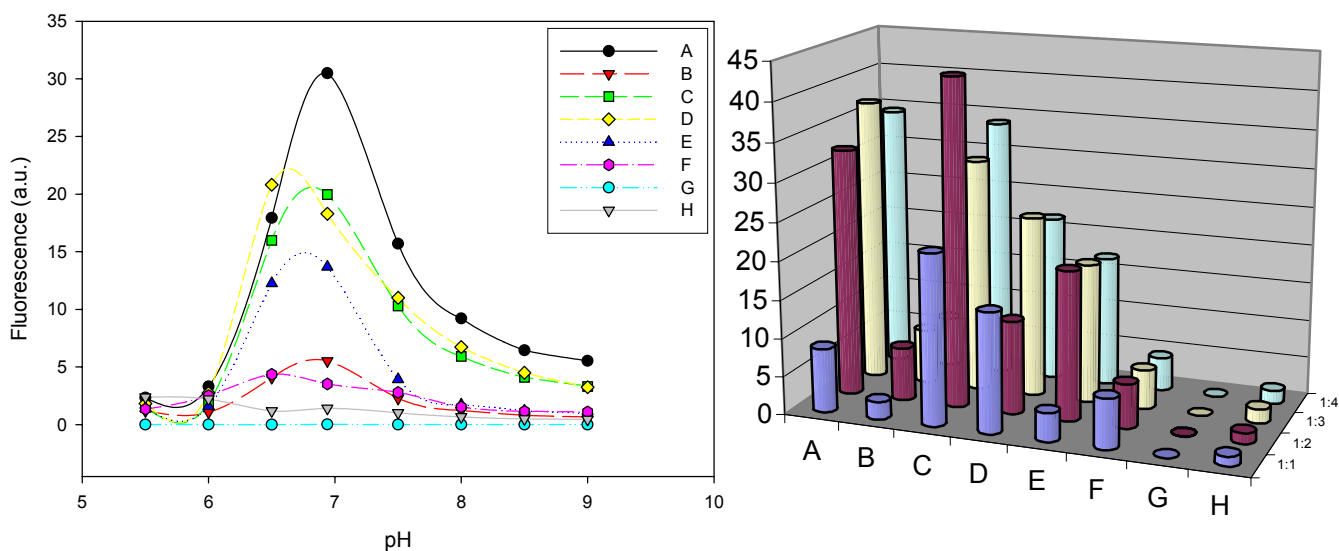


Figure 6.15 pH optimum(A) and optimal molar ratios of Eu to Tx (B) of all EuTx-HP

A-H as in Table 6.3

The pH optimum and optimal molar ratios of all EuTx-HP is shown in Figure 6.15.

These knowledge provides the basis for the further molecule design for the better lanthanide probes for H_2O_2 .

6.5. Experimental (Please see Chapter 7 for the reagents and instruments)

6.5.1. Protocol of GOx-labeled Immunoassay

The scheme of sandwich GOx-ELISA is shown in Figure 6.2. The affinity reaction is proceeded as: (1) add 200 μ l rabbit anti-bovine-IgG at a concentration of 5 μ g/ml in PBS into each well of a polystyrene U-bottom microplate, incubate at 37 °C for 1 hour. Alternatively, incubate at 4 °C overnight; (2) block remaining binding sites in each well by incubating with 220 μ l of 1% BSA, incubate at 37 °C for 30 min; (3) add 200 μ l diluted sample antigen bovine IgG in PBS to each well, incubate at 37 °C for 1 hour; (4) add 200 μ l of monoclonal anti-bovine IgG biotin conjugate at 1:1000 in each well, incubate at 37 °C for 1 hour; (5) add 200 μ l of 10 μ g/ml streptavidin in PBS to each well of microplate, incubate at room temperature for 30 min, then add 200 μ l of 3 U/mL GOx-biotin in PBS to each well of the microplate, incubate at room temperature for 30 min. Between two coatings, rinse 3 times by PBS. Last rinse with MOPS buffer before adding the EuTc probe. PBS was used for the incubation steps and later was washed out at last step of washing.

The fluorescence detection is as following: 250 μ l of of EuTc and glucose mixture (as prepared by mixing 5.0 ml of EuTc stock solution, 5.0 ml of 27 mmol/L glucose solution, and MOPS buffer to make up volume to 25 ml. The solution should be prepared fresh every times.) is added to each well of samples. The kinetic curve of the change or the end-point of fluorescent intensity of EuTc-HP system after incubating 50 - 60 min was record on Fluoroskan Ascent fluorescence microplate reader.

The direct GOx-ELISA process is the same as the sandwich GOx-ELISA except for coating with 200 μ l diluted bovine IgG to each well and incubate at 37 °C for 1 hour.

6.5.2. Coupled GOx-Catalase Enzymatic System

650 μL of the EuTc stock solution were placed in a cuvette, upon which 40 μL of glucose (0.2 M) and 1010 μL of MOPS buffer were added. After fluorescence intensity remained constant, the following solutions were sequentially added: 200 μL of H_2O_2 (5 mM), 5 μL of catalase ($1.28 \times 10^4 \text{ U} \cdot \text{mL}^{-1}$), 160 μL of GOx ($47.1 \text{ U} \cdot \text{mL}^{-1}$), 70 μL of 3-AT (28 mM), 2.0 μL of a saturated solution of $\text{Hg}(\text{NO}_3)_2$ in MOPS, another 70 μL of 3-AT, and 2 μL of catalase, and the time trace of fluorescence intensity monitored as shown in Figure 6.6(A). The images, video and animation pictures were obtained by monitoring a similar sequence involving addition of **a**: 650 μL of the EuTc stock solution, 40 μL of glucose (0.2 M) and 1010 μL of MOPS buffer. **b**: further addition of 200 μL of H_2O_2 (5 mM), **c**: 5 μL of catalase ($1.28 \cdot 10^4 \text{ U} \cdot \text{mL}^{-1}$), **d**: 200 μL of GOx ($47.1 \text{ U} \cdot \text{mL}^{-1}$), **e**: 70 μL of 3-AT (28 mM), **f**: 2.0 μL of a saturated solution of $\text{Hg}(\text{NO}_3)_2$ in MOPS, and **g**: 5 μL of catalase ($1.28 \times 10^4 \text{ U} \cdot \text{mL}^{-1}$). The images of different stages (**a** to **g** in Fig. 6.6(B)) were processed for the histogram and the mean values of the red fluorescence intensities as shown in Figure 6.6(B).

6.5.3. Construction of Microplate Sensors and Arrays

The microplate sensors and arrays are constructed by the by the immobilization of biotinylated glucose oxidase (biotinamidocaproyl labeled GOx) on the streptavidin coated microplate (Greiner 96 Well Platte F-form Black, μClear , Streptavidin coated) through the biotin-avidin interactions. The composition of the wells in the microplate is specified in Table 6.1 and 6.2. After the addition of biotinamidocaproyl labeled GOx in streptavidin coated plate, shake for 30-45 min. on Miniature Akku-Shaker from Edmund Bühler (KM2, www.edmund-buehler.de/english/index.html); then wash with MOPS for three times; finally add the other substrates and shake 30-40 min. After reading the plate composition by

fluorescence microplate readers, the fluorescence imaging of constructed sensors and arrays is performed same as that for GOx alone.

6.6. References

1. Miller, J.N.; Niessner, R.; Knopp, D. (2001) Enzyme- and immunoassays, in : Guenzler H, Williams A (eds) Handbook of analytical techniques, Wiley, p 162-166.
2. Kemeny, D.M. and Challacombe, S.J. (eds) (1988). ELISA and other solid phase immunoassays, John Wiley & Son Ltd.
3. www.immunochemistry.com
4. Dasgupta, A; Chow, L; Nazareno, L; Tso, G; Datta, P. (2000) J. Clin. Lab. Anal. 14(5), 224-229.
5. Van Dyke, K. and Van Dyke R (1990) Luminescence immunoassay and molecular applications, CRC Press, Boca Raton, p 35.
6. Sokoll, L. J.; Chan, D. W. (1999) Anal. Chem. 71(12), 356R-362R.
7. Hage, D. S. (1999) Immunoassays. Anal. Chem. 71(12), 294R-304R.
8. Hopkins, J. (2002) Veterinary Immunology and Immunopathology 87(3-4), 245-249.
9. Pines, J. (1997) Methods in Enzymology , 283(Cell Cycle Control), 99-113.
10. Nakayama, G. R. (1998) Curr. Opin. in Drug Discov. & Develop. 1(1), 85-91.
11. Self, C. H.; Cook, D. B. (1996) Curr. Opin. in Biotechn. 7(1), 60-5.
12. Augustin, Ch. M.; Oswald, B.; Wolfbeis, O. S. (2002) Anal. Biochem. 305(2), 166-172.
13. Parker, C. W. (1981) Annu. Rev. Pharmacol. Toxicol. 21 113-32.
14. Diamandis, E. P. (1988) Clin. Biochem.21(3), 139-50.
15. Stoellner, D; Stoecklein, W; Scheller, F; Warsinke, A. (2002) Anal. Chim. Acta 470(2), 111-119.
16. Puget, K.; Michelson, A. M.; Avrameas, S. (1977) Anal. Biochem. 79(1), 447-56.
17. Markela, E.; Stahlberg, T. H.; Hemmilae, I. (1993) J. of Immun. Methods 161(1), 1-6.
18. Hemmilä, I; Soini, E; and Lövgren T, (1982) Fresenius Z. Anal. Chem. 311, 357.
19. Meyer, Jorg; Karst, Uwe. (2001) Analyst 126(2), 175-178.
20. Hard, R. C., Jr.; Miller, W; Romagnoli, G. J. Histochem. and Cytochem. (1989), 37(6), 909-12.
21. Yoshioka, M.; Aso, C.; Hiraoka, T.; Kitajima, M.; Kuroda, M.; Sugi, M.; Parvez, H. Microchemical Journal (1994), 49(2-3), 235-43.
22. Borrebaeck, C. A. K. (2000) Immunology Today 21(8), 379-382.
23. Zeravik, J.; Ruzgas, T.; Franek, M. Biosensors & Bioelectronics (2003), 18(11), 1321-1327.
24. Mueller, S. et al. Biochem. J. 363, 483-491 (2002).
25. Sato, M., Ozawa, T., Inukai, K., Asano, T. Umezawa, Y. Nature Biotech. 20, 287-294(2002).
26. Nagai, Y. et al. Nature Biotechnology, 18, 313-316 (2000).

27. Mueller, S., Pantopoulos, K., Hentze, M. W. & Stremmel, W. In: *Bioluminescence and Chemiluminescence: molecular reporting with photons* (ed. Hastings, J. W., Kricka, L. J. and Stanley, P. E.) 338-341, Wiley & Sons Ltd, Chichester, 1997.
28. Pantopoulos, K. et al. *J. Biol. Chem.* 272, 9802-9808 (1997)
29. Toren, E. & Burger, F. *Mikrochim. Acta.* (3), 538-45 (1968).
30. Barlow, C; Lockhart, D. J. *Current Opinions in Neurobiology* (2002), 12(5), 554-561.
31. Epstein, J. R.; Walt, D. R. *Chemical Society Reviews* (2003), 32(4), 203-214.
32. Mayr, T; Igel, C; Liebsch, G; Klimant, I; Wolfbeis, O. S. *Anal. Chem.* (2003), 75(17), 4389-4396.
33. Butterfield, D. A.; Bhattacharyya, D. *Membrane Science and Technology Series* (2003), 8(New Insights into Membrane Science and Technology: Polymeric and Biofunctional Membranes, 2003), 233-240.
34. Diaz, A., Rangel, P., Montes de Oca, Y., Lledias, F. Hansberg, W. *Free Radical Biology & Medicine* 31, 1323-1333(2001).
35. Dickins, R. Batsanov, S, A. Beeby, A. Botta, M. Bruce, J. Howard, J. C. Love, D. Parker, R. Peacock, H Puschmann. *J. Am. Chem. Soc.* (2002)124, 12697 - 12705
36. Hirschy, L. M.; Van Geel, T. F.; Winefordner, J. D.; Kelly, R. N.; Schulman, S. G. *Analytica Chimica Acta* (1984), 166 207-19.
37. Liu, X; Li, Y; Ci, Y. *Analytica Chimica Acta* (1997), 345(1-3), 213-217.
38. L. M. Hirschy, E. V. Dose, J. D. Winefordner, *Anal. Chim. Acta* 147 (1983) 311.
39. Wessels, J. M.; Ford, W. E.; Szymczak, W.; Schneider, S.. *Journal of Physical Chemistry B* (1998), 102(46), 9323-9331.
40. De Paula, Flavia C. S.; Carvalho, Sandra; Duarte, Helio A.; Paniago, Eucler B.; Mangrich, Antonio S.; Pereira-Maia, Elene C.. *Journal of Inorganic Biochemistry* (1999), 76(3-4), 221-230.
41. Martin, R. B. In *Metal Ions in Biological Systems*; Siegel, H., Ed.; Marcel Dekker: New York, 1985; Vol. 19, pp 20-52.
42. Leeson, L. J.; Krueger, J. E.; Nash, R. A. *Tetrahedron Lett.* 1963, 18, 1155.
43. Kamitani, Jun; Sumaoka, Jun; Asanuma, Hiroyuki; Komiyama, Makoto. *Journal of the Chemical Society, Perkin Transactions 2: Physical Organic Chemistry* (1998), (3), 523-528.
44. Lis, S.; Hnatejko, Z.; Barczynski, P.; Elbanowski, M. *Journal of Alloys and Compounds* (2002), 344(1-2), 70-74.

7. Materials and Instruments

7.1. Materials and Reagents

All inorganic salts were of analytical purity and were obtained from Sigma-Aldrich (www.sigmaaldrich.com) unless otherwise stated. All solutions were prepared in a 10 mmol L⁻¹ 3-(N-morpholino)propanesulfonate (MOPS; from Carl Roth GmbH, www.carl-roth.de) buffer of pH 6.9 unless otherwise described. High-purity H₂O₂ was obtained from Merck (www.vwr.com) as a 30% solution. Working concentrations of H₂O₂ (5 mmol L⁻¹) were prepared daily fresh.

The EuTc reagent was prepared from EuCl₃ · 6 H₂O (from Alfa Products, www.alfa.com) and tetracycline hydrochloride (either from Serva, www.serva.de; or from Sigma). The EuTc stock solution was prepared by mixing 10 mL of a 6.3 mM EuCl₃ solution with 10 mL of a 2.1 mM tetracycline solution in MOPS buffer and diluted to 100 mL. This reagent is available from Chromeon GmbH (www.chromeon.com); and it may be further diluted to concentration required. Phosphate buffers should be avoided since phosphate binds to EuTc. Chlortetracycline hydrochloride, roli-tetracycline hydrochloride, oxytetracycline hydrochloride, demeclocycline hydrochloride, doxycycline hydrochloride, minocycline hydrochloride, meclocycline sulfosalicylate salt, and glucose were from Sigma-Aldrich.

Catalase (EC 1.11.1.6, from bovine liver; as a suspension, unit as defined by the provider) and 3-amino-1,2,4-triazole, as a specific inhibitor of CAT, were purchased from Sigma. Glucose oxidase (GOx, EC 1.1.3.4, from *Aspergillus niger*, 185,000 unit/g; unit as defined by the provider), and other oxidases (Uricase (urate oxidase), galactose oxidase, lactate oxidase, sarcosine oxidase) were from Sigma-Aldrich and were used without further

purification. The glucose stock solution was stored overnight before use to allow the equilibrium of α - and β -anomers. Rabbit anti-bovine IgG, bovine IgG, biotin-conjugated monoclonal anti-bovine IgG, biotinamidocaproyl labeled glucose oxidase, streptavidine, and bovine serum albumin (BSA), were from Sigma.

7.2. Instruments

Quantitative fluorescence measurements were performed on three microplate readers, one Fluoroskan Ascent (from Thermo Labsystems, www.labsystems.fi) for steady state fluorescence intensity measurement, one GENios+ (from Tecan, www.tecan.com) for time-resolved (“gated”) detection, and one FLUOstar OPTIMA for time-resolved and rapid lifetime determination detections (from BMG Labtechnologies GmbH, www.bmglabtech.com). The excitation filters were set to 405 nm, and the emission filters to 620 nm or 612 nm. All experiments were performed at a programmed temperature of 30.0 °C.

Fluorescence spectra and time traces of the coupled GOx-catalase system studies were acquired on an SLM AB2 luminescence spectrometer (Spectronic Unicam, www.unicaminstruments.com) in rectangular cells with stirring. Varian Eclipse fluorometer (Varian, www.varian.com) with microplate accessory has also been applied for the fluorescence spectra. Absorption spectra and spectrophotometric detection of catalase were performed on a Cary 50 Bio photometer (Varian).

Circular dichroism (CD) spectra were obtained from J-710 spectropolarimeter (Jasco Inc. www.jascoinc.com). Data were processed either with Spectra Manager Software from Jasco or with Excel. For videos and photos, a DCR-TRV8E Sony camcorder and an Olympus C4040 digital camera were used.

Either U-bottom transparent microtiterplates (MTP, microplate), or black Fluotrac 200, or flat bottom black MTPs with transparent bottom (96 wells; from Greiner bio-one, <http://www.greiner-lab.com>) were used. In some cases, a Hamilton Microlab dispensing robot was used for preparation of the microplates.

8. Summary

The thesis describes the development of a novel reversible H₂O₂ fluorescent probe comprising the ternary complex of europium(III), tetracycline and hydrogen peroxide; and its application in the assays of H₂O₂, of H₂O₂ producing oxidases and their substrates, and of H₂O₂ consuming catalase and its inhibitors. The probe is applied in steady-state intensity-based, time-resolved “gated”, or lifetime-based detection modes both for microplate fluorescence measurement and imaging.

The fluorescent probe’s advantages include the reversibility of the EuTc-HP system, the possibility of a kinetic real-time detection of the production and the consumption of H₂O₂, and the system works best at pH 6.9 - 7.0. It also exhibits the typical spectral characteristics of a ligand-to-europium energy transfer system which include a Stokes shift of ~210 nm, line-like emission, excitation at 380-420 nm (e.g. by the 405-nm blue diode laser), and a μ s decay time (~60 μ s) facilitating time-resolved fluorometry and imaging.

For the probe study, *Chapter 1* gives an overview of the state of art of the H₂O₂ measurements. In the following first part of *Chapter 2* is presented the characterization of the fluorescent EuTc-HP probe for its absorbance, circular dichroism and fluorescence spectra, fluorescence lifetime and decay profile, optimal pH and stability, and the influence of temperature, buffers, quenchers and interferents. In the last part of *Chapter 6*, the peculiar molar ratio of the EuTc-HP probe is further investigated for its possible structure and a combinatorial approach for discovery of new lanthanide probes is preliminarily proceeded as well.

Different assays have been developed for H₂O₂, glucose, glucose oxidase and catalase, as examples for the detection of enzyme substrates and enzymes. Furthermore, different fluorometric schemes have been applied, such as the steady-state intensity-based detection (*Chapter 5*, catalase), the time-resolved gated detections (*Chapter 3*, glucose), the rapid lifetime determination method (*Chapter 2*, H₂O₂, novel on microplate) and the time-correlated single photon counting method of the lifetime-based detection (*Chapter 2*, H₂O₂), for both microplates and cuvettes, compatible with high-throughput screening.

The μ s range lifetime of the EuTc-HP probe has greatly facilitated fluorescence imaging, a means for visualization and mapping of the analyte with multiple chemical information. Four schemes of imaging, those are the conventional fluorescence intensity imaging (FII), the time-resolved ("gated") imaging (TRI), the phase delay ratioing imaging (PDI), and the rapid lifetime determination imaging (RLI), have been tested for the quantitative analysis. Hydrogen peroxide, glucose, and glucose oxidase have been determined by the fluorescent imaging system, with *Chapter 4* highlighting the fluorescence imaging of glucose oxidase.

There are possible further applications in perspective for the EuTc-HP probe. *Chapter 6* summarizes the initial attempts, such as glucose oxidase based ELISA, the coupled catalase/glucose oxidase system as a platform for screening, and the construction of microplate arrays and sensors.

10. Patent and List of Recent Publications

Patent

German patent: Ger. Offen. DE 10155160 *Determination of catalases and peroxidases, their conjugates, substrates, activators and inhibitors using europium (III) complexes with ligands and hydrogen peroxide*. 2003, May 22.

US patent in application

Recent Publications

1. Wu, Meng; Lin, Z.; Wolfbeis, O. S. *Determination of the Activity of Catalase Using a Europium(III)-tetracycline Derived Fluorescent Substrate* Anal. Biochem. (2003), 320, 129–135.
2. Wolfbeis, O. S.; Duerkop, A.; Wu, Meng; Lin, Z. *A Europium-ion-based luminescent sensing probe for hydrogen peroxide*. Angew. Chem., Int. Ed. (2002), 41, 4495-4498.
3. Wolfbeis, O. S.; Boehmer, M.; Duerkop, A.; Enderlein, J.; Gruber, M.; Klimant, I.; Krause, C.; Kuerner, J.; Liebsch, G.; Lin, Z.; Oswald, B.; Wu, M. *Advanced luminescent labels, probes and beads, and their application to luminescence bioassay and imaging*. Springer Series on Fluorescence (2002), 2 (Ed. R. Kraayenhof, Fluorescence Spectroscopy, Imaging and Probes), 3-42.
4. Michael Schäferling, Meng Wu, Jörg Enderlein, Henrik Bauer, Otto S. Wolfbeis *Time-Resolved Luminescence Imaging of Hydrogen Peroxide Using Sensor Membranes in a Microwell Format* Applied Spectroscopy. in press (2003).
5. Wu Lei, Axel Dürkop, Zhihong Lin, Meng Wu, and Otto S. Wolfbeis *Detection of Hydrogen Peroxide in River Water via a Microplate Luminescence Assay with Time-Resolved ("Gated") Detection* Microchimica Acta. in press (2003).
6. Meng WU; Zhihong. LIN; Michael Schaeferling, Axel Dürkop; O. S. Wolfbeis *Direct Imaging Determination of Glucose Oxidase Activity Using a Fluorescent Europium (III) Tetracycline Probe*, submitted (2003).
7. Wu, Meng; Lin, Z.; Dürkop, A.; Wolfbeis, O. S., *Direct and Time-Resolved Enzymatic Determination of Glucose Using a Fluorescent Europium Probe for Hydrogen Peroxide*, submitted (2003).
8. Michael Schäferling, Meng Wu and Otto S. Wolfbeis. *Fluorescent Imaging of Glucose*, submitted (2003).

Poster and Presentation

1. Meng WU, Zhihong LIN, Axel Dürkop, Michael Schäferling, Otto Wolfbeis *Direct high-throughput detection and imaging of glucose and glucose oxidase using a fluorescent europium probe*. MAF - 8th Conference on Methods and Applications of Fluorescence Spectroscopy, Imaging and Probes, Aug. 24-27 2003, Prague, Czech.
2. Michael Schäferling, Meng Wu, Otto S. Wolfbeis *Time-Resolved Luminescent Imaging of Hydrogen Peroxide Using Sensor Membranes Containing Europium-Tetracycline in a Microarray Format*. BSS2003; 3th German BioSensorSymposium, 30, March, 2003 – 01, April, 2003 (Berlin).
3. Wu, M., LIN, Z, Dürkop, A, Wolfbeis, O, *A Europium(III)-derived Molecular Probe for the Detection and Differentiation of Oligonucleotides, ss-DNA and ds-DNA* Euroanalysis-12 European Conference on Analytical Chemistry, Dortmund, Germany, September 8 - 13, 2002 P2-083.
4. Otto S. Wolfbeis, Meng Wu, Zhihong Lin, Axel Dürkop, and Torsten Mayr *Fluorescent Europium(III) Chelates as Labels and Molecular Probes for Bioassays*. Analytica 2002, Munich, on 24 April 2002.

11. Appendix

11.1. Abbreviations and Symbols

3-AT	3-Amino-1,2,4-triazole
A6550	N-Acetyl-3,7-dihydrophenoxazine
BOD/COD	Biological oxygen demand/ Chemical oxygen demand
CAT	Catalase.
DELFA	Dissociation enhanced lanthanide fluoroimmunoassay
DTQ	8-(4,6-Dichloro-1,3,5-triazinoxy)quinoline
EALL	Enzyme-amplified lanthanide luminescence
ELISA	Enzyme-linked immunosorbent assay
ESR	Electron spin resonance
Eu	Europium
EuTc	Europium tetracycline complex, in 3:1 ratio, if not othrewise specified
EuTc-HP	Europium tetracycline hydrogen peroxide complex, usually in 3:1 ratio of Eu : Tc.
FAD	Flavin adenine dinucleotide
FII	Fluorescent intensity imaging
FLIM	Fluorescence lifetime imaging microscopy
GalOx	Galactose oxidase
GFP	Green fluorescent protein
GOx	Glucose oxidase
HP	Hydrogen peroxide, H ₂ O ₂
HPMQ	N-(4'-Hydroxyphenyl)-N-(4-methylquinolinyl)amine
HST	High throughput screening
IDL	Interactive data language
LOx	Lactate oxidase
MOPS	3-(N-Morpholino)propanesulfonate.
MTP	Microtiter plate, or microplate
NADH	β-Nicotinamide adenine dinucleotide
PAR	4-(2-Pyridylazo)resorcinol
PDR, PDI	Phase delay ratioing, Phase delay ratioing imaging
pHPA	p-Hydroxyphenylacetate
POx	Peroxidase
PTQA	2-α-Pyridylthioquinaldinamide
RLD, RLI	Rapid lifetime determination, Rapid lifetime determination imaging
ROS	Reactive oxygen species
S/N	Signal-to-noise ratio
SCE	Saturated calomel electrode
SOx	Sarcosine oxidase
TBDRH	Tris(2,2'-bipyridyl)dichlororuthenium(II) hexahydrate
Tc	Tetracycline
TCSPC	Time-correlated single photon counting
TRI	Time-resolved (gated) imaging
UOx	Urate oxidase

11.2. Programs

A. Matlab codes for imaging processing of GOx images

```

1. function [ output_args ] =
   GOx_all1( input_args )
2. %GOX_ALL1 Summary of this function
   goes here
3. clear
4. %reading the files
5. g1= imread('GOx_Glu1_img1.tif');
6. g2= imread('GOx_Glu1_img2.tif');
7. g3= imread('GOx_Glu1_dark1.tif');
8. g4= imread('GOx_Glu1_dark2.tif');
9.
10. %crop the file to the interested part
11. g1a=imcrop(g1,[5 20 315 78]);
12. g2a=imcrop(g2,[5 20 315 78]);
13. g3a=imcrop(g3,[5 20 315 78]);
14. g4a=imcrop(g4,[5 20 315 78]);
15.
16. %windows1 subtraction
17. ga1=imsubtract(g1a,g3a);
18. ga1b=ga1>10;
19. ga2=(double(ga1)/65535).*(double
   (ga1b)/255);
20.
21. %windows2 subtraction
22. gb1=imsubtract(g2a,g4a);
23. gb1b=gb1>10;
24. gb2=(double(gb1)/65535).*(double
   (gb1b)/255);
25.
26. %divide of window1 and windows2
27. ga3=ga2;
28. gb3=gb2;
29. gc=ga3./gb3;
30.
31. %further exclude the inf in the array.
32. gc1=gc<500000;
33. gd1=gc.*gc1;
34. gd2=mat2gray(gd1);
35. imwrite((mat2gray(gd1)),'GOx_RLI_1.ti
   f','Compression','none');
36. figure, pcolor(mat2gray(gd1))
37.
38. %crop to the targeted dots
39. % in the row, upper row
40. gda12 = imcrop(gd1, [0 0 26 25]);
41. gda12a= imcrop(gda12, [8 9 15 12]);
42. a12i=mean2(gda12a);
43. a12s=std2(gda12a);
44.
45. gda11 = imcrop(gd1, [28 0 26 25]);
46. gda11a= imcrop(gda11, [8 9 15 12]);
47. a11i=mean2(gda11a);
48. a11s=std2(gda11a);
49.
50. gda10 = imcrop(gd1, [54 0 26 25]);
51. gda10a= imcrop(gda10, [8 9 15 12]);
52. a10i=mean2(gda10a);
53. a10s=std2(gda10a);
54.
55. gda9 = imcrop(gd1, [80 0 26 25]);
56. gda9a= imcrop(gda9, [8 9 15 12]);
57. a9i=mean2(gda9a);
58. a9s=std2(gda9a);
59.
60. gda8 = imcrop(gd1, [106 0 26 25]);
61. gda8a= imcrop(gda8, [8 9 15 12]);
62. a8i=mean2(gda8a);
63. a8s=std2(gda8a);
64.
65. gda7 = imcrop(gd1, [134 0 26 25]);
66. gda7a= imcrop(gda7, [8 9 15 12]);
67. a7i=mean2(gda7a);
68. a7s=std2(gda7a);
69.
70. gda6 = imcrop(gd1, [159 0 26 25]);
71. gda6a= imcrop(gda6, [8 9 15 12]);
72. a6i=mean2(gda6a);
73. a6s=std2(gda6a);
74.
75. gda5 = imcrop(gd1, [185 0 26 25]);
76. gda5a= imcrop(gda5, [8 9 15 12]);
77. a5i=mean2(gda5a);
78. a5s=std2(gda5a);
79.
80. gda4 = imcrop(gd1, [211 0 26 25]);
81. gda4a= imcrop(gda4, [8 9 15 12]);
82. a4i=mean2(gda4a);
83. a4s=std2(gda4a);
84.
85. gda3 = imcrop(gd1, [237 0 26 25]);
86. gda3a= imcrop(gda3, [8 9 15 12]);
87. a3i=mean2(gda3a);
88. a3s=std2(gda3a);
89.
90. gda2 = imcrop(gd1, [264 0 26 25]);
91. gda2a= imcrop(gda2, [8 9 14 12]);
92. a2i=mean2(gda2a);
93. a2s=std2(gda2a);
94.
95. gda1 = imcrop(gd1, [288 0 26 25]);
96. gda1a= imcrop(gda1, [8 9 14 12]);
97. a1i=mean2(gda1a);

```

```

98. als=std2(gda1a);
99.
100.    % middle row
101.    gdb12 = imcrop(gd1, [0 27 26 25]);
102.    gdb12a= imcrop(gdb12, [8 9 15 12]);
103.    b12i=mean2(gdb12a);
104.    b12s=std2(gdb12a);
105.
106.    gdb11 = imcrop(gd1, [28 27 26 25]);
107.    gdb11a= imcrop(gdb11, [8 9 15 12]);
108.    b11i=mean2(gdb11a);
109.    b11s=std2(gdb11a);
110.
111.    gdb10 = imcrop(gd1, [54 27 26 25]);
112.    gdb10a= imcrop(gdb10, [8 9 15 12]);
113.    b10i=mean2(gdb10a);
114.    b10s=std2(gdb10a);
115.
116.    gdb9 = imcrop(gd1, [80 27 26 25]);
117.    gdb9a= imcrop(gdb9, [8 9 15 12]);
118.    b9i=mean2(gdb9a);
119.    b9s=std2(gdb9a);
120.
121.    gdb8 = imcrop(gd1, [106 27 26 25]);
122.    gdb8a= imcrop(gdb8, [8 9 15 12]);
123.    b8i=mean2(gdb8a);
124.    b8s=std2(gdb8a);
125.
126.    gdb7 = imcrop(gd1, [134 27 26 25]);
127.    gdb7a= imcrop(gdb7, [8 9 15 12]);
128.    b7i=mean2(gdb7a);
129.    b7s=std2(gdb7a);
130.
131.    gdb6 = imcrop(gd1, [159 27 26 25]);
132.    gdb6a= imcrop(gdb6, [8 9 15 12]);
133.    b6i=mean2(gdb6a);
134.    b6s=std2(gdb6a);
135.
136.    gdb5 = imcrop(gd1, [185 27 26 25]);
137.    gdb5a= imcrop(gdb5, [8 9 15 12]);
138.    b5i=mean2(gdb5a);
139.    b5s=std2(gdb5a);
140.
141.    gdb4 = imcrop(gd1, [211 27 26 25]);
142.    gdb4a= imcrop(gdb4, [8 9 15 12]);
143.    b4i=mean2(gdb4a);
144.    b4s=std2(gdb4a);
145.
146.    gdb3 = imcrop(gd1, [237 27 26 25]);
147.    gdb3a= imcrop(gdb3, [8 9 15 12]);
148.    b3i=mean2(gdb3a);
149.    b3s=std2(gdb3a);
150.
151.    gdb2 = imcrop(gd1, [264 27 26 25]);
152.    gdb2a= imcrop(gdb2, [8 9 14 12]);
153.    b2i=mean2(gdb2a);
154.    b2s=std2(gdb2a);
155.
156.    gdb1 = imcrop(gd1, [288 27 26 25]);
157.    gdb1a= imcrop(gdb1, [8 9 14 12]);
158.    b1i=mean2(gdb1a);
159.    b1s=std2(gdb1a);
160.
161.    %lower row
162.    gdc12 = imcrop(gd1, [0 52 26 25]);
163.    gdc12a= imcrop(gdc12, [8 9 15 12]);
164.    c12i=mean2(gdc12a);
165.    c12s=std2(gdc12a);
166.
167.    gdc11 = imcrop(gd1, [28 52 26 25]);
168.    gdc11a= imcrop(gdc11, [8 9 15 12]);
169.    c11i=mean2(gdc11a);
170.    c11s=std2(gdc11a);
171.
172.    gdc10 = imcrop(gd1, [54 52 26 25]);
173.    gdc10a= imcrop(gdc10, [8 9 15 12]);
174.    c10i=mean2(gdc10a);
175.    c10s=std2(gdc10a);
176.
177.    gdc9 = imcrop(gd1, [80 52 26 25]);
178.    gdc9a= imcrop(gdc9, [8 9 15 12]);
179.    c9i=mean2(gdc9a);
180.    c9s=std2(gdc9a);
181.
182.    gdc8 = imcrop(gd1, [106 52 26 25]);
183.    gdc8a= imcrop(gdc8, [8 9 15 12]);
184.    c8i=mean2(gdc8a);
185.    c8s=std2(gdc8a);
186.
187.    gdc7 = imcrop(gd1, [133 52 26 25]);
188.    gdc7a= imcrop(gdc7, [8 9 15 12]);
189.    c7i=mean2(gdc7a);
190.    c7s=std2(gdc7a);
191.
192.    gdc6 = imcrop(gd1, [159 52 26 25]);
193.    gdc6a= imcrop(gdc6, [8 9 15 12]);
194.    c6i=mean2(gdc6a);
195.    c6s=std2(gdc6a);
196.
197.    gdc5 = imcrop(gd1, [185 52 26 25]);
198.    gdc5a= imcrop(gdc5, [8 9 15 12]);
199.    c5i=mean2(gdc5a);
200.    c5s=std2(gdc5a);
201.
202.    gdc4 = imcrop(gd1, [211 52 26 25]);
203.    gdc4a= imcrop(gdc4, [8 9 15 12]);
204.    c4i=mean2(gdc4a);
205.    c4s=std2(gdc4a);
206.
207.    gdc3 = imcrop(gd1, [237 52 26 25]);
208.    gdc3a= imcrop(gdc3, [8 9 15 12]);
209.    c3i=mean2(gdc3a);

```

```

210.  c3s=std2(gdc3a);
211.
212.  gdc2 = imcrop(gd1, [264 52 26 25]);
213.  gdc2a= imcrop(gdc2, [8 9 14 12]);
214.  c2i=mean2(gdc2a);
215.  c2s=std2(gdc2a);
216.
217.  gdc1 = imcrop(gd1, [288 52 26 25]);
218.  gdc1a= imcrop(gdc1, [8 9 14 12]);
219.  c1i=mean2(gdc1a);
220.  c1s=std2(gdc1a);
221.
222.  % Further caculation of the ratios:
223.  B=[a1i a12i a11i a10i a9i a8i a7i a6i
    a5i a4i a3i a2i;b1i b12i b11i b10i b9i b8i
    b7i b6i b5i b4i b3i b2i; c1i c12i c11i c10i
    c9i c8i c7i c6i c5i c4i c3i c2i];
224.  C=[a1s a12s a11s a10s a9s a8s a7s
    a6s a5s a4s a3s a2s;b1s b12s b11s b10s
    b9s b8s b7s b6s b5s b4s b3s b2s; c1s c12s
    c11s c10s c9s c8s c7s c6s c5s c4s c3s
    c2s];
225.  D= mean(B);
226.  E=std(B);
227.  F= mean(C);
228.
229.  A=[0 0.05412 0.1353 0.2706 0.5412
    1.353 2.706 5.412 13.53 27.06 54.12
    135.3];
230.  % Glucose conc. A=[0 0.001386
    0.002772 0.00693 0.01386 0.02772
    0.0693 0.1386 0.2772 0.693]
231.
232.  S=[A D E F];
233.
234.  save GOx_Ratio.out S -ASCII
235.
236.  %regional filtration for 3D graphs
237.  h2=fspecial('average',12);
238.  ga1b1=ga1>10;
239.  gg1=roifilt2(h2,gd1,ga1b1);
240.  gg2=mat2gray(gg1);
241.  gg3=imcrop(gg2,[6.5 6.5 300 65]);
242.  %imwrite((gg2,'Glu_RLI_For3D.tif',
    'Compression','none');
243.  %figure, surf(gg3)
244.
245.  % invert the color
246.  f1=200; k1=256; k=k1/f1;
247.  [m,n]=size(gg3);
248.  X2=double(gg3);
249.  for i=1:m
250.      for j=1:n
251.          f=X2(i,j);
252.          gg4(i,j)=0;
253.          if(f>=0)&(f<=f1)
254.              gg4(i,j)=k1-k*f;
255.          else
256.              gg4(i,j)=0;
257.          end
258.      end
259.  end
260.
261.  %crop to the targeted dots
262.  % in the row, upper row
263.
264.  gga12 = imcrop(gg4, [0 0 26 25]);
265.  gga12a= imcrop(gga12, [8 6 3 2]);
266.  ga12i=(mean2(gga12a)-254.72)*10;
267.  ga12s=std2(gga12a);
268.
269.  gga11 = imcrop(gg4, [27 0 26 25]);
270.  gga11a= imcrop(gga11, [8 6 3 2]);
271.  ga11i=(mean2(gga11a)-254.72)*10;
272.  ga11s=std2(gga11a);
273.
274.  gga10 = imcrop(gg4, [54 0 26 25]);
275.  gga10a= imcrop(gga10, [8 6 3 2]);
276.  ga10i=(mean2(gga10a)-254.72)*10;
277.  ga10s=std2(gga10a);
278.
279.  gga9 = imcrop(gg4, [80 0 26 25]);
280.  gga9a= imcrop(gga9, [8 6 3 2]);
281.  ga9i=(mean2(gga9a)-254.72)*10;
282.  ga9s=std2(gga9a);
283.
284.  gga8 = imcrop(gg4, [106 0 26 25]);
285.  gga8a= imcrop(gga8, [8 6 3 2]);
286.  ga8i=(mean2(gga8a)-254.72)*10;
287.  ga8s=std2(gga8a);
288.
289.  gga7 = imcrop(gg4, [133 0 26 25]);
290.  gga7a= imcrop(gga7, [8 6 3 2]);
291.  ga7i=(mean2(gga7a)-254.72)*10;
292.  ga7s=std2(gga7a);
293.
294.  gga6 = imcrop(gg4, [159 0 26 25]);
295.  gga6a= imcrop(gga6, [8 6 3 2]);
296.  ga6i=(mean2(gga6a)-254.72)*10;
297.  ga6s=std2(gga6a);
298.
299.  gga5 = imcrop(gg4, [185 0 26 25]);
300.  gga5a= imcrop(gga5, [8 6 3 2]);
301.  ga5i=(mean2(gga5a)-254.72)*10;
302.  ga5s=std2(gga5a);
303.
304.  gga4 = imcrop(gg4, [211 0 26 25]);
305.  gga4a= imcrop(gga4, [8 6 3 2]);
306.  ga4i=(mean2(gga4a)-254.72)*10;
307.  ga4s=std2(gga4a);
308.
309.  gga3 = imcrop(gg4, [237 0 26 25]);

```

```

310. gga3a= imcrop(gga3, [8 6 3 2]);
311. ga3i=(mean2(gga3a)-254.72)*10;
312. ga3s=std2(gga3a);
313.
314. gga2 = imcrop(gg4, [264 0 26 25]);
315. gga2a= imcrop(gga2, [8 6 3 2]);
316. ga2i=(mean2(gga2a)-254.72)*10;
317. ga2s=std2(gga2a);
318.
319. gga1 = imcrop(gg4, [287 0 26 25]);
320. gga1a= imcrop(gga1, [8 7 3 2]);
321. ga1i=(mean2(gga1a)-254.72)*10;
322. ga1s=std2(gga1a);
323.
324. % middle row
325. ggb12 = imcrop(gg4, [0 28 26 25]);
326. ggb12a= imcrop(ggb12, [8 6 3 2]);
327. gb12i=(mean2(ggb12a)-254.72)*10;
328. gb12s=std2(ggb12a);
329.
330. ggb11 = imcrop(gg4, [27 28 26 25]);
331. ggb11a= imcrop(ggb11, [8 6 3 2]);
332. gb11i=(mean2(ggb11a)-254.72)*10;
333. gb11s=std2(ggb11a);
334.
335. ggb10 = imcrop(gg4, [54 28 26 25]);
336. ggb10a= imcrop(ggb10, [8 6 3 2]);
337. gb10i=(mean2(ggb10a)-254.72)*10;
338. gb10s=std2(ggb10a);
339.
340. ggb9 = imcrop(gg4, [80 28 26 25]);
341. ggb9a= imcrop(ggb9, [8 6 3 2]);
342. gb9i=(mean2(ggb9a)-254.72)*10;
343. gb9s=std2(ggb9a);
344.
345. ggb8 = imcrop(gg4, [106 28 26 25]);
346. ggb8a= imcrop(ggb8, [8 6 3 2]);
347. gb8i=(mean2(ggb8a)-254.72)*10;
348. gb8s=std2(ggb8a);
349.
350. ggb7 = imcrop(gg4, [133 28 26 25]);
351. ggb7a= imcrop(ggb7, [8 6 3 2]);
352. gb7i=(mean2(ggb7a)-254.72)*10;
353. gb7s=std2(ggb7a);
354.
355. ggb6 = imcrop(gg4, [159 28 26 25]);
356. ggb6a= imcrop(ggb6, [8 6 3 2]);
357. gb6i=(mean2(ggb6a)-254.72)*10;
358. gb6s=std2(ggb6a);
359.
360. ggb5 = imcrop(gg4, [185 28 26 25]);
361. ggb5a= imcrop(ggb5, [8 6 3 2]);
362. gb5i=(mean2(ggb5a)-254.72)*10;
363. gb5s=std2(ggb5a);
364.
365. ggb4 = imcrop(gg4, [211 28 26 25]);
366. ggb4a= imcrop(ggb4, [8 6 3 2]);
367. gb4i=(mean2(ggb4a)-254.72)*10;
368. gb4s=std2(ggb4a);
369.
370. ggb3 = imcrop(gg4, [237 28 26 25]);
371. ggb3a= imcrop(ggb3, [8 6 3 2]);
372. gb3i=(mean2(ggb3a)-254.72)*10;
373. gb3s=std2(ggb3a);
374.
375. ggb2 = imcrop(gg4, [264 28 26 25]);
376. ggb2a= imcrop(ggb2, [8 6 3 2]);
377. gb2i=(mean2(ggb2a)-254.72)*10;
378. gb2s=std2(ggb2a);
379.
380. ggb1 = imcrop(gg4, [287 28 26 25]);
381. ggb1a= imcrop(ggb1, [8 6 3 2]);
382. gb1i=(mean2(ggb1a)-254.72)*10;
383. gb1s=std2(ggb1a);
384.
385. %lower row
386. ggc12 = imcrop(gg4, [0 54 26 25]);
387. ggc12a= imcrop(ggc12, [7 6 3 2]);
388. gc12i=(mean2(ggc12a)-254.72)*10;
389. gc12s=std2(ggc12a);
390.
391. ggc11 = imcrop(gg4, [27 52 26 25]);
392. ggc11a= imcrop(ggc11, [7 6 3 2]);
393. gc11i=(mean2(ggc11a)-254.72)*10;
394. gc11s=std2(ggc11a);
395.
396. ggc10 = imcrop(gg4, [54 52 26 25]);
397. ggc10a= imcrop(ggc10, [7 6 3 2]);
398. gc10i=(mean2(ggc10a)-254.72)*10;
399. gc10s=std2(ggc10a);
400.
401. ggc9 = imcrop(gg4, [80 52 26 25]);
402. ggc9a= imcrop(ggc9, [8 6 3 2]);
403. gc9i=(mean2(ggc9a)-254.72)*10;
404. gc9s=std2(ggc9a);
405.
406. ggc8 = imcrop(gg4, [106 52 26 25]);
407. ggc8a= imcrop(ggc8, [8 6 3 2]);
408. gc8i=(mean2(ggc8a)-254.72)*10;
409. gc8s=std2(ggc8a);
410.
411. ggc7 = imcrop(gg4, [132 52 26 25]);
412. ggc7a= imcrop(ggc7, [7 6 3 2]);
413. gc7i=(mean2(ggc7a)-254.72)*10;
414. gc7s=std2(ggc7a);
415.
416. ggc6 = imcrop(gg4, [159 52 26 25]);
417. ggc6a= imcrop(ggc6, [8 6 3 2]);
418. gc6i=(mean2(ggc6a)-254.72)*10;
419. gc6s=std2(ggc6a);
420.
421. ggc5 = imcrop(gg4, [185 52 26 25]);

```

```

422.   ggc5a= imcrop(ggc5, [8 6 3 2]);
423.   gc5i=(mean2(ggc5a)-254.72)*10;
424.   gc5s=std2(ggc5a);
425.
426.   ggc4 = imcrop(gg4, [211 52 26 25]);
427.   ggc4a= imcrop(ggc4, [8 6 3 2]);
428.   gc4i=(mean2(ggc4a)-254.72)*10;
429.   gc4s=std2(ggc4a);
430.
431.   ggc3 = imcrop(gg4, [237 52 26 25]);
432.   ggc3a= imcrop(ggc3, [8 6 3 2]);
433.   gc3i=(mean2(ggc3a)-254.72)*10;
434.   gc3s=std2(ggc3a);
435.
436.   ggc2 = imcrop(gg4, [264 52 26 25]);
437.   ggc2a= imcrop(ggc2, [8 6 3 2]);
438.   gc2i=(mean2(ggc2a)-254.72)*10;
439.   gc2s=std2(ggc2a);
440.
441.   ggc1 = imcrop(gg4, [287 54 26 25]);
442.   ggc1a= imcrop(ggc1, [8 6 3 2]);
443.   gc1i=(mean2(ggc1a)-254.72)*10;
444.   gc1s=std2(ggc1a);
445.
446.   % Further caculation of the ratios:
447.   GB=[gali ga12i gal1i ga10i ga9i ga8i ga7i
        ga6i ga5i ga4i ga3i ga2i;gbl1i gbl2i gbl1i gbl0i
        gb9i gb8i gb7i gb6i gb5i gb4i gb3i gb2i; gcli
        gc12i gc11i gc10i gc9i gc8i gc7i gc6i gc5i gc4i
        gc3i gc2i]
448.   GC=[gals ga12s gal1s ga10s ga9s ga8s
        ga7s ga6s ga5s ga4s ga3s ga2s;gbls gbl2s gbl1s
        gb10s gb9s gb8s gb7s gb6s gb5s gb4s gb3s gb2s;
        gcls gc12s gc11s gc10s gc9s gc8s gc7s gc6s
        gc5s gc4s gc3s gc2s]
449.   GD= mean(GB)
450.   GE=std(GB)
451.   GF= mean(GC)
452.   GS=[A GD GE GF]
453.
454.   save GOx_Ratio_afterreverse.out GS -
        ASCII
455.
456.   gg5=mat2gray(gg4);
457.   %imwrite((gg5,'Glu_RLI_For3D_fin.tif','Co
        mpresion','none');
458.   figure,imshow(gg5)
459.   %figure, surf(gg5)
460.   pixval on

```

B. Source codes for filling microplates with the Hamilton Microlab dispensing robot

Number Line

```

1
2           Program for hydrogen peroxide detection
4   Initialise single needle arm
5   Initialise dispenser 1
6   Open Excel :C:\...\Methods\Meng\HP\Well_composition_HP_Test3.xls
8   Dispensing MOPS from A1 to C9
9       Loop 9
10      zeile=_sysloop[1]+1
11      Read from Excel : Sheet1
12      vol=3*mops
13      Aspirate 5 + vol ul from Polymer with syringe 1 , speed 50 seconds per stroke
14      Loop 3
15      Dispense mops ul to Meng_HP1 with syringe 1 , speed 30 seconds per stroke
16      End of loop
17      Wash needle with syringe 1, 5 mm above bottom in Waschen, 0 ul 1 times, lift 20 mm
18      End of loop
19      Wash needle with syringe 1, 5 mm above bottom in Waschen, 1000 ul 2 times, lift 20 mm
21      Dispensing MOPS from D1 to F9
22      Loop 9
23      zeile=_sysloop[1]+10
24      Read from Excel : Sheet1
25      vol=3*mops
26      Aspirate 5 + vol ul from Polymer with syringe 1 , speed 50 seconds per stroke
27      Loop 3
28      Dispense mops ul to Meng_HP2 with syringe 1 , speed 30 seconds per stroke

```

```
29     End of loop
30 Wash needle with syringe 1, 5 mm above bottom in Waschen, 0 ul 1 times, lift 20 mm
31     End of loop
32 Wash needle with syringe 1, 5 mm above bottom in Waschen, 1000 ul 2 times, lift 20 mm
35 Set new position in Proben to 1 for single needle arm
36 Set new position in Meng_HP1 to 1 for single needle arm
37 Set new position in Meng_HP2 to 1 for single needle arm
40 Dispensing of HP4
41 Loop 6
42     zeile=_sysloop[1]+1
43     Read from Excel : Sheet1
44         vol2=3*HP4+10
45         Aspirate 5 + vol2 ul from Proben with syringe 1 , speed 50 seconds per stroke
46     Loop 3
47         Dispense HP4 ul to Meng_HP1 with syringe 1 , speed 30 seconds per stroke
48     End of loop
49 Wash needle with syringe 1, 5 mm above bottom in Waschen, 0 ul 1 times, lift 20 mm
50 End of loop
51 Wash needle with syringe 1, 5 mm above bottom in Waschen, 1000 ul 2 times, lift 20 mm
54 Set new position in Proben to old position plus 1 for single needle arm
56 Dispensing of HP3
57 Loop 3
58     zeile=_sysloop[1]+7
59     Read from Excel : Sheet1
60         vol3=3*HP3+10
61         Aspirate 5 + vol3 ul from Proben with syringe 1 , speed 50 seconds per stroke
62     Loop 3
63         Dispense HP3 ul to Meng_HP1 with syringe 1 , speed 30 seconds per stroke
64     End of loop
65 Wash needle with syringe 1, 5 mm above bottom in Waschen, 0 ul 1 times, lift 20 mm
66 End of loop
67 Wash needle with syringe 1, 5 mm above bottom in Waschen, 1000 ul 2 times, lift 20 mm
70 Set new position in Proben to old position plus 1 for single needle arm
72 Dispensing of HP2
73 Loop 6
74     zeile=_sysloop[1]+10
75     Read from Excel : Sheet1
76         vol4=3*HP2+10
77         Aspirate 5 + vol4 ul from Proben with syringe 1 , speed 50 seconds per stroke
78     Loop 3
79         Dispense HP2 ul to Meng_HP2 with syringe 1 , speed 30 seconds per stroke
80     End of loop
81 Wash needle with syringe 1, 5 mm above bottom in Waschen, 0 ul 1 times, lift 20 mm
82 End of loop
83 Wash needle with syringe 1, 5 mm above bottom in Waschen, 1000 ul 2 times, lift 20 mm
85 Set new position in Proben to old position plus 1 for single needle arm
87 Dispensing of HP1
88 Loop 3
89     zeile=_sysloop[1]+16
90     Read from Excel : Sheet1
91         vol5=3*HP1+10
92         Aspirate 5 + vol5 ul from Proben with syringe 1 , speed 50 seconds per stroke
93     Loop 3
94         Dispense HP1 ul to Meng_HP2 with syringe 1 , speed 30 seconds per stroke
95     End of loop
96 Wash needle with syringe 1, 5 mm above bottom in Waschen, 0 ul 1 times, lift 20 mm
```

97 End of loop
 98 Wash needle with syringe 1, 5 mm above bottom in Waschen, 1000 ul 2 times, lift 20 mm
 102 Set new position in Polymer to 2 for single needle arm
 103 Set new position in Meng_HP1 to 1 for single needle arm
 104 Set new position in Meng_HP2 to 1 for single needle arm
 107 Dispensing of EuTc for A1 to C9
 108 Aspirate 5 + 1900 ul from Polymer with syringe 1, speed 50 seconds per stroke
 109 Loop 27
 110 Dispense 65 ul to Meng_HP1 with syringe 1, speed 30 seconds per stroke
 111 End of loop
 112 Wash needle with syringe 1, 5 mm above bottom in Waschen, 0 ul 1 times, lift 20 mm
 114 Dispensing of EuTc for D1 to F9
 115 Aspirate 5 + 1900 ul from Polymer with syringe 1, speed 50 seconds per stroke
 116 Loop 27
 117 Dispense 65 ul to Meng_HP2 with syringe 1, speed 30 seconds per stroke
 118 End of loop
 119 Wash needle with syringe 1, 5 mm above bottom in Waschen, 1000 ul 2 times, lift 20 mm
 120 Initialise single needle arm
 121 End of method

Layout of the excel-worksheet for filling microtiterplates

	MOPS	HP1	HP2	HP3	HP4	EuTc	HP (mM)
A1	185				0	65	0
A2	180				5	65	0.00001
A3	175				10	65	0.00002
A4	165				20	65	0.00004
A5	145				40	65	0.00008
A6	105				80	65	0.00016
A7	165			20		65	0.0004
A8	145			40		65	0.0008
A9	125			60		65	0.0012
D1	185		0			65	0
D2	180		5			65	0.001
D3	175		10			65	0.002
D4	145		40			65	0.008
D5	125		60			65	0.012
D6	105		80			65	0.016
D7	145	40				65	0.08
D8	125	60				65	0.12
D9	105	80				65	0.16

Conc. HP1: 0.5mM, HP2: 0.05mM, HP3: 0.005mM, HP4: 0.0005mM,
 EuTc: 0.2 mM, MOPS: 10 mM, pH 6.9.

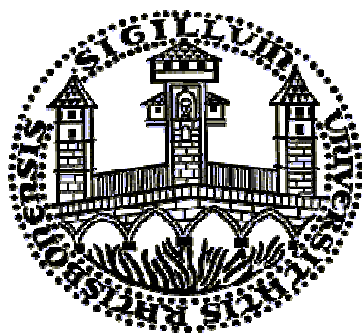
11.3. Chinese Summary 中文摘要

博士论文

用荧光时间分辨法和荧光影像法研究

新型镧系过氧化氢荧光探针及其在酶和酶底物分析中的应用

吴 蒙



联邦德国
雷根斯堡大学
化学和药学院

二〇〇三年十二月

本论文研究和发了一种基于铈-四环素-过氧化氢三元络合物并具有可逆性的荧光探针. 该探针的突出优点在于 (1) 其可逆性, 可以实现动态实时检测过氧化氢的生成与消耗. (2) 6.9-7.0 的最佳 pH, 尤其适合生物测定的要求. (3) 具有镧系元素荧光的三大特征, 即较大的 Stokes 位移(~210nm), 线性尖锐发射光谱和较长的微秒级荧光寿命; 并且可在 380-420 nm 范围内激发 (如可使用 405 nm 半导体蓝色激光), 极大地方便了时间分辨荧光检测和荧光影像测定. 因此该荧光探针可被用于稳态荧光强度测定法, 时间分辨弛预测定法, 和荧光寿命测定法等检测技术和相对应的多种荧光影像技术.

基于过氧化氢的荧光探针在生物研究领域有着广泛的应用前景. 因为过氧化氢作为活性氧物质(reactive oxygen species, ROS) 的一员, 普遍存在于生物体系中并参与了很多重要的氧化还原反应, 成为细胞氧化的生物标志物和新的神经递质而受到重视.

在本论文中, 首先研究的是探针特性. 第一章对目前的过氧化氢分析技术作了简单的概述, 第二章的前半部分则主要讨论了该探针的表征, 包括其吸收光谱, 圆二色光谱, 荧光光谱, 荧光寿命和衰变. 同时还讨论了其最佳的 pH, 稳定性, 温度, 缓冲溶剂, 猝灭和干扰的影响等问题. 第六章的后半部分进一步讨论了该荧光探针特别的结构特征, 并提供了用组合化学的方式研究新型镧系荧光探针结构的初步结果.

其次是测定方法的研究. 多种不同荧光分析原理和测定方法分别用于过氧化氢, 葡萄糖, 葡萄糖氧化酶, 过氧化氢酶的测定. 如稳态荧光强度测定法测定过氧化物酶 (第五章), 时间分辨弛预测定法测定葡萄糖 (第三章), 荧光寿命测定法中的快速寿命测定法 (Rapid Lifetime Determination, RLD) 测定过氧化氢 (第二章, 首次的微点滴板 (microtiter plate) 上实现), 及时间相关单光子计数测定法检测过氧化氢 (第二章). 这些测定方法既适用于比色池(cuvette), 又适用于微点滴板 (microtiter plate) 检测, 还可用于高通量筛选研究.

另外对基于该探针的荧光影像技术也做了进一步的研究. 由于该荧光探针具有微秒级荧光寿命, 因此其荧光影像装置被大大简化, 还可以同时使用多种时间分辨的手段获取被测物的多重信息. 四种影像分析方式, 包括常规荧光影像, 时间分辨弛预, 相弛预比例法(Phase delay ratioing PDR) 影像, 及快速寿命测定法(RLD) 影像, 被应用于过氧化氢, 葡萄糖, 葡萄糖氧化酶的荧光影像测定, 其中重点在第四章介绍了葡萄糖氧化酶的荧光影像.

最后, 在第六章的前半部分总结了该探针在其他领域中的应用, 包括葡萄糖氧化酶酶标免疫分析(ELISA), 过氧化氢酶/葡萄糖氧化酶酶联体系用于筛选平台的研究, 及基于微点滴板的阵列和传感器的研究.

注明: 中文摘要仅供参考, 具体内容以英文原文为准.

12. Acknowledgements

First and foremost I acknowledge my supervisor, Professor Otto S. Wolfbeis. I would like to thank him for offering the opportunity for me to study under his supervision on the topic of fluorescent probes, for his exceptional guidance, his unconditional willingness to lend assistance, such as reviewing the manuscripts in the weekends or discussing the project in after-work hours.

Special thanks in particular to Dr. Christian Krause, who shares the same lab with me, for the helpful straightforward discussions, and assistance with the fluorescent beads; Dr. Axel Dürkop for raising the topic and all the helps, especially for the arrangements of try-outs of the state-of-art instruments; Dr. Michael Schäferling for productive cooperation on the imaging research; Dr. Ruess for sharing his expertise on pH; Dr. Stefan Woelki for his help with theoretical mathematical problems.

Thanks also to Bernhard Weidgans for interesting discussion and always available helping hands, Athanasios Apostolidis for helps with the Hamilton dispensing robot and its programming, Claudia Schröder for helps with imaging devices and programs, Sarina Arain for helps with FluoroSkan Ascent reader, Thomas Hirsch for helps with programs. Acknowledgement extends to Bianca Wetzl, Alexander Karasyov, Torsten Mayr, Michael Meier, Qingli Hao and all other colleagues at our institute for their friendship, assistance, and for making work in the lab so enjoyable.

Thanks to PD. Dr. Vladimir Mirsky and Angela Haberkern for their helps, especially when I was first in Regensburg. I would also like to acknowledge the helps of Edeltraud Schmid, our secretary, for her kindly help and patience with “meine schlechte Deutsch”.

A very kind thanks to Dr. Jörg Enderlein of Institute for Biological Information Processing, Research Center Jülich, Mr. Thomas Gensch of the same center, and Mr. Henrik Bauer of PicoQuant GmbH, Berlin, for many helpful discussions and assistance, and the provision of laboratory resources, and equipment time. Thanks also to Prof. Ingo Klimant for helpful discussions and advices, in addition to the wonderful experience in Prague.

Chromeon GmbH and University of Regensburg are gratefully acknowledged for the provision of financial support. Appreciation also to Dr. Petra Bastian and Dr. Michaela Gruber of Chromeon for their hospitality and kindly helps.

The love, support, and patience of my wife, my son and the family are appreciated more than words can say.